

AD-A191 498

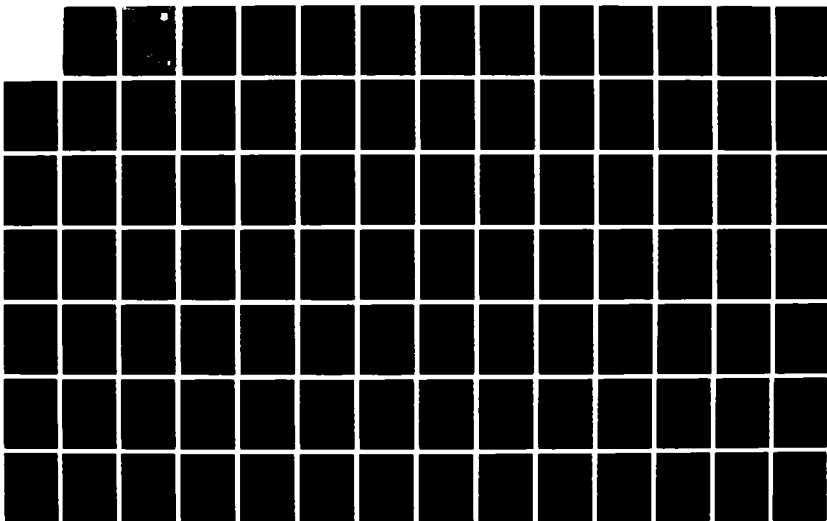
A SCIENTIFIC BASIS FOR AN ALTERNATE CATHODE
ARCHITECTURE(U) ROME AIR DEVELOPMENT CENTER GRIFFISS
AFB NY E J DANISZEWSKI FEB 88 RADC-TR-88-33

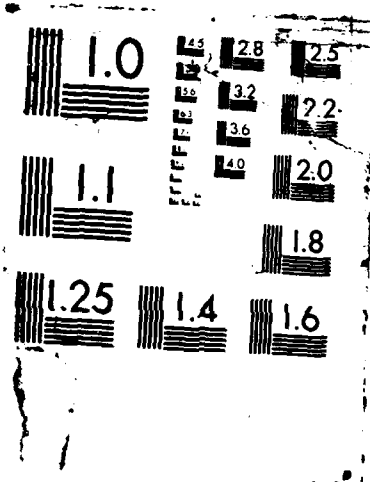
1/2

UNCLASSIFIED

F/G 7/4

NL





FILE COPY

(4)

AD-A191 498

RADC-TR-88-33

In-House Report

February 1988



A SCIENTIFIC BASIS FOR AN ALTERNATE CATHODE ARCHITECTURE

Edward J. Dantszoweld

APPROVED FOR PUBLIC RELEASE; DISTRIBUTION UNLIMITED

This effort was funded in part by the Laboratory Directors' Fund

**ROME AIR DEVELOPMENT CENTER
Air Force Systems Command
Griffiss Air Force Base, NY 13441-5700**

**DTIC
ELECTE
FEB 24 1988
S E D**

88 2 23 106

This report has been reviewed by the RADC Public Affairs Office (PA) and is releasable to the National Technical Information Service (NTIS). At NTIS it will be releasable to the general public, including foreign nations.

RADC-TR-88-33 has been reviewed and is approved for publication.

APPROVED:



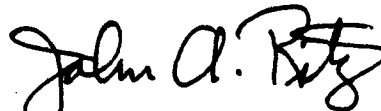
FRED J. DEMMA
Chief, Surveillance Technology Division
Directorate of Surveillance

APPROVED:



FRANK J. REHM
Technical Director
Directorate of Surveillance

FOR THE COMMANDER:



JOHN A. RITZ
Directorate of Plans & Programs

If your address has changed or if you wish to be removed from the RADC mailing list, or if the addressee is no longer employed by your organization, please notify RADC (OCTP) Griffiss AFB NY 13441-5700. This will assist us in maintaining a current mailing list.

Do not return copies of this report unless contractual obligations or notice on a specific document requires that it be returned.

UNCLASSIFIED

SECURITY CLASSIFICATION OF THIS PAGE

| REPORT DOCUMENTATION PAGE | | | | Form Approved OMB No 0704-0188 | |
|--|-------|--|--|--|-----------------------------------|
| 1a. REPORT SECURITY CLASSIFICATION UNCLASSIFIED | | | 1b. RESTRICTIVE MARKINGS N/A | | |
| 2a. SECURITY CLASSIFICATION AUTHORITY N/A | | | 3. DISTRIBUTION/AVAILABILITY OF REPORT Approved for public release; distribution unlimited. | | |
| 2b. DECLASSIFICATION/DOWNGRADING SCHEDULE N/A | | | | | |
| 4. PERFORMING ORGANIZATION REPORT NUMBER(S) RADC-TR-88-33 | | | 5. MONITORING ORGANIZATION REPORT NUMBER(S) N/A | | |
| 6a. NAME OF PERFORMING ORGANIZATION Rome Air Development Center | | 6b. OFFICE SYMBOL (if applicable) OCTP | 7a. NAME OF MONITORING ORGANIZATION N/A | | |
| 6c. ADDRESS (City, State, and ZIP Code) Griffiss AFB NY 13441-5700 | | | 7b. ADDRESS (City, State, and ZIP Code) N/A | | |
| 8a. NAME OF FUNDING/SPONSORING ORGANIZATION AFOSR | | 8b. OFFICE SYMBOL (if applicable) NE | 9. PROCUREMENT INSTRUMENT IDENTIFICATION NUMBER N/A | | |
| 8c. ADDRESS (City, State, and ZIP Code) Bolling AFB Wash DC 20332 | | | 10. SOURCE OF FUNDING NUMBERS | | |
| | | | PROGRAM ELEMENT NO 61102F | PROJECT NO LDFF 2305 | TASK NO 06 J9 |
| 11. TITLE (Include Security Classification) A SCIENTIFIC BASIS FOR AN ALTERNATE CATHODE ARCHITECTURE | | | | | |
| 12. PERSONAL AUTHOR(S) Edward J. Daniszewski | | | | | |
| 13a. TYPE OF REPORT In-House | | 13b. TIME COVERED FROM Sep 84 TO Dec 87 | | 14. DATE OF REPORT (Year, Month, Day) February 1988 | |
| 15. PAGE COUNT 154 | | | | | |
| 16. SUPPLEMENTARY NOTATION This effort was funded in part by the Laboratory Directors' Fund. | | | | | |
| 17. COSATI CODES | | | 18. SUBJECT TERMS (Continue on reverse if necessary and identify by block number) | | |
| FIELD | GROUP | SUB-GROUP | Thermionic Emission ; Crystal Field Theory ; | | |
| 09 | 03 | | Mossbauer Spectroscopy ; Metal-Metal Bond | | |
| | | | Differential Thermal Analysis | | |
| 19. ABSTRACT (Continue on reverse if necessary and identify by block number) <p>The main effort of this research has been to try to bring together in a simplified manner both theoretical and experimental studies basic to the analysis of thermionic emission from Impregnated Dispenser Cathodes (IDC) as it is understood at this time. This study revealed two major areas of uncertainty: (1) the electronic and steric nature of the cathode emissive surface, and (2) the lack of a reproducible impregnation procedure.</p> <p>Mossbauer Spectroscopy was used to probe cathode surfaces and revealed that enhanced thermionic emission was concomitant with the presence of a low-spin state transition metal ion. The existence of the low-spin Mossbauer probe led to a formulation of a hypothetical surface molecular configuration consistent with the constraints imposed by surface symmetry considerations. This model had a striking parallelism with similar systems in the field of heterogeneous supported catalysis (HSC), viz., the hexagonal barium titanates (HBT). The structure of the HBT appeared advantageous for thermionic emission because it exhibits</p> | | | | | |
| 20. DISTRIBUTION/AVAILABILITY OF ABSTRACT <input checked="" type="checkbox"/> UNCLASSIFIED/UNLIMITED <input type="checkbox"/> SAME AS RPT <input type="checkbox"/> OTIC USERS | | | 21. ABSTRACT SECURITY CLASSIFICATION UNCLASSIFIED | | |
| 22a. NAME OF RESPONSIBLE INDIVIDUAL Edward J. Daniszewski | | | 22b. TELEPHONE (Include Area Code) (315) 330-4381 | | 22c. OFFICE SYMBOL RADC (OCTP) |

UNCLASSIFIED

the strong metal-metal surface bond which culminates in a covalent bond between a d-electron donor cation, or atom, in an epiphase, and an acceptor cation at the surface of an oxide.

Utilizing the standard practices of HSC, and monitoring the solid state chemistry with Raman Spectroscopy and differential thermal analysis (DTA) to insure reproducibility, three prototype cathodes were fabricated. Zero field emission from these devices were in excellent agreement with the theoretical Richardson equation, and the emission densities of two of the cathodes were comparable to state-of-the-art IDCs, but at much lower temperatures (900K vs 1200K).

| | |
|--------------------|--|
| Accession For | |
| NTIS GRA&I | <input checked="checked" type="checkbox"/> |
| DTIC TAB | <input type="checkbox"/> |
| Unannounced | <input type="checkbox"/> |
| Justification | |
| By _____ | |
| Distribution/ | |
| Availability Codes | |
| Dist | Avail and/or Special |
| A-1 | |



UNCLASSIFIED

PREFACE

Basic research consists of a systematic inquiry or investigation into a subject in order to discover or revise facts, theories, or applications. The researcher himself must decide whether his ultimate goal is the attainment of knowledge or the exploitation of knowledge. However, depending upon the subject of the research, a third option can be synthesized if a dialectic process is considered. In this approach, an iterative method between theory and application can be developed. This has been the approach used in my research.

I believe that any personal goal needs encouragement from others in order to be realized. It is my humble pleasure to pay a tribute of appreciation to the many researchers before me; it is my hope that this effort exhibits the same elegance and vigor as theirs, and that it will foster the same spirit in future investigators.

I acknowledge especially my friends and supervisors (really no difference) at Rome Air Development Center who taught and supported me: my advisors, and now good friends, Peter and Jim, who cared, fostered, and directed my efforts; Drs Horst Wittmann and John Dimmock of the Air Force Office of Scientific Research who believed in my work and conveyed genuine professional concern; my dear wife who listened, and listened, and finally understood what I was going through (I love you for it); and finally my two best friends, my father Joseph, and Bishop David Cunningham. I humbly dedicate this work to you, because you dedicated your lives to me...*Łc z panem w Bogiem.*

CONTENTS

Chapter

| | | |
|------|------------------------------------|-----|
| I. | INTRODUCTION..... | 1 |
| A. | HISTORICAL BACKGROUND..... | 5 |
| B. | EARLY THEORY..... | 6 |
| C. | CATHODE DEVELOPMENT..... | 9 |
| D. | SUMMARY..... | 20 |
| II. | EXPERIMENTAL..... | 22 |
| A. | MOSSBAUER THEORY..... | 22 |
| B. | CRYSTAL FIELD THEORY..... | 42 |
| C. | MOSSBAUER EXPERIMENTAL..... | 50 |
| D. | DIFFERENTIAL THERMAL ANALYSIS..... | 55 |
| E. | TEMPERATURE CALIBRATION..... | 57 |
| F. | IMPREGNATION PROCEDURES..... | 62 |
| G. | DTA EXPERIMENTAL..... | 67 |
| H. | EMISSION DIAGNOSTICS..... | 71 |
| III. | EXPERIMENTAL RESULTS..... | 74 |
| A. | MOSSBAUER RESULTS..... | 74 |
| B. | DISCUSSION..... | 92 |
| IV. | EXPERIMENTAL RESULTS..... | 106 |
| A. | DTA RESULTS..... | 106 |
| B. | DISCUSSION..... | 116 |
| V. | EMISSION RESULTS..... | 126 |
| A. | FABRICATION AND TESTING..... | 126 |
| B. | DISCUSSION..... | 136 |
| VI. | SUMMARY | 139 |

I. INTRODUCTION

Even though there has been tremendous advances in the field of solid state electronics, the vacuum tube still retains its usefulness and superiority in a number of applications, ranging from television picture tubes to sophisticated communication satellites. The fundamental principle of operation of the vacuum tube is the generation and propagation of an intense, focused electron beam that then interacts with a radio frequency (RF) wave in such a way that the RF wave is amplified. As the device name implies, this process occurs in a vacuum environment.

The heart of vacuum tube electronics is the source of the free electrons, i.e., the cathode. This component provides a copious supply of electrons by the process known as thermionic emission. First observed by Thomas Edison in 1883, this phenomenon refers to the thermally stimulated liberation of electrons from a metal or conducting solid.

Since Edison's discovery, much work has gone into both the development of the theory of thermionic emission, and the subsequent technology transfer to cathode fabrication. By employing an iterative technique between advances in these two areas, researchers have succeeded in producing excellent thermionic cathodes, i.e., high current densities at low temperatures for extended periods of lifetime. The prime objective, however, still remains; the

identification of the physics and chemistry germane to thermionic emission in order to establish a causal relationship between cathode preparation and performance.

Modern day cathodes consist of a porous, sintered tungsten matrix that is "impregnated" with a calcined melt of barium-calcium carbonates and aluminum oxide. A series of chemical reactions initiated at the cathode activation temperature, 1523K, and then sustained at the cathode operating temperature, 1273K, results in the formation of an electropositive monolayer adsorbate, a vertically oriented barium on oxygen ligand on the tungsten surface which drastically lowers the effective work function (from 4.54 eV to 2.0 eV). The evaporation of this monolayer necessitates a continuous dispensing mechanism for these cathodes, which have been named "B-type" impregnated dispenser cathodes, IDC's. In addition, if select 5-d transition metals are sputter coated onto the surfaces of the unactivated B-types, the effective work function is further lowered (to 1.8 eV), and thermionic emission is enhanced. These are known as the "M-type" IDCs, and they have replaced the B-type as the current state-of-the-art.

Although the IDC is an excellent performer, many questions remain unanswered; for instance, what ultimately determines the lifetime of an IDC? why are they so difficult to reproduce? Why does the M-type emit better than the B-type, and what inhibits the active element, barium, from diffusing to the surface of the

cathodes? These questions arise primarily from the evaluation of cathode performance, (electron emission as a function of time and temperature), but it is my contention that the answers are rooted in the physics and chemistry inherent to the theory of thermionic emission and predetermined in the fabrication of the IDC. This last statement is not meant to negate or neglect past research. Rather it reflects the realization and insight that early research was limited due to its place in history; relevant theories and experimental techniques weren't developed yet. It is my contention that if these advances, especially those in the solid state inorganic chemistry area of metal cluster compounds, are applied to the field of thermionic emission, a consistent theory would be developed and those areas of cathode fabrication that ultimately have an effect on actual thermionic emission could be identified.

Therefore, the central objective and rationale of my research is three-fold. First I present the results of an investigation of the emission enhancement of M-type IDC's by in situ Mossbauer spectroscopy to establish the reasons responsible for its performance. Mossbauer spectroscopy is ideally suited for this purpose since it is an accurate measure of exceedingly small perturbations in the nuclear energy levels caused by the solid-state properties of the local environment of the Mossbauer isotope.

The second part is directed at the procedures used to produce cathode structures. Differential thermal analysis (DTA) was the

experimental technique employed. The reason for this approach was dictated by the absence of any dynamic study of the plethora of solid-state reactions that can occur during cathode activation; previous studies formulated proposed "cathode structures" strictly on a thermochemical basis. The lifetime of an IDC is directly related to the evaporation of barium at the cathode operating temperature. In spite of an adequate barium supply in the original impregnant, the barium only originates from the top 10^7 \AA of the cathode, which certainly affects the lifetime of the device. Second, IDCs are very difficult to reproduce even if published fabrication sequences are followed. Third, there has been no systematic study of cathode fabrication techniques. It is my hypothesis that methods of salt deposition, particle size, drying, calcination, reduction, and decomposition times and temperatures, atmospheric composition and flow rate, all enter into the problem of producing and reproducing the optimal impregnant composition. Thus the effects of preparation variables have been systematically investigated by DTA.

The last part of my research is a synthesis of the knowledge gained in the first two parts. A hypothetical cathode, based on the concept of the strong metal-metal interaction (SMMI), was fabricated using the principles of heterogeneous supported catalysis. The recorded thermionic emission from these cathodes will illustrate the efficacy of employing the results of the first two parts of the research.

I.A.: HISTORICAL BACKGROUND OF THERMIONIC EMISSION

In 1883, Thomas Edison (1) noticed that the glass envelope of his new incandescent lamp was blackening during its operation. Edison wondered whether charged particles from the filament might be the cause. In an effort to discover the cause, he configured the circuit as depicted in Figure 1.

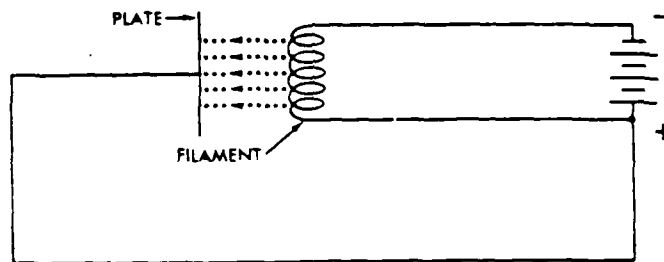


Figure 1
"Edison Effect" Circuit

He observed under these conditions that a current flowed from the plate through the external wire to the filament of his lamp, and he reasoned that charged particles were able to traverse the gap between the filament and the plate in his evacuated tube.

This phenomenon was quickly described as the "Edison Effect" by

Preece (2) in a paper to the Royal Society. The account by Preece of his own experiments on the "Edison Effect" did not separate the effect now recognized as thermionic emission from the "Blue Effect" which was probably the ionization of the residual gas by the accelerated particles.

I.B: EARLY THEORY

In 1897, Thomson (3) identified the particles emitted by the hot filament as electrons. In 1900, the Drude Theory of free electrons in metallic conductors paved the way for Richardson's (4) basic idea of the work function, which marked a better understanding of the thermionic emission process. In 1902 Richardson derived the first thermionic emission equation founded on the basic idea that the work function was a measure of the energy per electron required to transfer charge from the interior of the conductor to the field-free region outside of it. In it's original form, the equation was written:

$$I = ne(k/2\pi m)^{1/2} T^{3/2} \exp(-e\phi/kT) \quad (1)$$

where I is the saturation current expressed in Amperes/cm², n is the number of electrons, e and m are the electron charge and mass respectively, k is Boltzmann's constant, T is the absolute

temperature, and ϕ is the work function unique to individual conductors. In 1914, Wilson (5) considered thermionic emission as analogous to thermal evaporation of electrons and applied the Clausius-Clapeyron equation in his approach. This led to the following equation:

$$I = AT^2 \exp(-\phi/kT) \quad (2)$$

where A is a universal constant. Dushman (6) deduced this same equation in 1923 and argued from the Third Law of Thermodynamics that A was equal to 60.2 while ϕ would vary from emitter to emitter.

However, the introduction of quantum mechanics and the recognition by Sommerfeld (7) that the electrons in the metal obey the Fermi-Dirac distribution, led to a new treatment of thermionic emission. In 1928, Nordheim (8) obtained the relation

$$I = (1-r)AT^2 \exp(-\phi/kT) \quad (3)$$

by considering a statistical approach in which he introduced the occupation number of 2 to take into account the electron spin; this leads to a numerical value of the "universal" constant A of 120.4; and r is a reflection coefficient indicating the deviation from a "perfect" surface.

I.B.1: FIRST ATTEMPTS TO CORRELATE THEORY AND EXPERIMENTS

Early research established that regardless whether one chose a form of Equation (1) or (2), A and 0 are usually considered constants for a given emitter and they are fitted to the experimental data. Nottingham (9) has pointed out, however, that it has become more and more evident that little or no theoretical significance can be attributed to the application of this Richardson form to thermionic emission from a heterogeneous surface. It is his opinion that there are three main factors of thermionic measurements that prohibit direct use of this form of the equation:

- a. the true work function is temperature dependent
- b. the observed energy distribution of emitted electrons is deficient in the low energy range
- c. the evaluation of current density is seldom correct due to surface inhomogeneity.

It should also be pointed out that there are other factors that alter the current density at any given temperature. The first is the Schottky effect (10) which is the reduction in work function at constant temperature under the influence of an accelerating electric field that can be written

$$\phi_{\text{red}} = \phi_{\text{true}} - V \quad (4)$$

and it causes a further modification of the Richardson equation.

The second effect was realized when the thermionic emitter was employed in device technology. For a given cathode configuration and a specified accelerating voltage, the thermionic emission current increases exponentially with temperature up to a sharp limited current and shows no further increase as the temperature exceeds the critical temperature. This limiting current varies as the $(3/2)$ power of the applied voltage and the temperature at which this current limitation takes place is also voltage dependent.

As a reference for future discussions, this limitation of cathode emission current occurs at the "knee" temperature, which signifies the transition from temperature limited (TL) emission to fully space charge limited (FSCL) emission.

I.C.: DEVELOPMENT OF THERMIONIC CATHODES

To this day, thermionic cathodes are employed in a configuration called a close spaced diode or one that resembles a linear beam amplifier. The former is very similar to Edison's original circuit (Figure 1) except that it incorporates a series of focus electrodes to collimate the electrons as they are emitted from the cathode, focusing and retaining a majority of them within the confines of the accelerating field of the anode. The latter has the same basic structure of the close spaced diode, except the electrons are not

collected at the anode, rather they are allowed to drift past the anode into a multiple staged depressed collector. This latter device most closely resembles the primary device that employs thermionic emitters, viz., the traveling wave tube amplifier.

The major point of interest is, however, the noted deviation of the experimental data on thermionic cathodes from the theoretical emission equations. The effects mentioned above certainly contribute to this discrepancy, but they are not the only causes. As will be shown, the physical processes inherent to cathode performance are drastically predetermined in the actual device fabrication.

In spite of this disagreement between theory and experiment, early researchers continued to seek practical applications for this newly discovered phenomenon of thermionic emission. In 1904, Fleming (11) improved Edison's early circuit and used it to detect radio signals. Two years later DeForest (12) added a third grid between the filament and plate which could control the current flowing across the gap. In 1912, Armstrong (13) discovered the secret of amplification of DeForest's invention and was able to receive radio signals from Ireland, Germany, and even Honolulu at his laboratory at Columbia University. Thus, the inadvertant discovery by Edison in 1883 became the basis for modern day vacuum tube electronics. This occurred in spite of an incomplete theoretical understanding.

As noted in the introduction, the heart of the vacuum tube is the cathode, the source of the free electrons. If the full

usefulness of these devices is to be realized, it appears obvious that the main component must be optimized. The next section will briefly review the history of cathode development in order to establish the research background. History has shown that there are essentially six types of thermionic cathodes:

- (1) metal wire filaments
- (2) oxide cathodes
- (3) thoriated filaments
- (4) dispenser cathodes
- (5) impregnated dispenser cathodes (IDC)
- (6) lanthanum hexaboride, single crystal emitters

(Field emission cathodes and the so called "cold cathodes" used in crossed field devices will not be considered.)

I.C.1: METAL WIRE FILAMENTS

These cathodes are directly heated filaments of tungsten providing on the order of 300 mamps/cm^2 emission current density. The early use of tungsten can be traced to the utility of this element in the development of the incandescent light. These cathodes operate at 2500K, they are extremely brittle, and have short lifetimes. In parallel with the advent of tungsten filaments for the incandescent lamps, Coolidge (14) discovered that he could make tungsten ductile by hot working it below the annealing temperature.

However, when the filament operated above the annealing temperature, it recrystallized with boundries normal to the wire axis. As the crystals reoriented, the area between them became smaller, and the filament fails. To offset this, Coolidge added thorium to inhibit grain growth.

I.C.2: OXIDE CATHODES

Wehnelt (15) discovered in 1903 that barium oxide and other alkaline earth oxides could be applied to normally poor thermionic emitters with the result that such a coated emitter would yield an emission current many times greater than that characteristic of the base metal in the absence of the oxide coating. This particular cathode configuration has survived the test of time and, even with the advent of the IDC, is still used to this day in many pulsed applications. However, in spite of 83 years of extensive research, many of the fundamental problems of the oxide cathode emitting process remain speculation. These cathodes are capable of 500 mamps/cm² at 1073K. The interested reader is referred to excellent reviews of this device by Eisenstein, and Zalm (16).

I.C.3: THORIATED FILAMENTS

Langmuir and Rogers (17) in 1913, found that thoriated tungsten emitted 10,000 times the current of pure tungsten at a given temperature. Later analysis by Langmuir (18) showed that this enhanced emission could be related quantitatively to the average dipole moment per unit area created at the surface by the polarizable atoms absorbed on it. This discovery and the follow-on work, including the absorption of the alkalis, led to a far better understanding of the properties of thermionic emitters.

I.C.4: DISPENSER CATHODES

The original dispenser cathode, the Phillip's "L-Cathode" (19), consisted of a porous tungsten plug, (porosity in the range 17% to 27%), fixed atop a molybdenum cavity. The cavity was filled with a mixture of BaCO_3 and SrCO_3 , which were decomposed to their oxides by heating a vacuum at 1373K. After carbonate disassociation, barium oxide is chemically reduced by tungsten yielding barium vapor at a low pressure within the cavity. Barium is transported through the pores of the tungsten by migration of adatoms over internal surfaces and by Knudsen flow. On reaching the emitting surface, barium migrates out from each pore for a distance governed by the diffusion

coefficient and the absorption energy of barium on tungsten at the operating temperature of the cathode. The presence of barium on the tungsten surface, in conjunction with oxygen, provides the dipole layer which markedly lowers the work function of the metal. Since these cathodes operated at a temperature near 1400K, the active element, i.e., the barium, evaporated during the course of normal operation. Thus, the term "dispensing" indicates the practical novelty of this cathode, and accentuates the complexity of the fabrication process. These devices deliver 1 Ampere/cm² at 1373K, which is much higher than the oxide cathode, and exhibit extended lifetimes (20,000 hours).

I.C.5: IMPREGNATED DISPENSER CATHODE (IDC)

The IDC can be considered a type of dispenser cathode in which the alkaline earth oxide is not placed in a separate cavity, but is distributed throughout the tungsten matrix. First reported in 1953 by Levi (20), it consists of an indirectly heated porous tungsten matrix, made from 4 to 5 micron average grain size powder; this powder is isostatically pressed and sintered achieving an overall porosity of around 20% with good pore interconnectivity. This pellet is then impregnated with a melt of calcined BaO-Al₂O₃ drawn into the pores by capillary action in an atmosphere of dry hydrogen.

The original IDC, the "A-Cathode", had an impregnant ratio of 5 moles of BaCO_3 : 2 moles Al_2O_3 . This represented the lowest eutectic point in the binary phase diagram. This cathode was superseded by the "B-type" in which the starting impregnant was the same as the "A-type" except for the addition of 3 moles of CaCO_3 . The addition of the CaCO_3 lowered the inherent barium evaporation rate and thus produced a far superior thermionic emitter. These cathodes are activated at 1523K for up to four hours, and are capable of 2 Amperes/cm² at 1373K for extended periods of time.

In the 1960's Zalm (21) reported a further development in the emission density by sputter coating the surface of the B-type IDC with a thin layer (4000 Å) of osmium. Since then, several other workers have used other selected 4-d and 5-d transition metal layers in cathode fabrication, and the resulting "M-type" IDC (M stands for magic) have shown major improvements over the B-type.

The B-type cathode can deliver 2 Amperes/cm² at 1373K for thousands of hours. The M-type IDC requires approximately 350K less temperature for the same current densities, but as higher current loadings are necessary to meet demands, the elevated temperatures cause the thin sputter coating to diffuse into the tungsten matrix, and the M-type IDC becomes a B-type IDC, i.e., a pure tungsten surface.

In an effort to counter this diffusion, Falce (22) adopted a tungsten/iridium mixed metal matrix (MMM) IDC. In this device, the W and Ir metals are mixed in powder form to a composite matrix, and then impregnated in the usual way.

These cathodes have an excellent initial performance, exhibiting current densities of 4 Amperes/cm² at temperatures below 1300K. However, after 500 hours of operation there is a rapid decay in the emission characteristics. This decay is attributed to the failure of the W/Ir matrix to provide sufficient free Barium by reduction of the impregnant compounds. Once this reaction rate was discovered, large W islands were intentionally placed within the matrix, and the MMM cathode has become a standard of the tube industry.

About the same time, Green et al (23) were fabricating cathodes from 80/20 W/Os powders. These cathodes at first were comparable to B's; after 160 hours they were comparable to M's, and after 400 hours they had stabilized at a value some 50% better than the M. Auger analysis of these cathodes revealed the presence of a sigma phase W/Os alloy as well as several weak peaks consistent with the compounds barium tungstate and barium osmate.

The major difference between the MMM and the W/Os cathodes is evident upon inspection of the respective alloy phase diagrams. The 80/20 W/Ir mixture does not have a stable alloy phase at cathode operating temperature, the sigma phase annealing out to a beta and epsilon phase. The W/Os system does indeed have a stable sigma phase at cathode operating temperature. This stability appears to be extremely relevant to the choice of cathode surface fabrication, and will be the subject of a later section.

The next logical step was to eliminate the annealing time of these cathodes; this led Tuck (24) to deposit a sigma phase W/Os alloy on the tungsten matrix. This codeposited (CD) cathode is compared to its predecessors in Figure 2.

More recently a new type of dispenser cathode has been developed by Falce (25). It is called the controlled porosity dispenser (CPD) cathode and uses a thin foil (10^6 \AA) of tungsten with a controlled array of laser drilled or ion etched pores to allow dispensing of free barium from a reservoir behind the surface. The exact nature of the film, i.e., alloy composition and phase, thickness and texture, is the subject of ongoing research at the Naval Research Laboratory.

sputter coating of the same alloy composition. This combination provides lowest effective work function plus evaporation rate control, coupled with physical stability, immunity to interdiffusion and ion bombardment. The surface layers are backed with a thick layer of highly permeable segregated large grain-size porous tungsten to provide a deep chemically reactive barium reservoir.

I.C.6: LANTHANUM HEXABORIDE, SINGLE CRYSTAL EMITTERS

Lanthanum hexaboride cathodes are widely used in scanning electron microscopes and other instruments where a small, bright electron source is desirable. The work function and operating temperatures of these cathodes are much higher than the barium based IDC's, but the intrinsic evaporation rate is much lower. Typical cathodes deliver 1 Ampere/cm² at 1423-1573K. This temperature is not suitable for some applications, but these cathodes do not present the problems intrinsic to the IDCs.

I.D. SUMMARY AND CONCLUSIONS

The logic underlaying the design of thermionic cathodes is the culmination of both theoretical and engineering advances in the field of thermionic emission and related disciplines. However, the underlying effect of work function lowering by the absorption of a polar complex onto a metal surface, has been known since the classic work of Langmuir and Taylor (27) in 1933. Unfortunately, the past 50 years has seen a pragmatic application of their work. In spite of advances in vacuum technology, machining precision, more stable power supplies, purer materials, more sensitive analytical tools, and sound theory, the IDC still suffers from the problems that plagued the early researchers, viz., work function distributions, emission patchiness, surface diffusion, and unexplained emission properties. Modern day IDC's are excellent performers as shown in Figure 2, but they are far from being theoretically understood.

This short history of the development of the IDC was intended to familiarize the reader with the complex chemistry and physics inherent to achieving optimal thermionic emission. As noted in the preface, scientific advance and discovery is rooted in and established on the work of predecessors. To summarize these

endeavors, the early years of thermionic emission research were directed at the discrepancies between the theoretical emission equations and experimental results (1900-1940); the war years (1940-1945) led to the quest for practical devices especially in the radar field; the onset of solid state advances resulted in a great migration of thermionic researchers, but the subsequent realization that solid state devices could not replace thermionic devices for high power at high frequency, has given rise to a new resurgence into the field of thermionic emission (1975-1986).

The IDC enjoys the rank as the state-of-the-art cathode. Therefore, this research will be directed at this particular class of devices.

II. EXPERIMENTAL

This section describes the theory, experimental techniques, apparatus and procedures that I employed in my analysis of impregnated thermionic cathodes. First, Mossbauer spectroscopy, with its sensitivity to the local environment of the Mossbauer nucleus, could investigate perturbations in the nuclear levels caused by the solid-state properties of the host lattice. In combination with crystal field theory, the results could be incorporated into the identification of the electronic configuration of the active emissive sites of thermionic cathodes. Second, differential thermal analysis (DTA), being a qualitative indication of a change in a material or system which is temperature dependent, was used to analyze accepted cathode impregnant preparation sequences. Lastly, a novel cathode architecture, based on the Mossbauer results and fabricated under the scrutiny of DTA, was tested for thermionic emission under conditions identical to traditional thermionic emission experiments.

II.A: MOSSBAUER EFFECT AND MOSSBAUER SPECTROSCOPY

The Mossbauer Effect (28) is also known as recoil-free nuclear resonance absorption. It was discovered by R.L. Mossbauer in 1958, and in 1961, he was awarded the Nobel Prize for his work. A convenient starting point for a discussion of the theory of the Mossbauer Effect is the concept of resonance absorption.

Resonance absorption has long been known in connection with

electronic transitions where a system absorbs a quantum of energy equal to the difference between two of its energy levels. Since the energy states of an atomic nucleus are also quantized, it was expected that resonant absorption would also occur between a gamma radiating radioactive source that decayed by isomeric transition and a ground state isobar absorber.

The experimental verification of nuclear resonant absorption was difficult to obtain, however, because when a gamma photon with momentum E_0/c is emitted from a nucleus, the law of conservation of momentum states that the nucleus must acquire an equal but opposite momentum. If M is the mass of the nucleus, v the velocity component of the nucleus along the direction of the radiation propagation, Δv the change in velocity due to the gamma photon emission, and E_0 the energy of the radiation, then

$$Mv = M(v + \Delta v) = E_0/c \quad (5)$$

Therefore the nucleus acquires a recoil energy

$$E_r = E_0^2/2Mc^2 \quad (6)$$

Thus the energy of the photons of the radiation decreases by E_r when compared with the energy difference between the ground and excited states. The absorbing nucleus suffers a recoil energy of E_r and thus the photon energy available for excitation is now less by an amount

$2E_r$. The energy available to excite the absorbing nucleus is

$$E = E_r - 2E_r \quad (7)$$

The linewidth of the gamma radiation of energy E_0 can be calculated on the basis of the Heisenberg uncertainty principle. The natural linewidth (Γ) depends on the lifetime (τ) of the excited state by the relation

$$\Gamma \tau = h \quad (8)$$

where h is Planck's constant. This is illustrated in Figure 3.

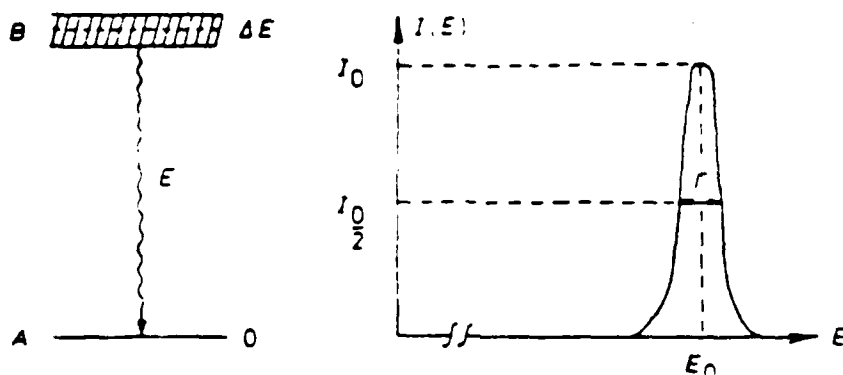


Figure 3

Line Width of Energy Distribution

The energy distribution of the radiation is described by a Breit-Wigner Lorentzian type of function:

$$I(E) = \text{constant } (\Gamma / 2\pi) ((E - E_0)^2 + (\Gamma / 2)^2)^{-1} \quad (7)$$

The measured linewidth is considerably greater than the natural linewidth as a consequence of thermal motion of the atoms of the source and absorber. This thermal motion changes the frequency of the gamma radiation via the Doppler Effect. The higher the temperature, the higher the average kinetic energy of the atoms, and thus the broader is the curve that describes the energy distribution.

If the radiation results from electronic transitions, the recoil energy is so small that E_0 will be within the line-width; in the event of nuclear transitions, the recoil energy is so large that even in spite of the Doppler broadening, there is no overlap of the emission and absorption bands. This is shown in Figure 4.

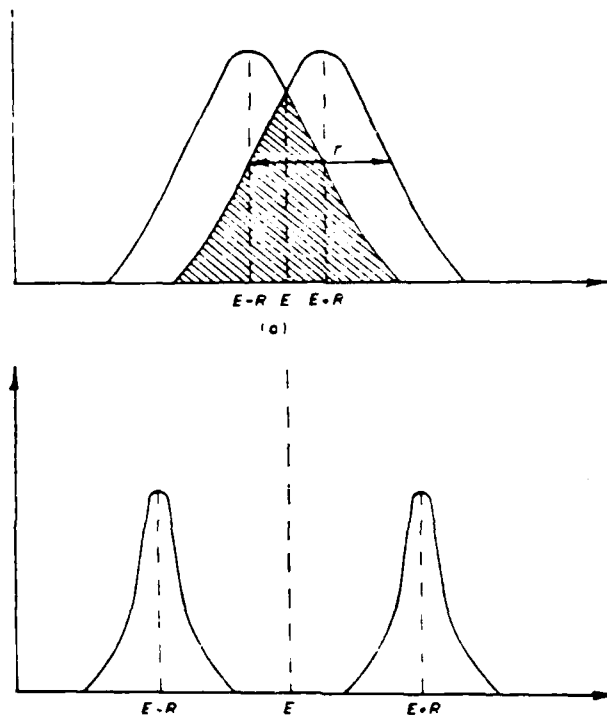


Figure 4

Relation of Emission and Absorption Bands for Optical and Gamma Transitions

As an example, consider the 14.4 keV transition of Iron 57; $\Gamma = 4.6 \times 10^{-9}$ and $E_r = 1.9 \times 10^{-3}$ eV. In contrast, infrared radiation energy has E_0 between 10^{-2} eV and 1 eV, $\Gamma = 10^{-5}$, and the associated E_r is on the order of 10^{-12} eV. Thus for Mossbauer isotopes, $\Gamma < E_r$ while for IR radiation, $\Gamma > E_r$.

The first attempts to experimentally detect nuclear resonance absorption were aimed at compensating for the recoil energy by increasing the temperature or by mechanical movement. This Doppler shift compensation was directed toward the overlapping of the energies of the source and absorbed.

In contrast, Mossbauer tried to reduce the resonance absorption

resulting from thermal Doppler broadening, and thus he cooled the Iridium 193 source and absorber in his original experiment. The absorption, however, increased considerably and in this manner Mossbauer discovered the conditions for recoil free nuclear resonance absorption.

To a first approximation, the lack of recoil energy can be explained by the cooling that causes the atomic nucleus to be bonded more firmly into the crystal lattice. (This is analogous to jumping from a boat frozen in ice and comparing it to jumping from a boat in water.) The M in Equation 6 is no longer just one nucleus; it now refers to a mass of crystal grains. E_r is thus negligible small. In a more exact interpretation, if one adopts the Einstein model of the crystal, the recoil energy would be applied to the excitation of the Mossbauer atoms as if they were represented as oscillators. In this framework, the lattice vibrations are quantized, and, therefore, they cannot absorb arbitrary energy. If $E_r < h\omega$ (where ω is the frequency difference between two levels of lattice vibrations), then the crystal is unable to absorb the recoil energy and recoil free nuclear resonant absorption may occur. The Mossbauer effect is thus a zero phonon event.

A more realistic picture can be presented by employing the Debye model of a crystal. In this representation, every value of ω from 0 to ω_p is permitted, with different probabilities. ω_p , the Debye frequency, is the upper limit of treating the crystal as a quantized

system.

The probability of recoil free emission or absorption, the f-factor or the Lamb-Mossbauer factor, is determined by the nucleus vibrating about its equilibrium position. Treating the nucleus as an oscillator, if it moves in a particular direction with a velocity $v(t)$ c , then the frequency of the electromagnetic wave in the sense of the Doppler effect is

$$\omega(t) = \omega_0 (1 + v(t)/c) \quad (10)$$

If the oscillator frequency is a function of time then the vector potential $A(t)$ of the electromagnetic wave emitted by a classical oscillator can be described as

$$A(t) = A_0 \int_0^t \exp(i\omega(t')) dt' \quad (11)$$

Substituting for $A(t)$ and integrating we can obtain

$$A(t) = A_0 \exp(i\omega_0 t) \exp(i\omega_0 x(t)/c) = A_0 \exp(i\omega_0 t) \exp(ix(t)/\lambda) \quad (12)$$

where λ is the wavelength of the photon radiation. The oscillator undergoes harmonic vibration with a frequency Ω and an amplitude x_0 such that

$$A(t) = A_0 \exp(i\omega_0 t) \exp(ix_0 \sin \Omega t / \lambda) \quad (13)$$

The exponential factor can be expanded in a series of Bessel functions to obtain

$$A(t) = A_0 \sum_n J_n(x_0/\lambda) \exp(\omega_0 + n\Omega)t \quad (14)$$

This last equation just represents an electromagnetic wave that is a superposition of waves with frequencies of ω_0 and $\omega_0 + n\Omega$. Its intensity is given by

$$f = |A(n=0)|^2 = J_0^2(x_0/\lambda) \quad (15)$$

Replacing the Einstein model which treats the lattice elements as independent oscillators, with the Debye model, which treats the crystal as a continuum of frequencies, then

$$f = \prod_m^{3N} J_0^2(x_m/\lambda) \quad (16)$$

where x_m is the amplitude of the mth oscillator and N is the number of oscillators (the actual number of vibrational modes is $3N-6$ but the 6 can be ignored when compared with $3N$).

The argument of the Bessel function is small which allows a power series expansion; this leads to

$$J_0(x_n/\lambda) = 1 - (1/4)(x_n/\lambda)^2 \quad (17)$$

which in turn allows us to write

$$\ln f = -2 \sum_m^{3N} (1/4) (x_n/\lambda)^2 \quad (18)$$

Introducing the mean square deviation of the vibrating nucleus from its equilibrium position as

$$\langle x^2 \rangle = (1/2) \sum_m^{3N} x_n^2 \quad (19)$$

we obtain

$$\ln f = -\langle x^2 \rangle / \lambda^2 \quad (20)$$

and for an infinite number of oscillators

$$f = \exp(-\langle x^2 \rangle / \lambda^2) \quad (21)$$

The average energy of each of the $3N$ oscillators is

$$\langle E \rangle = (\langle n_i \rangle + 1/2) h \omega_i \quad (22)$$

where $\langle n_i \rangle$ is given by

$$\langle n_i \rangle = (\exp(\hbar\omega_i/kT) - 1)^{-1} \quad (23)$$

The energy equation can be rewritten in terms of the displacement of the i th oscillator:

$$NM\omega_i^2 \langle r_i^2 \rangle = (\langle n \rangle + 1/2)\hbar\omega_i \quad (24)$$

This leads to an expression of the average displacement as

$$\langle r^2 \rangle = (\hbar/NM) \sum (1/\omega_i) (\langle n_i \rangle + 1/2) \quad (25)$$

From the Debye theory, the frequency distribution can be expressed as

$$p(\omega) = 9N\omega^2/\omega_m^3 \quad (26)$$

where ω_m is the upper limit of the frequencies that occur: this value arises by evaluating

$$\int_0^{\omega_m} p(\omega) d\omega = 3N \quad (27)$$

Combining this with Equation 25 we have

$$\langle r^2 \rangle = \frac{9\hbar}{M\omega_m^3} \int_0^{\omega_{\max}} \left[\frac{1}{2} + \frac{1}{\exp(\hbar\omega/kT) - 1} \right] \omega d\omega \quad (28)$$

If we now introduce the Debye temperature as $\hbar\omega = k\theta_D$, we obtain

$$\langle r^2 \rangle = \frac{9\hbar^2}{4Mk\theta_D} \left(1 + \frac{4T^2}{\theta_D^2} \int_0^{\theta_D/T} \frac{\mu d\mu}{e^\mu - 1} \right) \quad (29)$$

In the region where $T < \theta_D$, this reduces to

$$\langle r^2 \rangle = \frac{9\hbar^2}{4Mk\theta_D} \left(1 + \frac{2\pi^2 T^2}{3\theta_D^2} \right) \quad (30)$$

or

$$f = \exp \left[- \frac{E_R}{k\theta_D} \left(\frac{3}{2} + \frac{\pi^2 T^2}{\theta_D^2} \right) \right] \quad (31)$$

From this last equation the following conclusions can be drawn concerning the possibility of recoil free nuclear resonance absorption:

- a. The Mossbauer-Lamb factor increases if the temperature decreases.
- b. The higher the crystal Debye temperature, the higher is the probability of the Mossbauer Effect
- c. The Mossbauer Effect can only be predicted for relatively small gamma energies (less than 100 kev).

II.A.2: THE MOSSBAUER SPECTRUM

A solid matrix containing the excited nuclei of a stable isotope is used as the source of the gamma radiation. It is placed alongside a second matrix of identical material containing the same isotope in its ground state; this becomes the absorber. In the first experiment performed by Mossbauer, he measured the intensity of the gamma radiation transmitted through the absorber as a function of temperature. If there was no resonant absorption, then the counting rate would be independent of temperature. If resonant absorption occurred, then there would be a decrease in the transmission as the temperature decreases since the recoil free fraction was postulated as increasing. The resonantly absorbed gamma rays are lost from the transmitted beam; some are randomly re-emitted (resonance fluorescence), while others are lost by an internal conversion process during the decay of the excited state. In a proportion of events an atomic s-electron is ejected instead of a gamma ray. This is called internal conversion, and is defined as the ratio of the number of conversion electrons to the number of gamma rays emitted.

Although this was the first technique utilized by Mossbauer, he later pioneered another method that has now been universally adopted. This method is based on the fact that the definition of the energy of the gamma ray emitted by the source in a Mossbauer Event is on the

order of 1 part in 10^{12} . (For a typical nuclear excited state half-life, $t_{1/2} = 10^{-7}$ sec, $\Gamma = 4.562 \times 10^{-9}$ eV. If the energy of the excited state is 45.65 KeV, the emitted gamma ray will have an intrinsic resolution of 1 part in 10^{12} .) This resolution is on the order of the Doppler energy shifts produced by small movements. If the source and absorber are in relative motion with velocity v , then the effective value of E_0 as seen by the absorber differs from the true energy by a small Doppler energy of

$$E = (v/c) E_\gamma \quad (32)$$

If v is zero, the emission and absorption profiles completely overlap and the absorption is at a maximum. Any increases or decrease in v can only decrease the overlap. It follows then, that a record of transmission as a function of velocity will show an absorption spectrum. This is illustrated in Figure 5. By convention, a positive velocity is taken to be a closing velocity as this represents an increase in the apparent energy of the gamma ray arriving at the absorber.

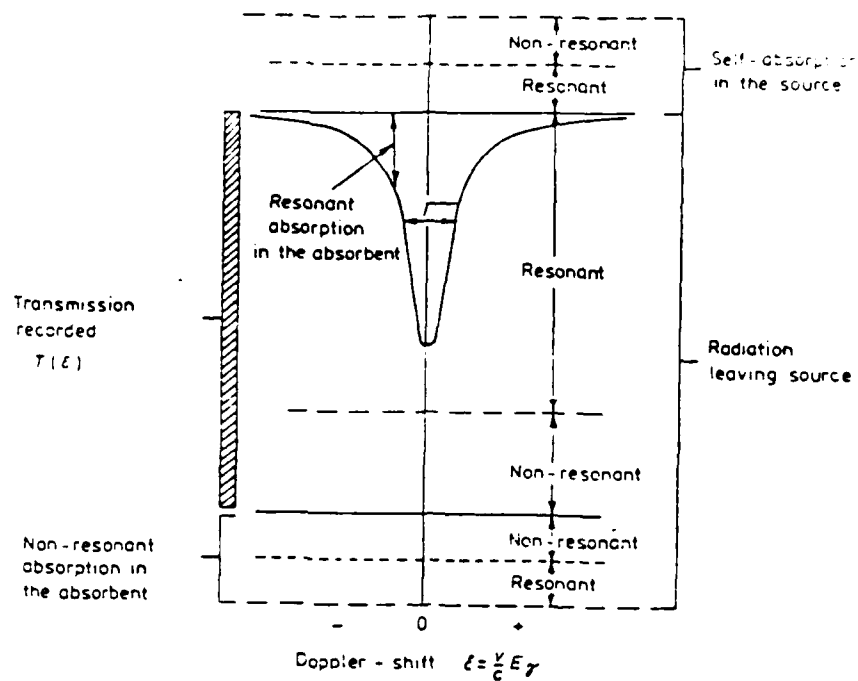


Figure 5

Mossbauer Transmission Spectrum

Since the half-widths of the Mossbauer spectra are fairly small, the probability of the Mossbauer effect is extremely sensitive to even quite small energy changes. Such small changes occur in the energy state of the nucleus as a result of interaction with the external environment, i.e., the electron shells and other atoms in the crystal. Thus, if the source and absorber do not have identical environments, the energy states of the atomic nuclei are also different and the probability of resonance absorption does not exist. However, if the source is moved relative to the absorber at various

rates, the resonance states can be created with the help of the Doppler energy shift. If the rate of movement is determined, conclusions can be drawn about the energy differences, that is, the effects of the chemical surroundings, of the Mossbauer atom.

The energy of the nuclear level is influenced by the s-electron density at the nucleus, as well as the electric and magnetic fields either internal or external to the sample. Thus, a Mossbauer spectrum can reflect the nature and the strengths of the hyperfine interactions between the Mossbauer nucleus and the surrounding fields. In what follows, we shall see how the chemical environment influences atomic electron configurations, especially those of the transition metals; this in turn has a direct effect on the Mossbauer nucleus, its nuclear energy levels, and the resultant Mossbauer spectra.

This influence of the chemical environment means that the spectrum need not consist of a single line, nor in the case of a single line, be centered at zero velocity. The parameters of interest pertinent to Mossbauer spectroscopy are the chemical isomer shift (δ), the electric quadrupole splitting (ΔE_Q), and the magnetic hyperfine interaction (ΔE_m). Any variations in these parameters or comparison of them with other experimental results, means that the Mossbauer effect can provide information on any change that results in a difference in the electronic structure of the Mossbauer atom.

The isomer shift is the displacement of the resonance absorption

from zero velocity and it is a function of s-electron density at the nucleus. Thus, information on oxidation states, types of bonding present (sigma, pi, or hybrid), as well as electronegativity measurements of nearest neighbors to the Mossbauer isotope may be obtained from the isomer shift.

Any nuclear state that has a spin $I > 1/2$, also has a non-zero quadrupole moment which can interact with an inhomogeneous electric field, described by the electric field gradient (EFG). There are two main contributions to the EFG; (1) charges on distant atoms or ions surrounding the Mossbauer atom in non-cubic symmetry, and (2) non-cubic electron contribution from partially filled valence orbitals of the Mossbauer atom. This interaction, the quadrupole splitting, is related to oxidation state, crystal or molecular symmetry, and the high-spin or low-spin nature of the Mossbauer atom.

The third interaction, that of the magnetic dipole ($I > 0$) with the internal or external magnetic field, results in a magnetic hyperfine splitting (ΔE_m). Also known as the nuclear Zeeman Effect, it can be used to measure dipole moments, the strengths of hyperfine magnetic fields, and can be used to determine Curie, Morin, and Neel temperatures.

Figures 6-8 illustrate schematically the resultant spectrum obtained from a Mossbauer isotope whose nuclear energy levels have been perturbed by its environment. These figures represent the basis for the interpretation of Mossbauer spectroscopy.

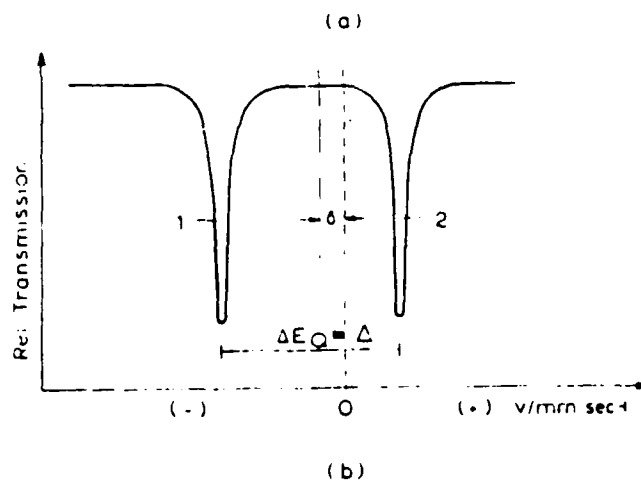
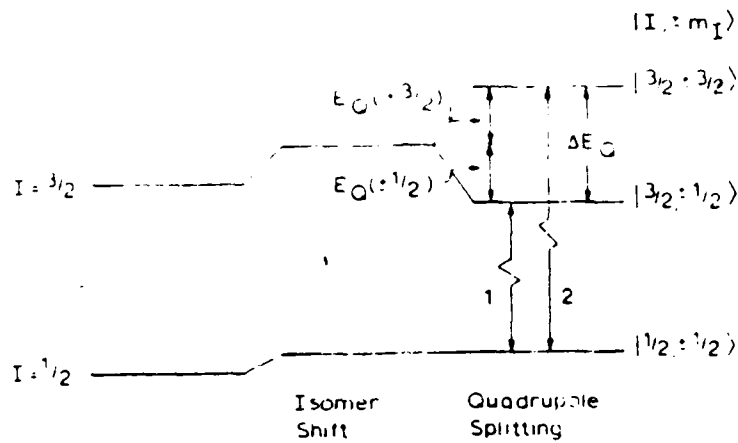


Figure 6a and b

Origin of the Isomer Shift

(a) s-electron density change at the nucleus shifts nuclear energy levels without lifting the degeneracy. (b) the resultant Mossbauer spectrum.

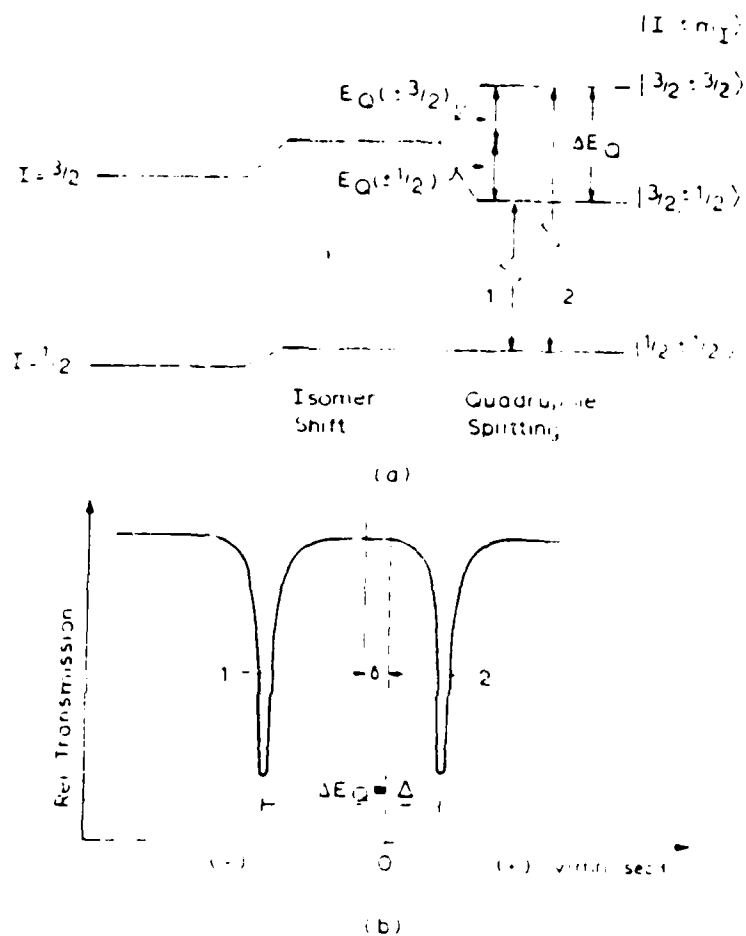


Figure 7a and b

Quadrupole splitting for a nucleus with spin $I = 3/2$. (a) $I = 3/2$ is split into two levels by electric quadrupole interaction. (b) resultant Mossbauer spectrum.

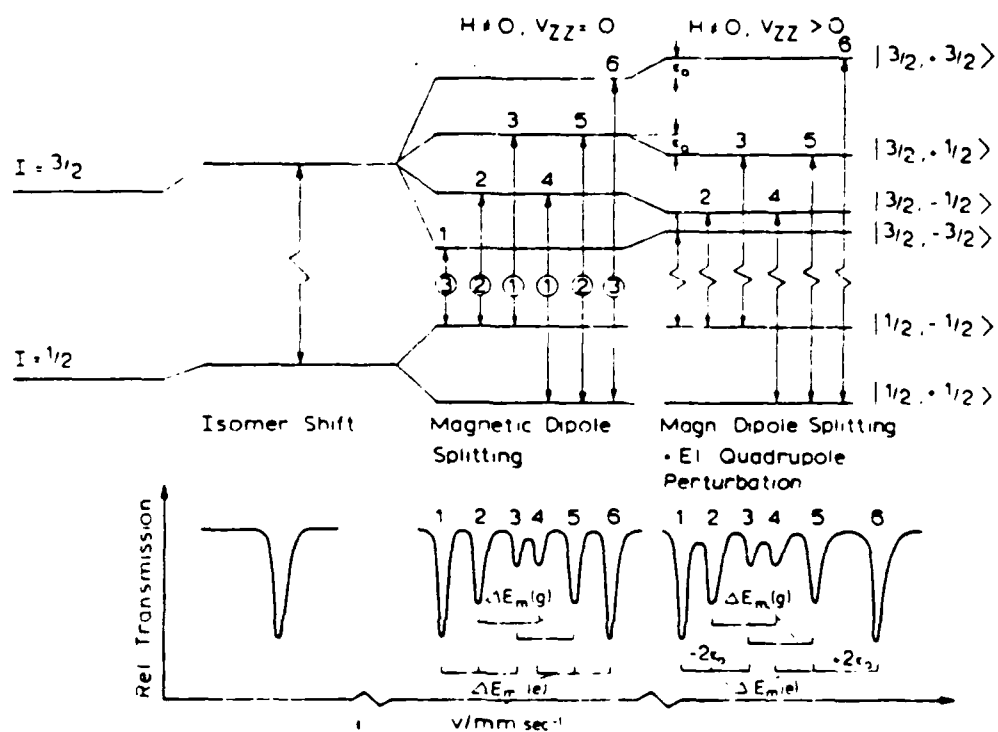


Figure 8a and b

(a) Magnetic dipole splitting with no external magnetic field. (b) Resultant Mossbauer spectrum

As mentioned previously, any variations in these three parameters or comparison of them with other experimental results, means that Mossbauer spectroscopy can provide information on any

change that results in a difference in the electronic structure of the Mossbauer atom. A wealth of such experimental results is provided in the "Mossbauer Effect Data Index". Thus once a Mossbauer spectrum is recorded, the isomer shift, quadrupole splitting, and magnetic hyperfine interaction, are measured and compared against reference spectra. In this manner, conclusions can be inferred as to the oxidation state, low-spin or high-spin nature, etc., of the Mossbauer atom being employed in the experiment.

II.B.: CRYSTAL FIELD THEORY

The d-orbitals of the transition metals are the outer most orbitals and are thus strongly influenced by their crystalline environment. In a crystal, the effective potential at an atomic site has the symmetry of the crystal structure rather than the spherical symmetry appropriate to free atoms in space. The atomic orbital representation given by Hund's Rule may thus be violated because the eigenvalues and eigenfunctions of the electron must now belong to the irreducible representations of the symmetry group of the Hamiltonian of the system in which the electron finds itself. For a free atom, the symmetry group is the three dimensional rotation group, for an atom in a crystal, the wave function of the electron must belong to one of the irreducible representations of the crystallographic point group, and for an absorbed complex, it must belong to one of the ten surface site groups (29, 30).

In order to investigate the effects of the crystalline potential on the d-electron wavefunctions and energy levels, and to establish the theoretical basis of my research, we begin with the pertinent crystal Hamiltonian:

$$H = \sum (p_i^2/2m) - Z_u e^2/r_{ij} + e^2/r_{ij} + \xi \vec{L}_i \cdot \vec{S}_j + \gamma \vec{J}_i \cdot \vec{I}_u + V_i + E_{iu} \quad (33)$$

where the terms in their respective order designate the following features of the reference atom in the crystalline environment:

- (1) Electron kinetic energy (T_i)
- (2) Coulomb attraction of electrons and nucleus (C_{iU})
- (3) Electron coulomb repulsion (F_{ij})
- (4) Spin-orbit interaction (L_{ij})
- (5) Magnetic interaction of nucleus and electrons (G_{iU})
- (6) Perturbing action due to neighboring atoms (V_i)
- (7) Energy interaction due to external fields (E_{iU})

It is convenient to think of each operator in the Hamiltonian as being "switched on" in the order of decreasing magnitude to determine the effects on the eigenfunctions of the unperturbed Hamiltonian. Since G_{iU} and E_{iU} are small ($.1$ to 1 cm^{-1}), they can be neglected and we can concentrate on the perturbing action of F_{ij} , L_{ij} , and V_i .

In general there are three important cases that classify the strength of the crystalline field. These are:

a. $F_{ij} > L_{ij} > V_i$. This is the weak field case usually found in ionic rare earth compounds.

b. $F_{ij} > V_i > L_{ij}$. This is the medium field case found in ionic compounds of the transition metals.

c. $V_i > F_{ij} > L_{ij}$. This is the strong field case found in covalent transition metal compounds.

The limiting cases, the weak and strong fields, dictate that an atom having identical d- or f- electrons may have energy levels which are determined primarily by the field, or the energy levels may be hardly affected by the crystal fields; in this latter case, the levels are determined by the forces present in the free atom and the ground state electron configurations are given by Hund's Rule. These configurations are listed below for those transition metals used in the M-type IDC.

| | | | | | | |
|----|--------|-----------------------------------|------------------|-----------------|-------------------------------|-------------------------|
| Re | [Xe] | ¹⁴ 4f | ⁵ 5d | ² 6s | ⁶ S _{5/2} | +> +> +> +> +> |
| Os | [Xe] | ¹⁴ 4f | ⁶ 5d | ² 6s | ⁵ D ₄ | ++> +> +> +> +> |
| Ir | [Xe] | ¹⁴ 4f | ⁷ 5d | ² 6s | ⁴ F _{9/2} | ++> ++> +> +> +> |
| Pt | [Xe] | ¹⁴ 4f | ¹⁰ 5d | ¹ 6s | ¹ S ₀ | ++> ++> ++> ++> ++> |
| | [Xe] | ^{OF} ¹⁴ 4f | ⁹ 5d | ² 6s | ² D _{5/2} | ++> ++> ++> +> +> |

Table 1

Hund Rule Ground State Electron Configurations of Transition Metals Used in IDC's

The basic idea of crystal field theory (CFT) is that an ion, atom, or molecule which has unfilled electron shells is perturbed by its neighbors in the solid to the extent that these unfilled shells become polarized, the spatial degeneracy of the free system is lifted, and the general physical properties are changed.

As an example, consider the effect of a cubic field, O_h , and a tetragonal field, D_{4h} , on the d-orbitals.

The contributions to characters of reducible representations for cartesian coordinates for d-orbitals are as follows:

| OPERATION | ATOMS CONTRIBUTING | d-ORBITALS |
|---------------|--|-----------------------------------|
| E | ALL | 5 |
| i | SINGLE ATOM AT CENTER | 5 |
| σ | ANY ATOM IN PLANE | 1 |
| C(θ) | ANY ATOM ON AXIS | $1 + 2\cos\theta + 2\cos 2\theta$ |
| S(θ) | ATOM AT INTERSECTION OF AXIS AND σ | $1 - 2\cos\theta + 2\cos 2\theta$ |

Table 2
d-electron Character Contributions

To illustrate the effects of the CFT, consider first the cubic field and then the tetragonal field. The following two tables give

the character tables for the O_h -group and the D_{4h} group.

IRREDUCIBLE

| <u>REPRESENTATIONS</u> | <u>E</u> | <u>$6C_4$</u> | <u>$3C_4^2$</u> | <u>$8C_3$</u> | <u>$6C_2$</u> |
|------------------------|----------|--------------------------|----------------------------|--------------------------|--------------------------|
| A_1 | 1 | 1 | 1 | 1 | 1 |
| A_2 | 1 | -1 | 1 | 1 | -1 |
| E | 2 | 0 | 2 | -1 | 0 |
| T_1 | 3 | 1 | -1 | 0 | -1 |
| T_2 | 3 | -1 | -1 | 0 | 1 |

Table 3

Character Table for the O_h -group

IRREDUCIBLE

| <u>REPRESENTATIONS</u> | <u>E</u> | <u>$2C_4$</u> | <u>C_4^2</u> | <u>$2C_2$</u> | <u>$2C_2'$</u> |
|------------------------|----------|--------------------------|---------------------------|--------------------------|---------------------------|
| A_1 | 1 | 1 | 1 | 1 | 1 |
| A_2 | 1 | 1 | 1 | -1 | -1 |
| B_1 | 1 | -1 | 1 | -1 | 1 |
| B_2 | 1 | -1 | 1 | 1 | -1 |
| E | 2 | 0 | -2 | 0 | 0 |

Table 4

Character table for D_{4h} -group

In the O_h -group, the d-electrons have the following characters:

| | <u>E</u> | <u>C₄</u> | <u>C₄²</u> | <u>C₃</u> | <u>C₂</u> |
|---|----------|----------------------|----------------------------------|----------------------|----------------------|
| d | 5 | -1 | 1 | -1 | 1 |

while in the D_{4h} representation the characters are:

| | <u>E</u> | <u>C₄</u> | <u>C₄²</u> | <u>C₂</u> | <u>C₂'</u> |
|---|----------|----------------------|----------------------------------|----------------------|-----------------------|
| d | 5 | -1 | 1 | 1 | 1 |

Using the orthogonality relationships for the characters of each representation, the d-orbitals in the field belonging to the O_h -group split into a T_{2g} and an E_g . When the symmetry is now lowered to the tetragonal field, the T_{2g} level splits into a B_{2g} and E_g while the E_g becomes a B_{1g} and A_{1g} . These level splittings for the two field symmetries are shown below.

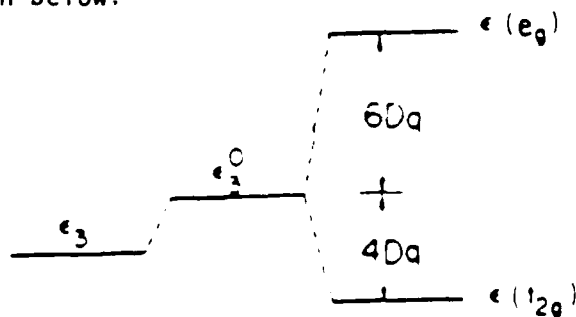


Figure 6

Splitting of the d-level in O_h -symmetry

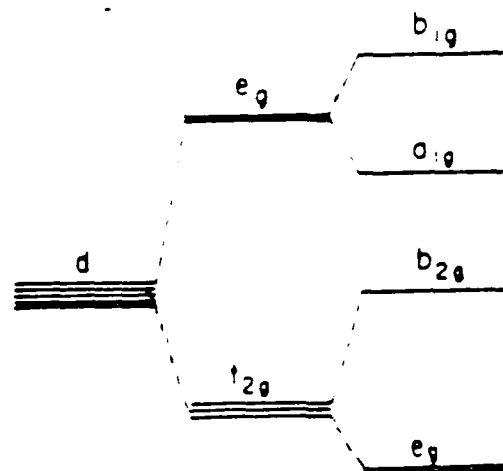


Figure 7

Splitting of the d-level in D_{4h} -symmetry

If we now consider atoms having more than one d-electron, the influence of a strong crystalline field can alter the Hund's Rule ground state electron configurations. This is especially important in the d-4, d-5, d-6, and d-7 configurations. In the weak field case (the Hund Rule ground state) the energy required for pairing electrons in the lower orbitals is greater than the energy required to promote an electron from the T_{2g} orbitals to the E_g orbitals where it may remain unpaired. In strong fields, the T_{2g} and E_g separation is so great that it requires less energy to pair the electrons in the lower T_{2g} orbitals than to promote one into the E_g orbitals. The large crystal field causes a breakdown of the Hund Rule, as illustrated in Figure 8.

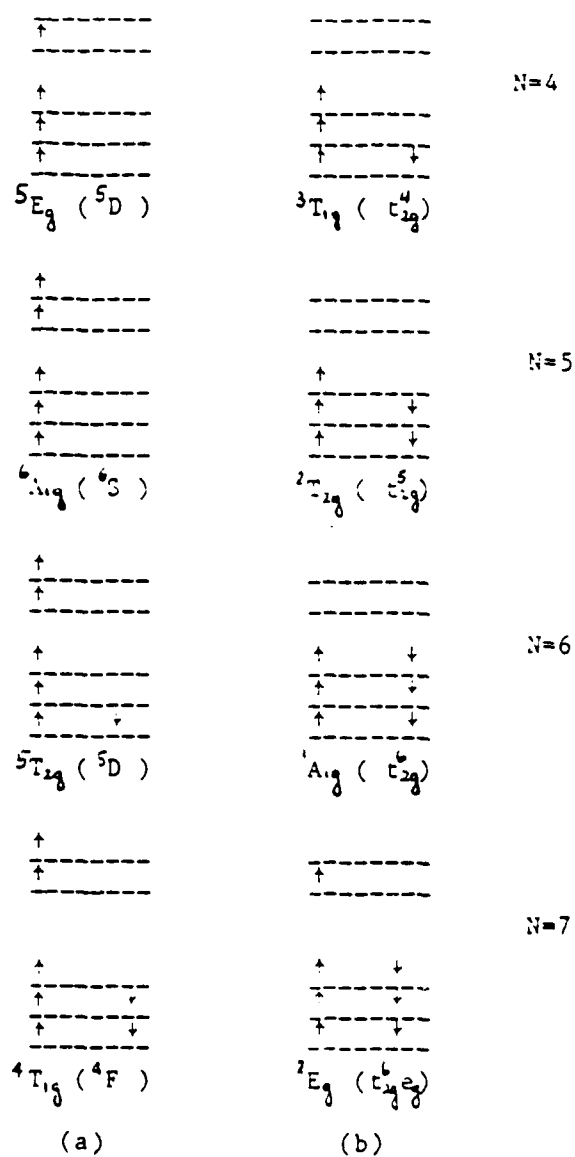


Figure 8

Ground State Spin Configuration: (a) high spin or weak field case,
(b) low spin or strong field case

II.C: MOSSBAUER EXPERIMENTAL

The elements intrinsic to the surface of the M-type IDC all have Mossbauer Isotopes; however, they all necessitate extremely low temperatures to record the Mossbauer effect. Therefore, in order to characterize the effects of temperature during activation of the M-type IDCs, it was decided to impurity dope these cathodes with Cobalt 57. The rationale behind this experimental procedure was that the deposition of the radioactive cobalt would be analogous to the transition metal sputter-coat used in the fabrication of M-type IDC's. The incorporation of this Mossbauer probe would then yield valuable information on the local electronic environment, as well as potentially giving information on the geometric structure and identity of the surface site group responsible for optimal thermionic emission. These data would be accumulated in a dynamic fashion. The ionic radii of cobalt, iron, osmium, iridium, and tungsten, given below in Table 5, indicate that it was indeed plausible to expect the Mossbauer probe impurity to occupy an osmium or tungsten site.

| ION | RADIUS |
|-------|--------|
| Fe 2+ | .81 |
| Co 2+ | .77 |
| W 4+ | .68 |
| Fe 3+ | .68 |
| Os 4+ | .67 |

Table 5
Ionic Radii of Cathode and Mossbauer Ions

The cathodes, a B-type and an M-type IDC, were obtained from Spectra-Mat, both with 5:3:2 molar ratio impregnants. They were impurity doped by the New England Nuclear Company according to the activation schedule of the cathodes, i.e., in vacuum at 1423K. Unfortunately this heat treatment caused tremendous outgassing in the New England Nuclear vacuum system, and resulted in a change of the doping procedure. As a result, the M-cathode was received without proper annealing, whereas the B-cathode was impurity doped and then annealed in hydrogen at 873K.

The spectra were recorded in the emission mode using an Austin Science Associates (ASA) Mossbauer spectrometer. It was recorded at room temperature and atmospheric conditions, and, at the suggestion of Dr. R. Collins of ASA, it was run at a velocity of ± 100 mm/sec in order to record possible unique absorptions. The initial count rate

was 50,000 counts/hour, and the spectrum was recorded for two hours. Since no lines appeared outside of ± 12 mm/sec, it was decided to limit the velocity range to not greater than ± 20 mm/sec; the computer data acquisition system of the spectrometer was then used to specify the velocity region of interest.

After the first spectrum was recorded, each cathode was placed in a vacuum oven and evacuated to a pressure of 10^{-8} Torr. The vacuum oven, also provided by ASA, was capable of temperatures to 1200K. For temperatures above this, another vacuum chamber was fabricated to utilize the potted heater in the cathode in order to complete the activation schedule. The second chamber had an optical port which allowed temperatures to be measured by means of a disappearing filament pyrometer.

The first set of spectra were recorded during the process of annealing the Mossbauer isotope. The temperature increments were initially chosen to be 323 K, however, it was difficult to stabilize the source at the prescribed temperatures. Therefore, the source was initially raised to the desired temperature, and then allowed to stabilize. This usually required 15-20 minutes. Another complication that arose during this first temperature cycling was the increase in pressure inside the vacuum oven. Whereas the vacuum oven had been previously baked out and outgassed, the procedure did not include the Mossbauer source. Therefore, the first set of spectra were recorded during the outgassing of the source. The cathode

source was raised to 873K and allowed to stabilize at this temperature, and was left there until the pressure stabilized (12 hours). The cathode was then allowed to cool to room temperature and a Mossbauer spectrum was taken. The initial spectrum was then recorded and the annealing procedure was monitored, from room temperature to 850K. Following this annealing, a total of 8 hours, the M-cathode was again allowed to cool to room temperature and another spectrum was recorded. This procedure was repeated until a reproducible Mossbauer spectrum was recorded at room temperature. This indicated that the Mossbauer source was annealed.

Once the annealing of the radioactive isotope was complete, the cathode was transferred to the second vacuum oven and pumped down overnight. This vacuum oven was used for this part of the research for two reasons:

- 1) the minimum detectable temperature of the optical pyrometer is 823K. If the cathode heater itself was used, there would have been the danger of overheating the source, thereby evaporating the deposited cobalt chloride.

- 2) as reported at the 1984 Tri-Service Cathode Workshop, barium is generated from the cathode at 1023K. Since there is interest in the bonding of this active element, it was decided to first anneal the source, and then to study a separate set of Mossbauer spectra at the onset of barium generation.

Utilizing the potted heater of the cathode, the temperature was

raised to 1023K (as determined by the optical pyrometer), the barium generation temperature. The next step was to reach cathode activation temperature, 1450K. Following the prescribed activation (four hours), the cathode was brought to 1253K, a temperature based on the operation of similar M-type IDC's on life test. After the spectrum was recorded, the cathode was allowed to cool freely to room temperature, 293K.

The B-cathode was analyzed in a manner very similar to that of the M-cathode, except no spectra were detectable at the activation temperature or the operating temperature.

All spectra were recorded against a single line stainless steel absorber, and the isomer shift of this absorber was included in the plotting routine of each spectrum.

II.D: DIFFERENTIAL THERMAL ANALYSIS

Differential thermal analysis (DTA), is a technique in which the temperature of a sample is compared with that of an inert reference material during the programmed change of temperature in a controlled atmosphere. The temperature of the sample and the reference should be the same until some thermal event, such as melting, decomposition, or change in the crystal structure, occurs in the sample in which case the sample temperature either lags behind (endothermic) or leads (exothermic) the reference temperature.

Sample sizes are usually small, a few milligrams, because then there is less trouble with thermal gradients within the sample which could lead to reduced sensitivity and accuracy. Heating and cooling rates must be empirically optimized because the change in temperature for a particular event decreases with a decrease in heating rate. DTA cells are usually designed for maximum sensitivity to thermal changes, but this is often at the expense of losing a calorimetric response; thus, peak areas or peak heights are only qualitatively related to the magnitude of the enthalpy changes occurring.

Uses of DTA in solid state science are many and varied. DTA detects such events as polymorphic transitions, thermal history changes on cooling and heating, glass transition temperatures, phase diagram determination, decomposition pathways, and kinetic studies. In addition, when DTA is employed to study mixtures and compound

preparations, the effects of mixing, ambient gas nature and flow rate, particle size, and dehydration time and temperature can be determined by comparing the DTA traces of the pure starting materials with those of the composites. Chemical reactions can be determined and monitored by comparing the mixture DTA trace with a superposition of the individual component traces. Also, reproducible preparation sequences can be determined by comparing temperature dependent chemical or physical changes indicated by the respective DTA traces.

II. E: TEMPERATURE CALIBRATION

In order to analyze thermionic cathodes with Mossbauer spectroscopy and DTA, it was necessary to duplicate, to some degree of accuracy, the temperatures reported in previous cathode studies. The accepted experimental procedure among cathode researchers employs either a disappearing filament pyrometer whose readings are corrected for the emissivity of tungsten, or a two-color ratio pyrometer which measures actual true temperature. It is not my purpose to argue this last point regarding true temperature. In fact, the measurement of the temperature of thermionic cathodes is relative to the emission current density. Under normal test conditions, the current density emitted by a cathode is recorded as a function of temperature (either brightness or true). At each temperature, the cathode heater power (voltage and current) is also recorded. It is this heater power that becomes the "yardstick" of cathode performance because in an actual thermionic device, there is no direct line-of-sight to the cathode; thus, optical pyrometry cannot be used, and conventional thermocouples would perturb the electron gun focusing fields. Therefore, when cathodes are evaluated as a function of lifetime, test temperatures are inferred from initial heater power values. This could, and probably does, present a problem, but some reference point must be chosen for both cathode performance and lifetime evaluation.

The Mossbauer spectrometer included a high temperature, 1150K, vacuum oven. The manufacturer, Austin Science Associates, assured temperature accuracy and stability within 20K. Since the vacuum oven was only to be used in the initial annealing of the cathode, temperatures below 900K, the temperature programmer and indicator of the spectrometer were found acceptable.

The differential thermal analyzer, a Perkin Elmer System 7/4 microprocessor controlled device, offered its own temperature calibration scheme. Representatives of the company, Mr. D. Sudlik and Mr. D. Johnson, installed the apparatus, and calibrated it manual using a gold standard. This temperature calibration trace is shown below in Figure 9.

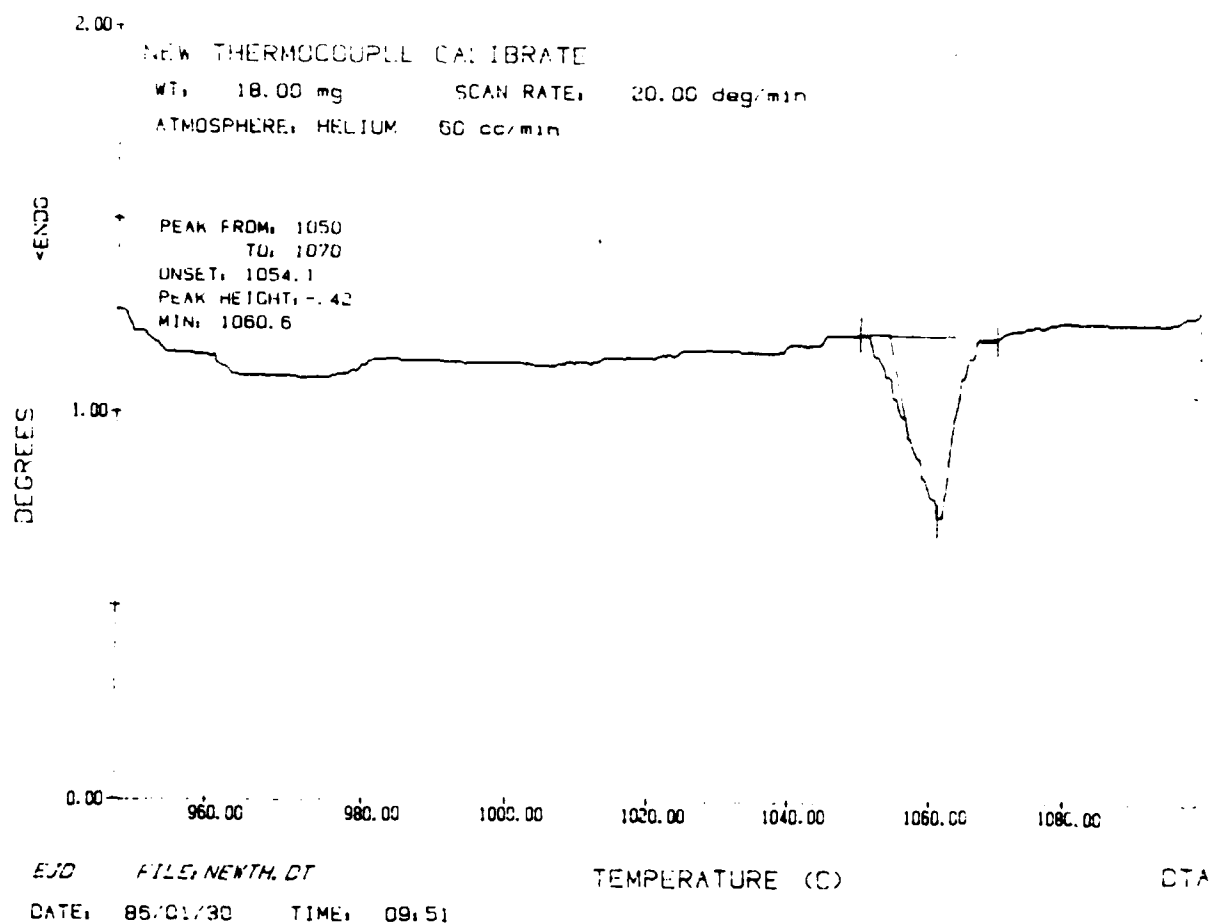


Figure 9

DTA Temperature Calibration Trace of Gold Sample;
heating rate of 20C/min, 60 cc/min helium atmosphere.

Thereafter, the DTA was calibrated on a regular basis
(weekly) or after replacement of the reference and sample

thermocouples. The calibration procedures duplicated the proposed experimental heating rates, ambient nature and flow rates. In general, the discrepancies obtained were less than 10K.

When Mossbauer and emission experiments required temperatures above 900K, an alternate vacuum chamber was fabricated, in order to take advantage of the potted heater configuration of the samples. This vacuum chamber was equipped with an optical viewing port so that optical pyrometry could be used (disappearing filament pyrometer). For temperatures below the pyrometer's minimum detectable temperature (1000K), the heater power values of similar cathodes on life test were extrapolated. The corresponding current and voltage values were then assigned to the heater, and allowed to stabilize. The heater power curve used in this temperature determination is shown in Figure 10.

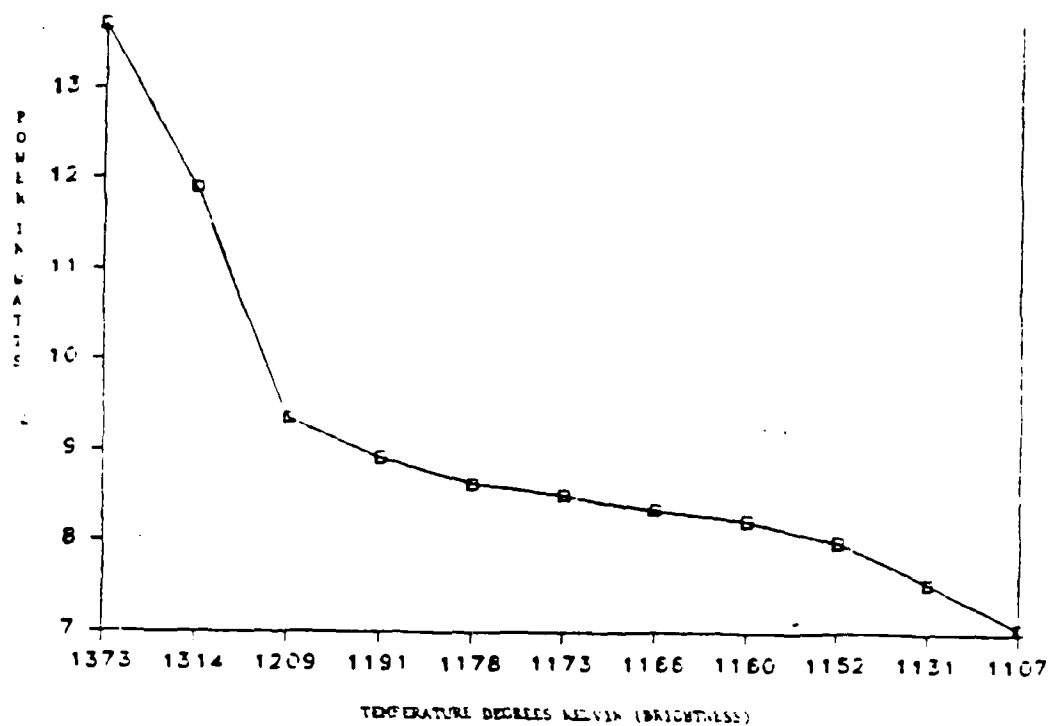


Figure 10
Cathode Heater Power Curve

II.F: CATHODE IMPREGNANT PREPARATION AND THERMOCHEMISTRY

The obvious starting point for a discussion of impregnant preparation and thermochemistry is to ascertain the choice of impregnant material. Private discussions with cathode researchers at the four Tri-Service Cathode Workshops have led to the following conclusions:

a) Since the IDC is a derivative of the L-cathode, it was a natural choice to keep the BaO. The L-cathode needed a large physical dimension for its reservoir, was difficult to machine to prescribed dimensions, and had a limited space to devote to its heater. As higher current densities were needed, the L-cathode had to be improved. Thus the IDC was born out of practical necessity. The BaO had to be "supported" within the porous tungsten plug and the "support" had to be compatible with the chemistry that resulted in the formation of free barium. Al_2O_3 was chosen as the "support" based on the binary phase diagram as well as the fact that it would not outgas significantly within the cathode vacuum environment (31).

b) BaO and CaO were found to be extremely hygroscopic. Shelf storage of the impregnant materials, the impregnant mixtures, and the finished cathodes was impractical due to the absorption of water vapor. Thus the carbonates were chosen. In addition, it was found that the carbonates of both barium and calcium were extremely

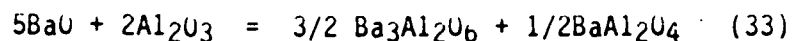
pure, much more so than the oxides.

These two observations led to the formulation of the Philips Emet procedure to synthesize impregnant compositions (32). Pure starting materials, barium and calcium carbonates, and aluminum oxide, are carefully weighed in the amounts required for the final composition. The starting materials are homogenized by ball milling of the dry ingredients, and a slurry is formed manually with distilled water, achieving the consistency of mud or heavy creme. The slurry is dried at low temperatures (400K) and then is calcined at high temperature (1600K) to form the barium calcium aluminate.

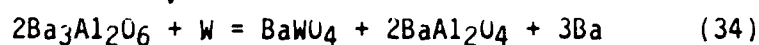
The porous tungsten plugs are then placed within the calcined impregnant mixture and together they are fired to 1875K in an atmosphere of dry hydrogen. The porous tungsten is thus impregnated with a chemical compound that, when properly activated, reacts with the interior pore walls of the tungsten to liberate free barium for subsequent adsorption on the cathode surface. The identity of the chemical compound within the tungsten matrix remains, to this very day, speculation.

It is believed that the free barium arises from a series of chemical reactions initiated by heating the impregnated tungsten matrix. In its original composition, cathode impregnants in the ratio of $5\text{BaO}:2\text{Al}_2\text{O}_3$ were chosen because this is the lowest melting point eutectic not containing free BaO (Brodie (33) showed that free BaO in the impregnant was undesirable from the standpoint of the

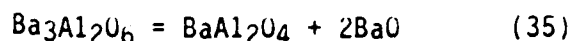
ratio of electron emission and Ba evaporation). According to the binary phase diagram, the equilibrium eutectic composition is



Due to its low reactivity with tungsten to form free barium, the monobarium aluminate is considered inert (34). The primary reaction responsible for generating free barium is



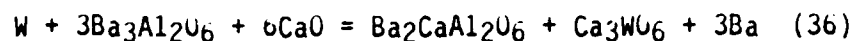
A further reaction that must be considered is



Rittner (35) has calculated the thermochemical equilibrium pressure for these last two reactions and predicted a ratio of the pressure of Ba/BaO = 5 at 1460K. The experimental value he obtained was 1.3, from which he concluded that a portion of the free barium was oxidized to BaO during transport to the surface.

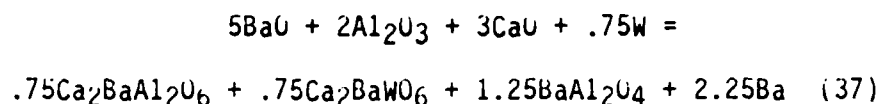
In 1953, Levi (36) introduced an improved version of the IDC, which was identical to the original except that 3 moles of CaO were added to the impregnant. Brodie and Jenkins (37) conducted a detailed study of barium evaporation from IDC's and they concluded

that the addition of the CaO did in fact reduce the evaporation rate of barium, and that the end products of the reaction of a Type B impregnant and the tungsten matrix were $\text{Ba}_3\text{Al}_2\text{O}_6$, BaWO_4 , and Ba_2CaWO_6 . In 1966, Zalm and von Stratum (38) proposed the following reaction:



This equation was later quoted by Forman (39) in 1977 in his paper in which he proposed his theory of monolayer barium coverage on the surface of IDC's.

In 1976, Rittner (40) had proposed a different chemical reaction to explain the production of barium from a Type B impregnant:



Although both Equations (36) and (37) are valid from a material point of view, neither had the advantage of the phase diagram of the barium-calcium-alumina system; hence only a speculation of the compounds which might take part in the reaction could be made.

During the past eight years, work has been initiated at

both Georgia Tech and The Aerospace Corporation, the aim of which is to characterize the $\text{BaO}:\text{CaO}:\text{Al}_2\text{O}_3$ ternary phase diagram. An extensive literature search has uncovered just a few references, but none of them are given at cathode operating temperatures. In fact, private discussion with both research groups indicate that even though strict stoichiometric ratios for the cathode impregnants were originally measured out, analysis of the impregnant mixture within cathodes after activation differed vastly from the initial values. These research efforts are of critical importance since knowledge of the reaction sequences and kinetics involved in the formation of compounds in the phase diagram will help determine the time and preparation methods necessary to achieve chemical equilibrium.

Before elaborating on this plausible research direction, the next section will describe my early efforts to "fingerprint" the traditional cathode impregnant fabrication and activation sequence by means of DTA.

II.G: DTA EXPERIMENTAL PROCEDURE

(FOR THIS PART OF THE EXPERIMENTAL PROCEDURE I MUST REVERT TO DEGREES CELSIUS)

Traditional impregnant materials, BaO, CaO, BaCO₃, CaCu₃, alpha and gamma alumina, and 8-12 micron tungsten powder (Aesar puratronic grade) were obtained. They were analyzed with a Perkin Elmer microprocessor controlled DTA, capable of room temperature (20C) to 1500C. A standard gas handling system was fabricated and equipped with molecular sieves, de-oxifiers, and Brooks mass flow controllers. A heating rate of 20C/min was chosen to optimize DTA sensitivity, and a gas flow rate of 60 cc/min (hydrogen and/or helium) was used to insure that the sample volume was flushed clean every minute. The alumina cylinder covering the reference and sample thermocouple has a volume of 57 cc, and to minimize the effects of re-adsorption it was determined that this flow rate was acceptable. The samples and reference materials (usually alumina supplied with the instrument) were placed in 6 cc alumina crucibles, specifically designed for the DTA. The instrument was calibrated using a gold standard.

Equal weights of reference and sample were then placed in the DTA, and since there was no isothermal software for this particular application, each initial experiment was divided into two

parts. First, an increase to 107C and this was maintained for 1 hour in helium atmosphere to complete dehydration; second, after this 1 hour hold, the temperature was raised to 1500C, i.e., the highest attainable temperature of the instrument, while maintaining the helium ambient.

Following the DTA characterization of each of the impregnant constituent, the heating rate, dehydration time, ambient flow rate, particle size, and, in the case of mixtures, the mixing time and procedure were varied. The final temperature for each of these experiments was determined by reference to the first set of DTA traces. In general, this temperature did not exceed 1200C.

The heating rate and dehydration time were varied by use of the software accompanying the DTA. For variations in the particle size, 40-mesh and 80-mesh screen were used. The impregnant constituents were either ground in a glass mortar and pestle or poured directly from their containers in a nitrogen filled glove box. They were then deposited upon the larger mesh screen which was situated directly above the smaller mesh screen, and each of the screens was gently agitated. This determined the range of particle size for the experiments. The mixing time and procedure represented a difficult problem because I could not find a "standard" for the consistency of heavy cream or mud. Therefore I chose the criteria that if the impregnant conglomerate "just stuck" to the stainless steel spatula, it was done.

At this point in time, even before the first DTA experiments were run, it became obvious that something very fundamental was lacking in the traditional cathode impregnant preparation sequences. Thus, the time-honored materials were replaced with barium nitrate, titanium oxide, ammonium metatungstate, and aqueous chloridic acid (.2M). A modified tungsten matrix was fabricated (acknowledgement to Dr. J. Dutta at Hanscom AFB) using the 8-12 micron tungsten powder, mixed with an equal volume of the ammonium metatungstate. Following ball milling for 1 hour, it was calcined at 300C until the cessation of ammonia vapor. The dry mixture was then isostatically pressed at 16,000 psi in an argon atmosphere of 60 psi, and sintered at 1800C for 1 hour. At this point, SEM photographs were taken. I received the sample matrix, and R. Agarwal conducted BET area measurements of nitrogen physisorption at liquid nitrogen temperature. Three discs were cut from the original sample, each approximately 0.61 cm in diameter and 1 cm thick. From the remainder, the incipient wetness factor of this modified matrix was then determined, and the first disc was wet-impregnated with a solution of barium nitrate, 136gms/liter. A portion of this impregnated sample was chipped away and Dr. R. Benner of the University of Utah performed Raman spectroscopy on it along with a reference sample of BaO, alpha alumina, and a fabricated 5:3:2 impregnant mixture. Each of the steps prior to the Raman spectroscopy were subject to the identical DTA procedures of the

traditional impregnants as described above.

The second disc, heated to 300C, was placed in a saturated solution of titanium oxide, 100gms/liter, for 24 hours in an atmosphere of helium. It was dried at 120C in a 60 cc/min helium flow for 12 hours, and then impregnated with barium nitrate in accordance with the first sample. Again, representative DTA traces were taken at each fabrication step.

The third disc was immersed in a .2M solution of chloroiridic acid for 24 hours, dried for 12 hours at 120C in the 60 cc/min helium flow, and then wet impregnated with the barium nitrate solution at 300C. DTA traces were taken during each sequence of preparation.

Whereas there exists a multitude of thermionic emission data pertaining to conventionally produced impregnated cathodes, the three prototype cathodes did not have such a data base. Therefore they had to be subjected to actual thermionic emission procedures. The next sections will briefly describe the standard emission tests as well as the experimental procedure employed in testing these novice cathodes.

II.H: THERMIONIC EMISSION DIAGNOSTICS

Since my research is directed at the noted discrepancy between experimental emission data and its fit to the Richardson equation, I chose to conduct zero-field emission experiments. Referring to equation (2), a plot of $\ln(I/T^2)$ versus $(1/T)$ should be a straight line. The work function would be the slope of the line and "A", the universal constant, could be determined by inserting the slope value back into the original equation. I had to assume however, that the work function was temperature independent.

The three prototype samples prepared according to the details of the last section, were pressed into molybdenum sleeves, 3 cm long, so that only the front surface was exposed; the sleeves were mechanically fastened to a four-pin vacuum feedthrough. Two pins were connected to a cathode heater assembly and the finished test cathode assembly was placed around it (Figure 11). The total assembly was then placed in a four inch four-way stainless steel cross, the other three flanges consisted of an optical viewing port, a stainless steel anode (7.62 cm in diameter), and a Varian 15 l/sec vac-ion pump. The important temperatures and time for activation were ascertained by reference to the DTA traces, and the temperatures were determined by extrapolating the heater power curve.

Once the sample was in the test chamber, it was allowed two (2) days to outgas; the final pressure recorded, in all cases, was less than 10^{-8} Torr. Each cathode was heated slowly, i.e., .2 volts per time increment, to avoid the effects of any "cold" heater surge current. Once the current value stabilized, the Lambda regulated current power supply was adjusted to a judgemental fit of the heater power curve reference. This was a calibrated power supply, USAF PMEL, with a full scale reading of 10 volts and rated at 3 amps. Therefore the discrepancy was only in the parallelax factor of reading the meter. The pressure remained relatively constant, less than 10^{-7} Torr, throughout the process.

Heater power measurements were taken using Simpson volt and amp meters. These were not calibrated, only zeroed. A Simpson milliammeter was connected in the test circuit, analogous to the Edison effect circuit of Figure 1 without the battery. The circuit was completed by connecting the milliammeter to the mechanical support of the cathode structure (Figure 12). Each experimental cathode was first subjected to heat treatments as indicated by the DTA traces, and then raised from 550C (823K) to 650C (923K), in increments of 50C (323K). The cathode was allowed to stabilize at each temperature for 15 minutes before the current reading was recorded.

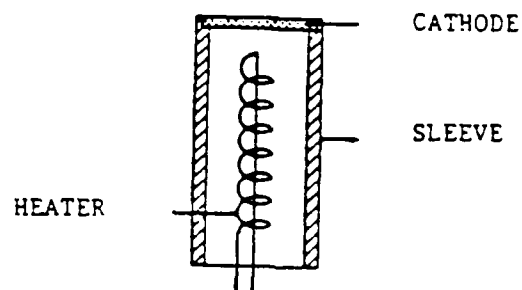


Figure 11
 Prototype cathode assembly

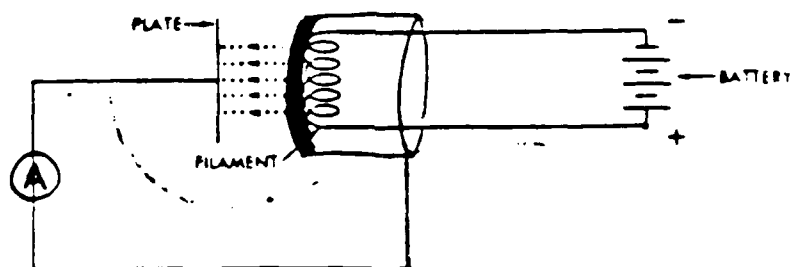


Figure 12
 Thermionic emission circuit for testing prototype cathodes

III.A: MOSSBAUER RESULTS

The first reported Mossbauer spectra of the "as received" Mossbauer sources are shown in Figures 13 and 14. Note the lack of any precise definition in each of the spectra. This is frequently the case in Mossbauer emission spectroscopy.

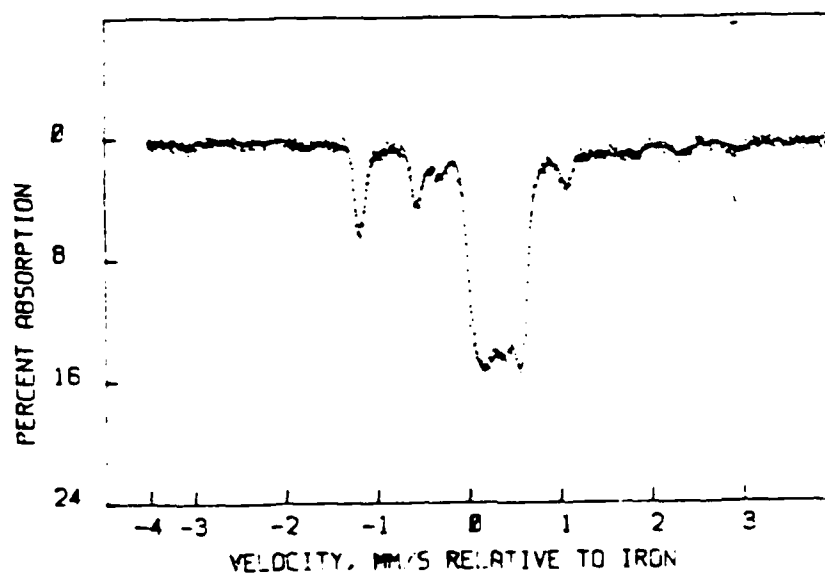


Figure 13

B cathode Mossbauer Source as received,
room temperature and atmospheric pressure

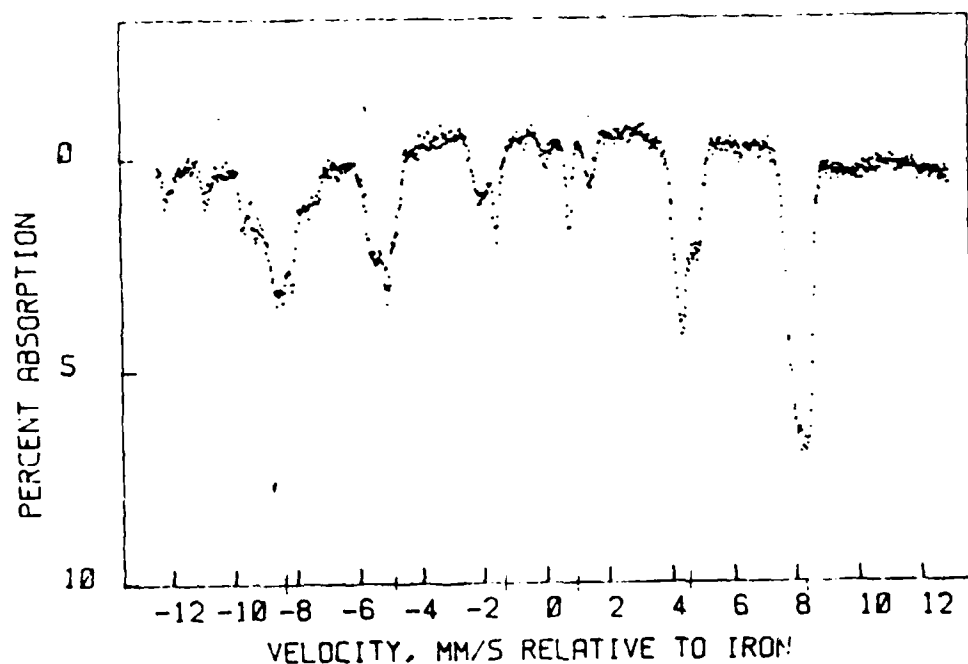


Figure 14

M cathode Mossbauer Source as received;
room temperature, atmospheric pressure

The Mossbauer spectrum after outgassing the cathode is shown in Figure 15. Note the difference between this spectrum and Figure 14; this clearly illustrates the effects of exposing this cathode to atmospheric conditions.

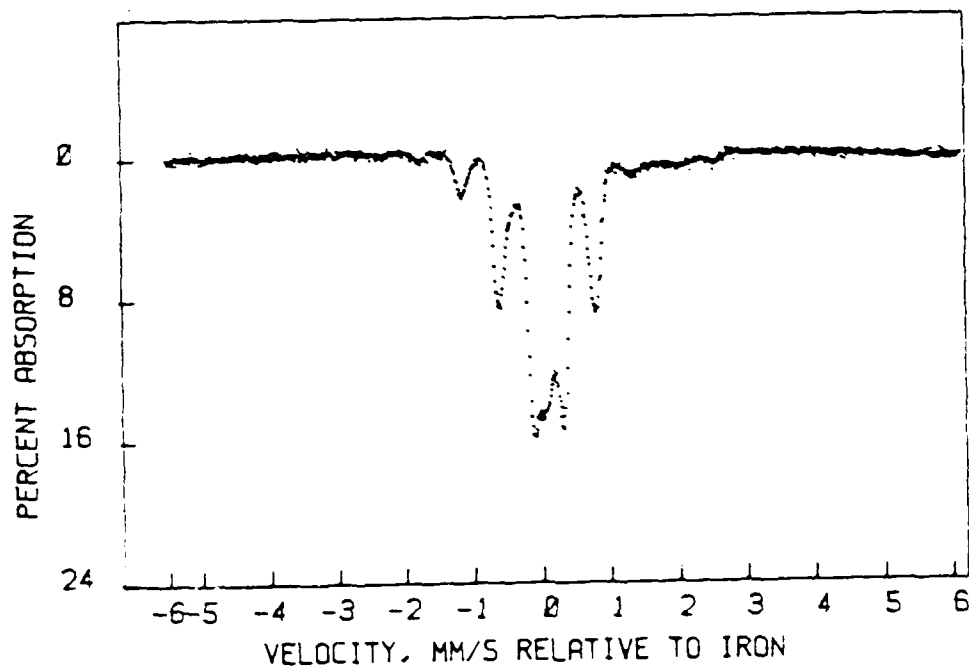


Figure 15

M cathode Mossbauer source after outgassing.

room temperature, 10^{-8} Torr

The annealing procedure is depicted in Figures 16-19. When viewing these figures, special attention should be paid to the disappearance of the Fe 2+ quadrupole doublet of Figure 15 (located at -1 mm/sec and +1 mm/sec) and the appearance of the Fe 3+ doublet at 0 mm/sec and +.5 mm/sec.

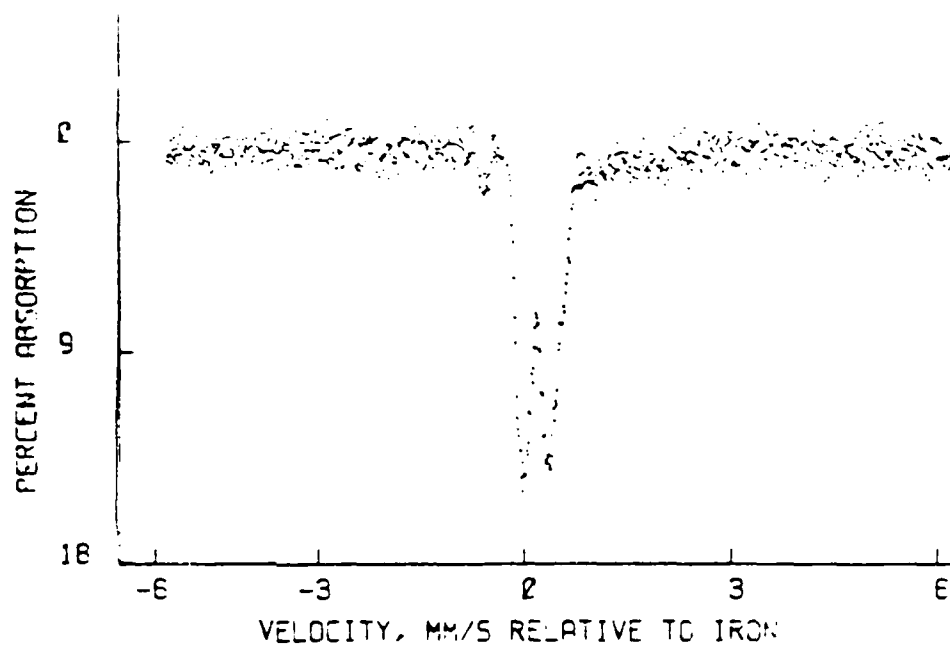


Figure 16

M-cathode Mossbauer source at 533K, 10^{-6} Torr

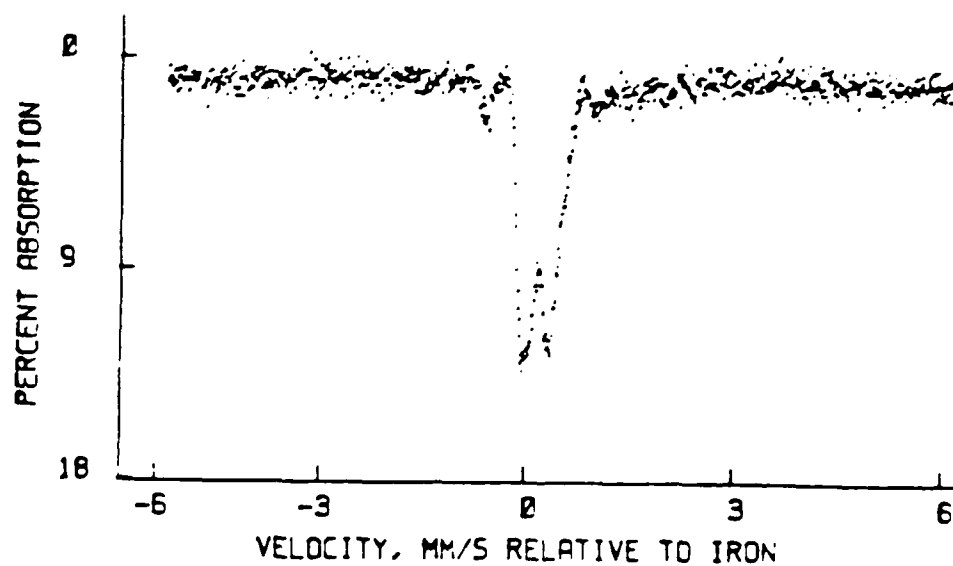


Figure 17

M-cathode Mossbauer source at 633K, 3×10^{-5} Torr

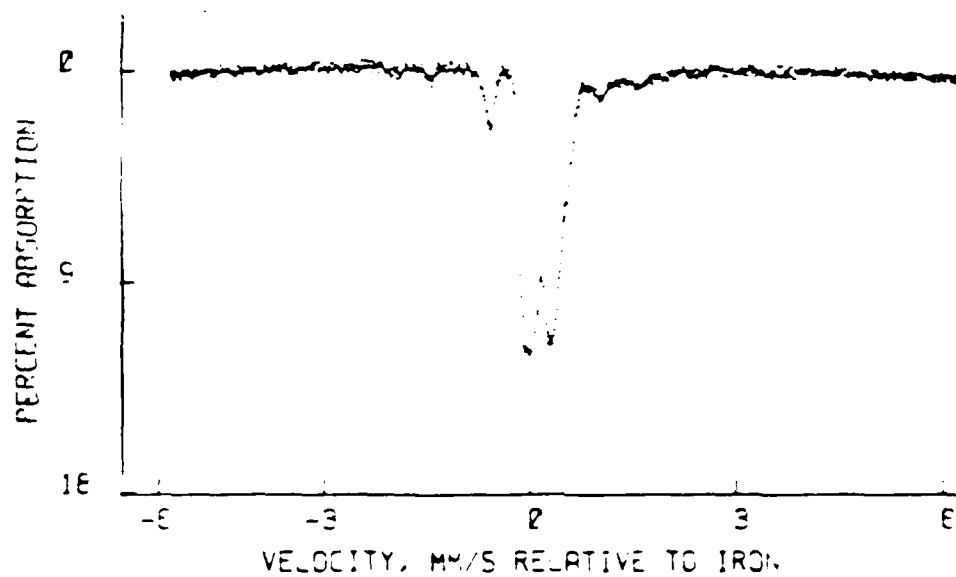


Figure 18

M-cathode Mossbauer source at 693K, 1×10^{-5} Torr

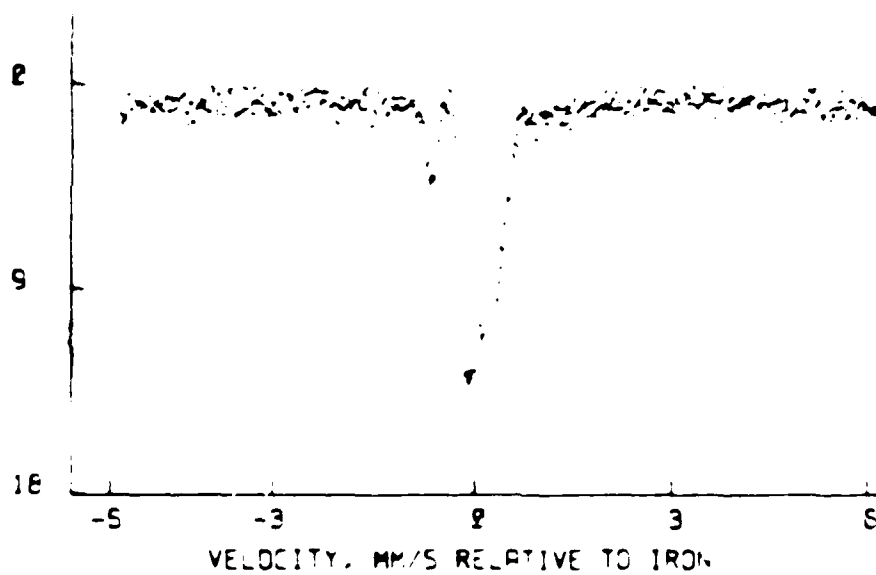


Figure 19

M-cathode Mossbauer source at 833K, 5×10^{-4} Torr

Figure 20 is the Mossbauer spectrum of the M-cathode following the annealing cycle.

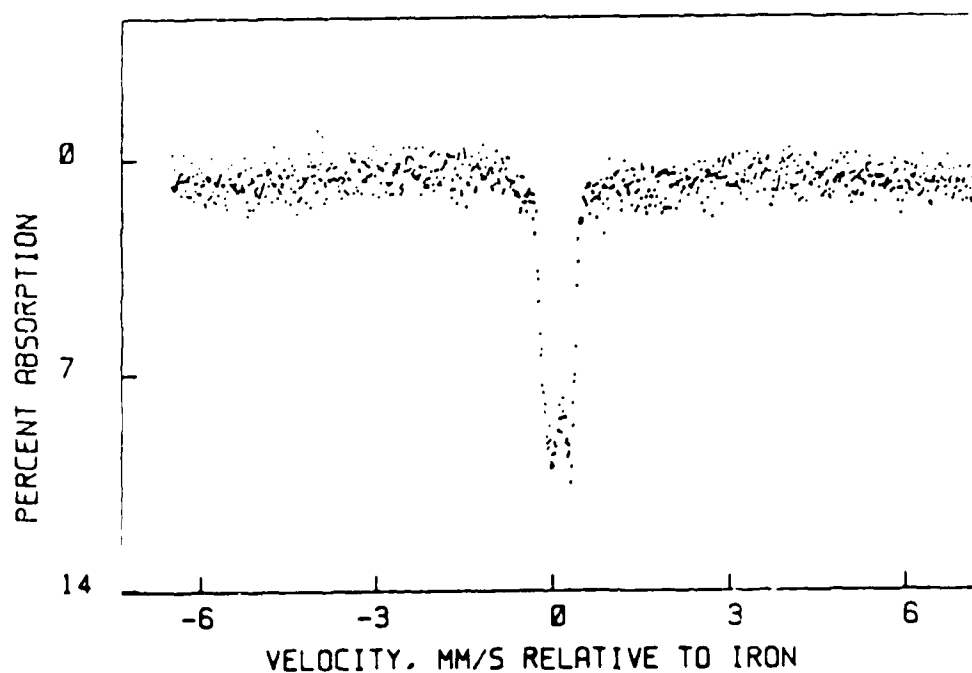


Figure 20

M-cathode Mossbauer source after annealing cycle;
room temperature, 10^{-8} Torr

The Mossbauer spectrum recorded to determine the annealing is shown in Figure 21, in good agreement with Figure 20. Thus it was concluded that the source was now annealed and outgassed, and it was transferred to the second vacuum oven for activation.

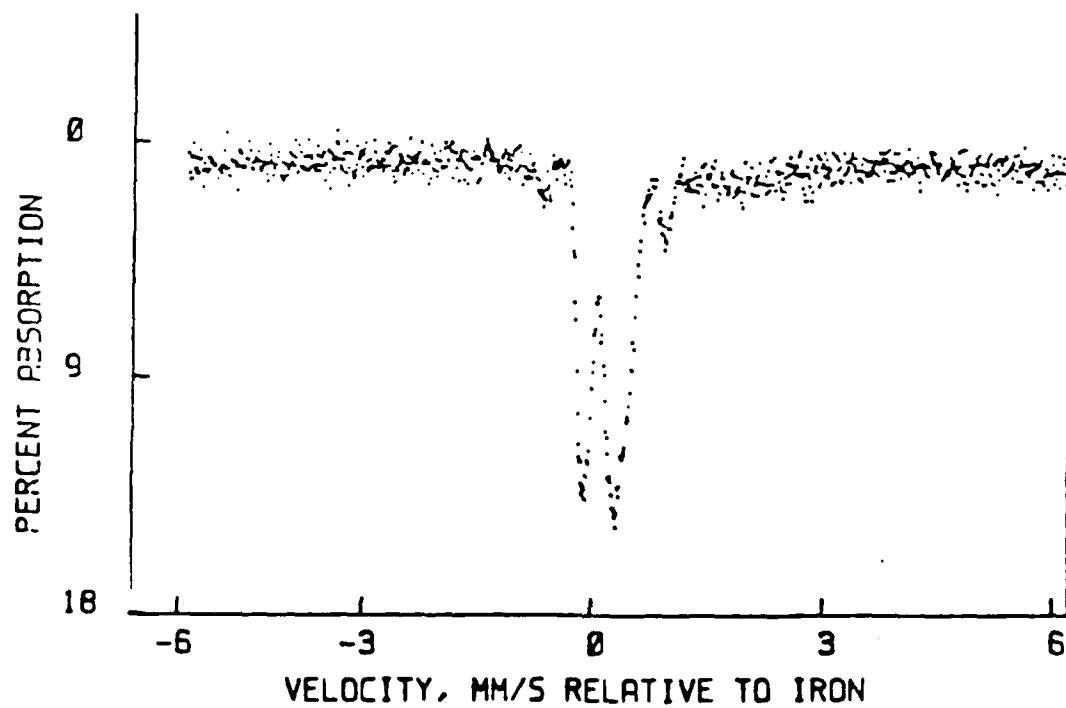


Figure 21

M-cathode Mossbauer source before activation;
room temperature, 10^{-8} Torr

At 1023K, the pressure increased drastically, and the resultant spectrum, Figure 22, reflects the dynamics occurring at the barium generation temperature.

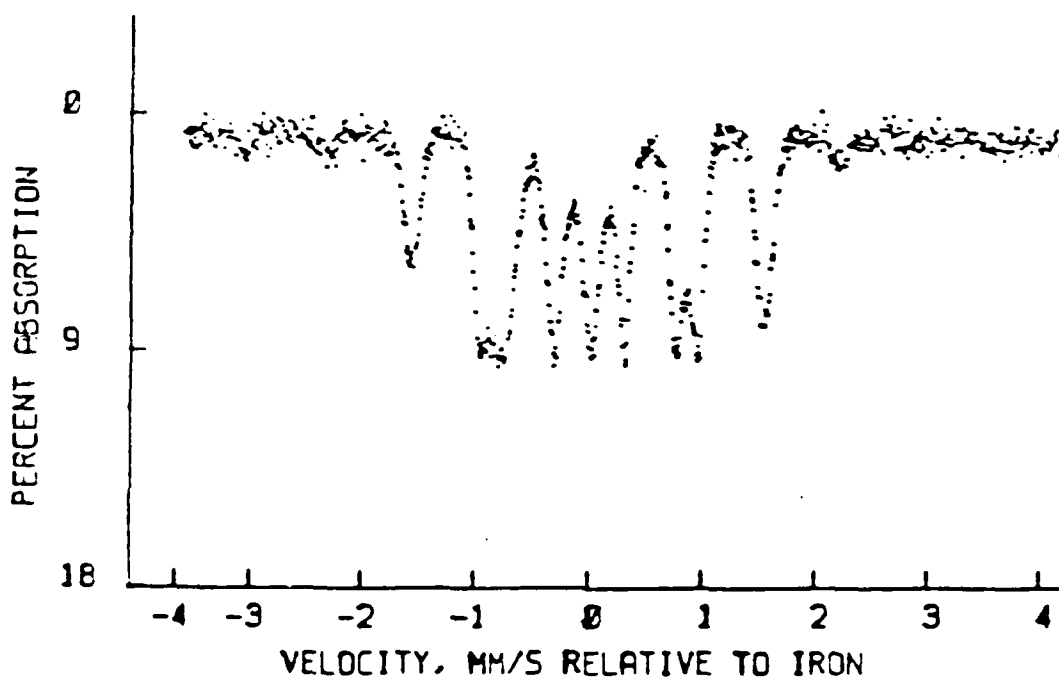


Figure 22

Mossbauer spectrum at barium generation temperature;

1023K, 3×10^{-3} Torr

Figure 23 is the recorded Mossbauer spectrum of the cathode source at cathode activation temperature (1500K). Note the relative simplicity of this spectrum when compared with Figure 22.

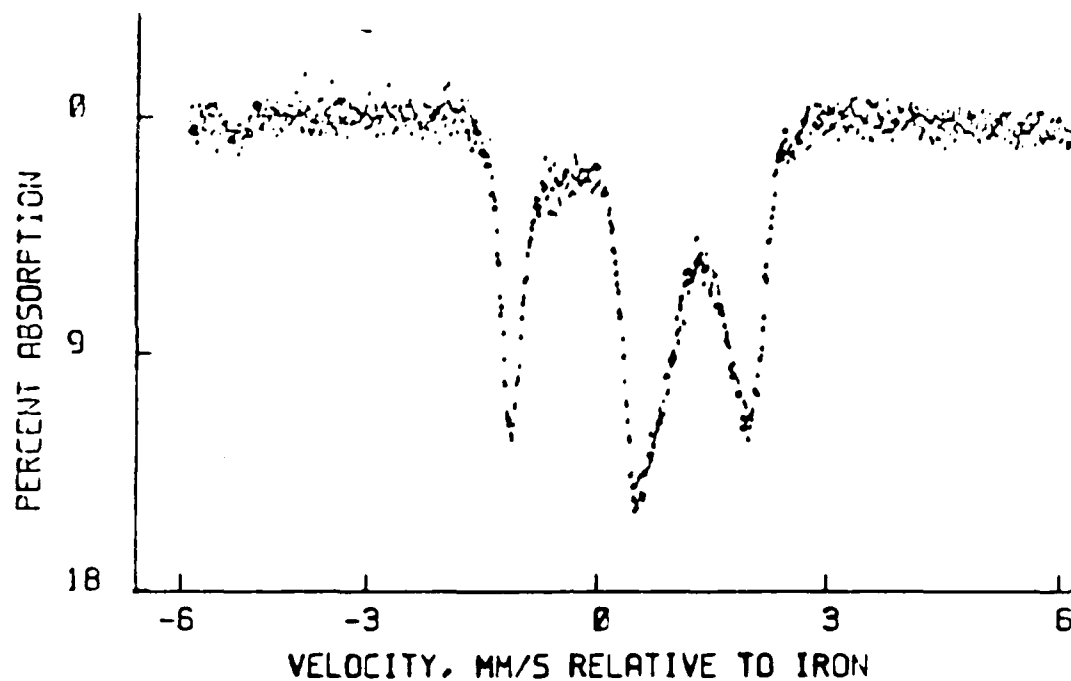


Figure 23

Mossbauer spectrum at cathode activation temperature;

1423K for four (4) hours

initial pressure 2×10^{-2} Torr, final pressure 10^{-6} Torr

Following activation (four hours), the cathode was brought to 1253K, a temperature based on the operation of similar M-type IDC's on life test. Figure 24 is the resultant spectrum, and it bears a close resemblance to Figure 22 except for the outer two absorption dips at -1.5 mm/sec and +1.5 mm/sec.

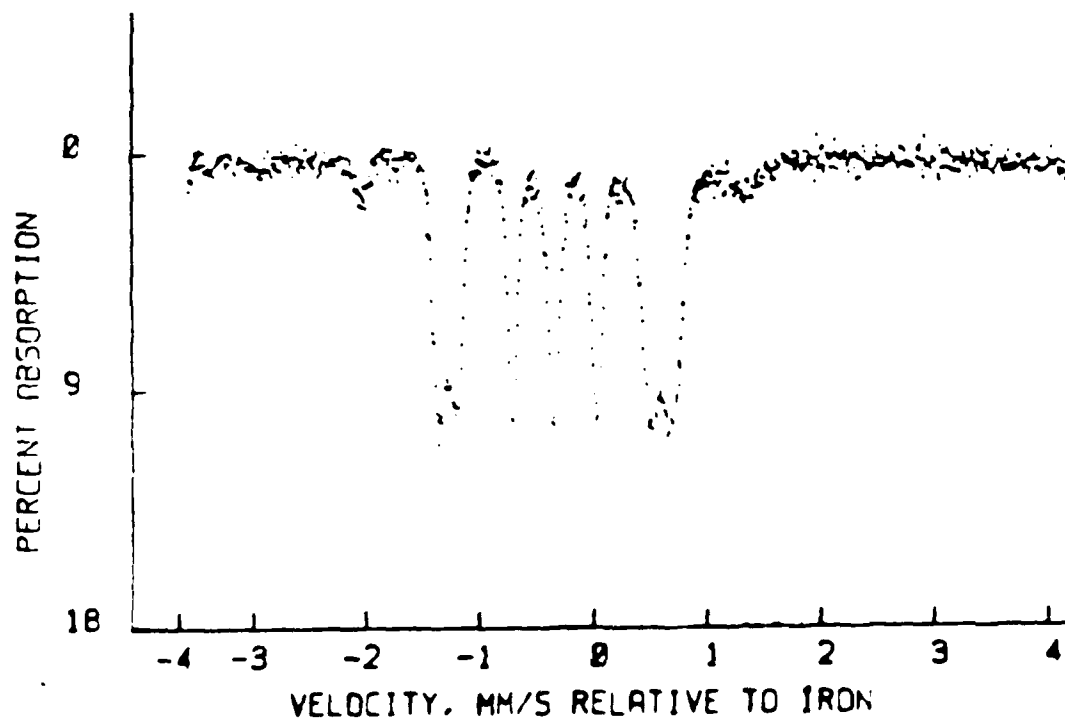


Figure 24

Mössbauer source at 1253K, cathode operating temperature;
 3×10^{-5} Torr

Figure 25 is the spectrum of an activated M-type IDC that was first operated at 1253K for eight hours. Note the good agreement with the initial annealed Mössbauer source spectrum, Figure 21.

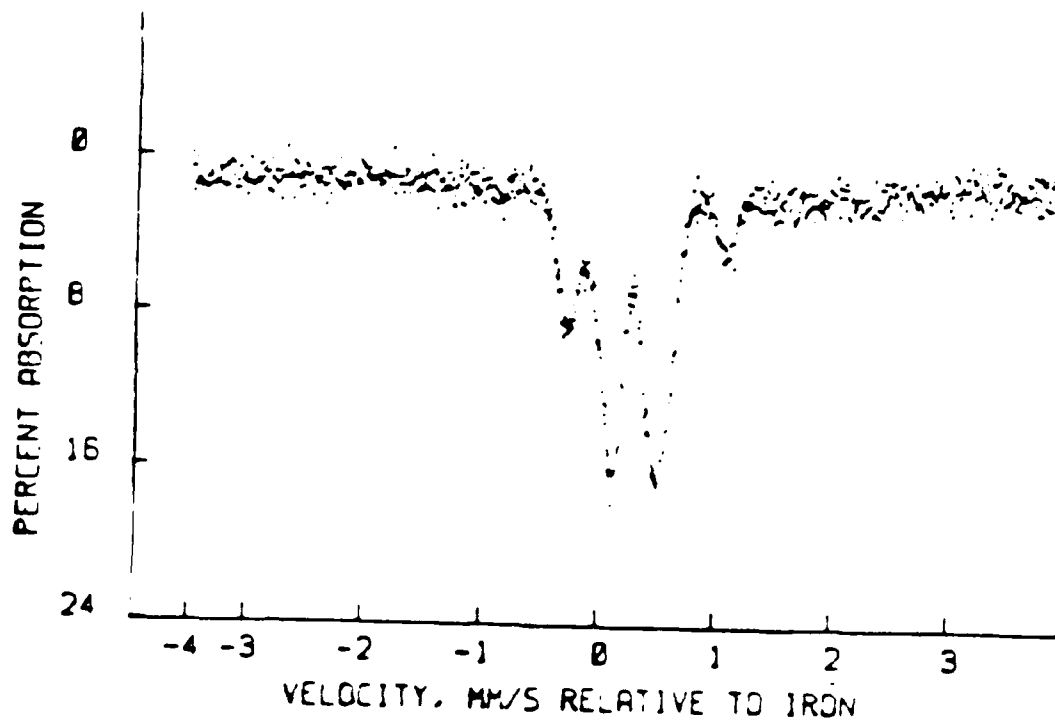


Figure 25

Mossbauer spectrum after activation and operation;
room temperature, pressure 10^{-8} Torr

In direct contrast to the spectra obtained from the M-cathode, Figure 26 shows the Mossbauer spectrum after outgassing the B-cathode source for 12 hours.

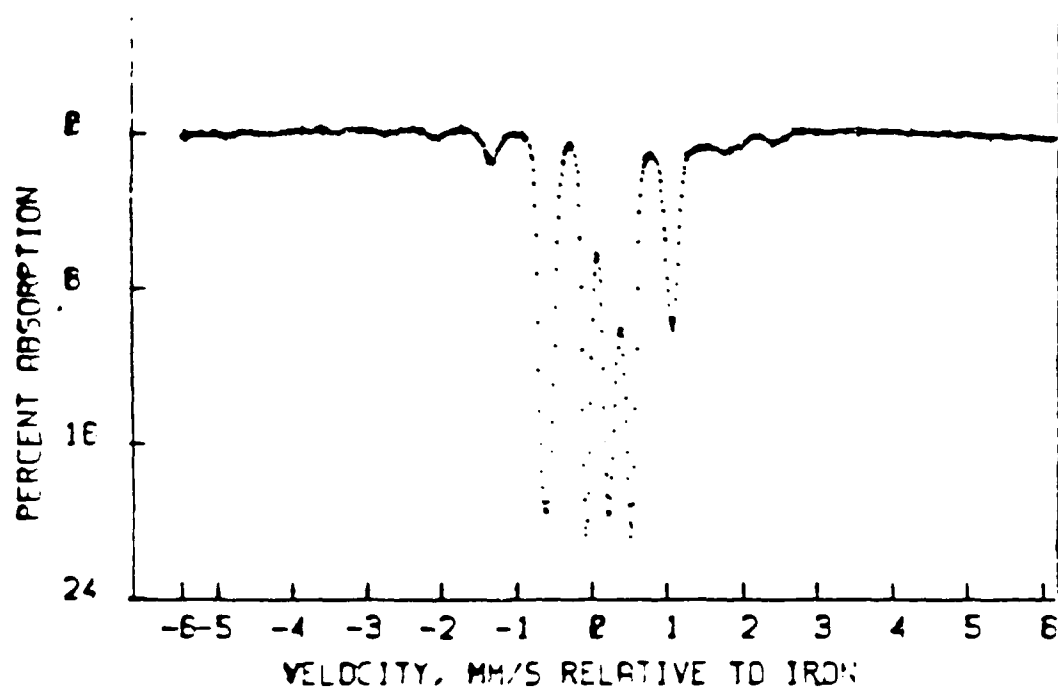


Figure 26

B-cathode Mossbauer source after initial outgassing
room temperature, pressure 10^{-8} Torr

The important feature of this spectrum is the resolution of the central absorption dip shown previously in Figure 13. Figure 27 is the Mossbauer spectrum of the B-cathode source after it was heated to 873K and allowed to cool to room temperature (293K).

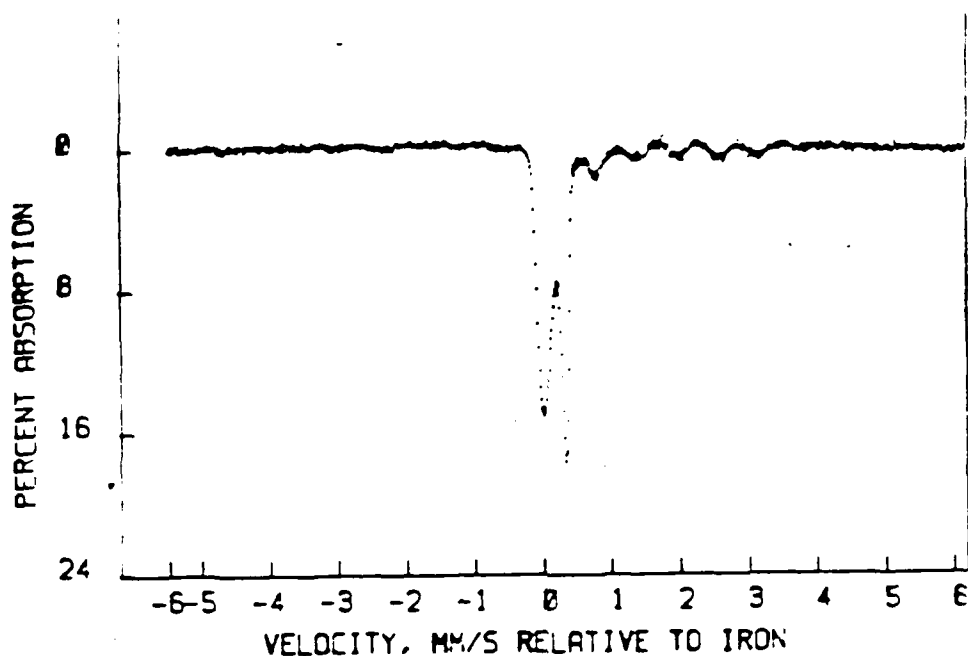


Figure 27

B-cathode Mossbauer source after outgassing
from 873K to room temperature, 10^{-8} Torr

The spectra appears to exhibit an anisotropic Fe $3+$ low-spin quadrupole doublet. Following this outgassing, the B-cathode was subjected to a similar annealing process as the M-cathode. Figures 28-31 depict this; attention should be paid to the definition of the maximum absorption dip (centered around zero velocity).

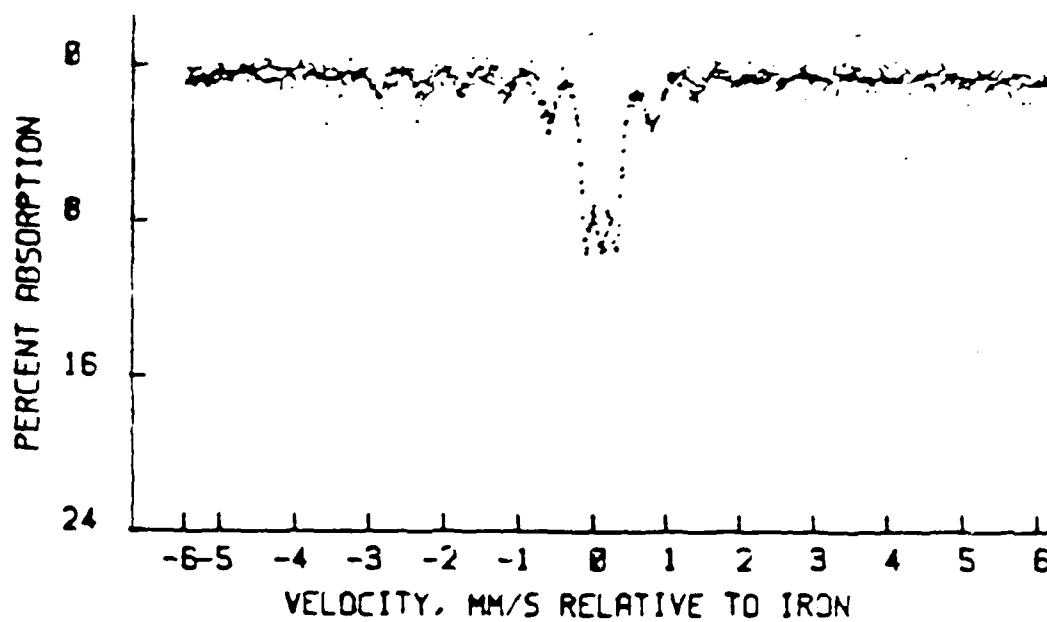


Figure 28

B-cathode Mossbauer source at 623K

pressure 5×10^{-5} Torr

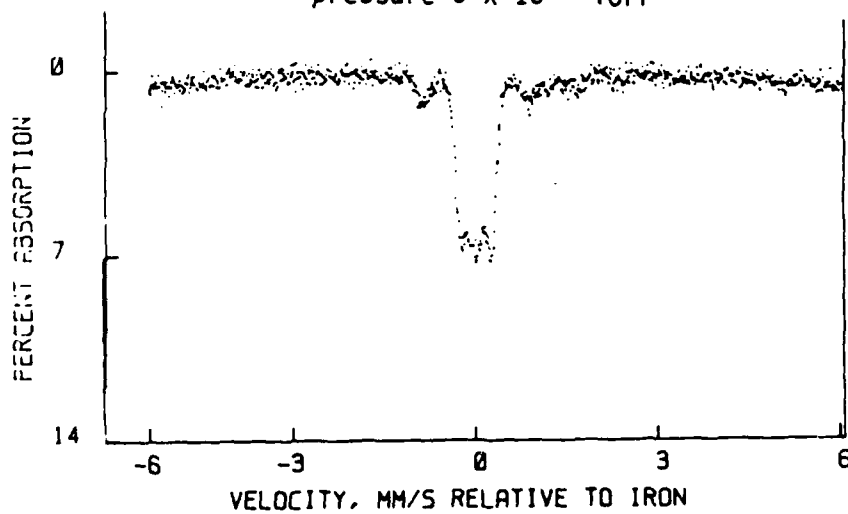


Figure 29

B-cathode Mossbauer source at 673K

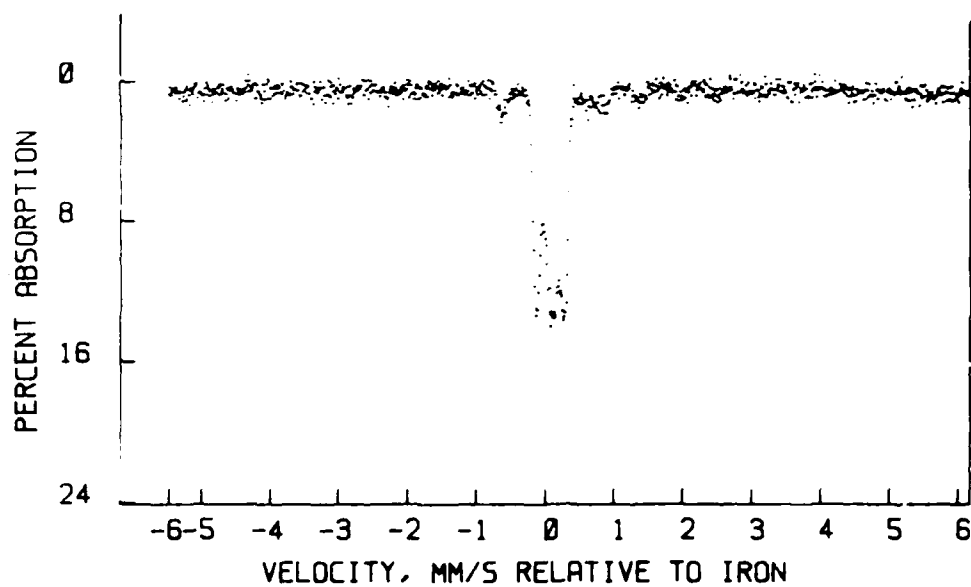


Figure 30

B-cathode Mossbauer source at 763K

pressure 3×10^{-4} Torr

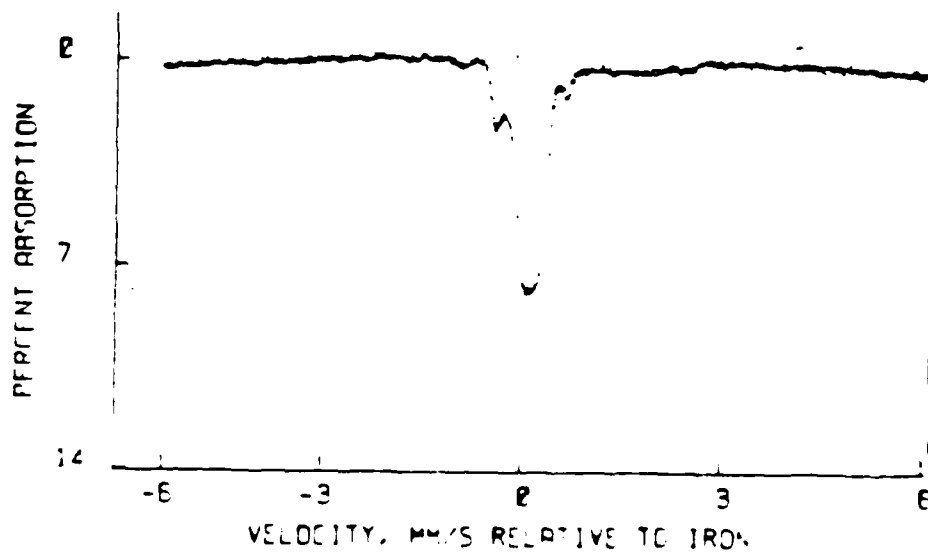


Figure 31

B-cathode Mossbauer source at 873K

pressure 8×10^{-3} Torr.



Figure 32

B-cathode Mossbauer source pre-activation;
room temperature, pressure 10^{-8} Torr

Figure 33 is the Mossbauer Spectrum at the barium generation temperature, and again reflects the dynamics of barium generation. This spectrum is similar in general shape to that of the M-cathode (Figure 22), but notice the increased isomer shift and the asymmetry of the two out dips at -1.5 mm/sec and +4 mm/sec.

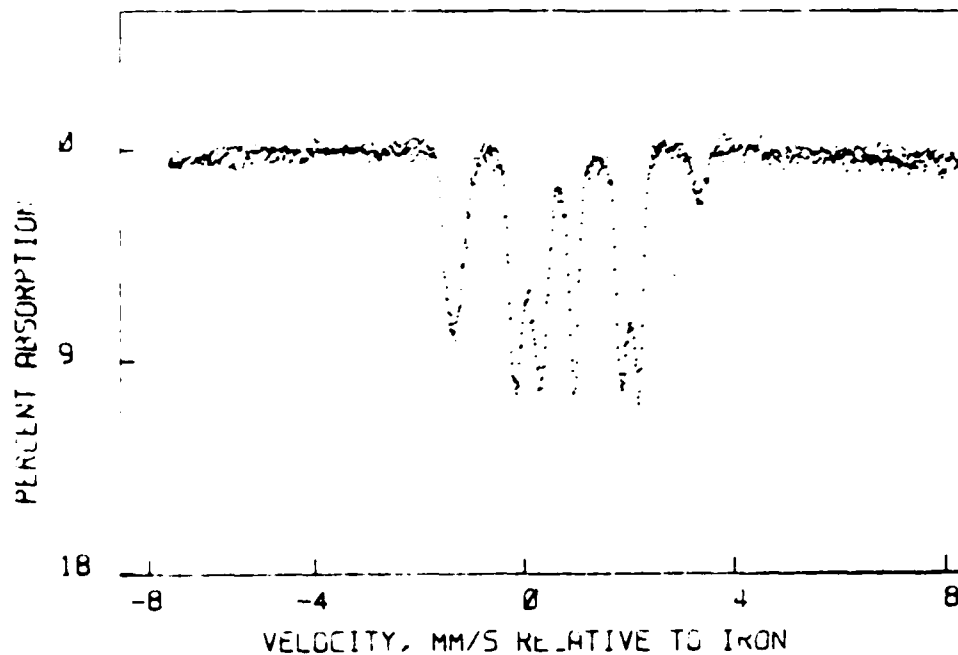


Figure 33

B-cathode Mossbauer source at barium generation temperature
1023K, pressure 10^{-3} Torr

No spectrum could be recorded at the cathode activation temperature. The same was true at the cathode operating temperature, in this case 1333K.

The cathode source was again allowed to cool to room temperature, 293K, and based on the original single line spectrum, it was decided to run a Mossbauer spectrum with a standard iron-enriched foil in order to determine if the single line spectrum was in fact a broadened quadrupole doublet. Figure 34 represents

AD-A191 498

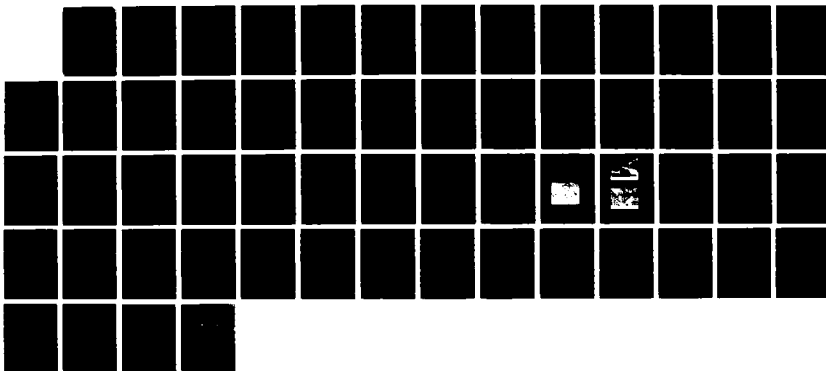
A SCIENTIFIC BASIS FOR AN ALTERNATE CATHODE
ARCHITECTURE(U) ROME AIR DEVELOPMENT CENTER GRIFFISS
AFB NY E J DANISZEWSKI FEB 88 RADC-TR-88-33

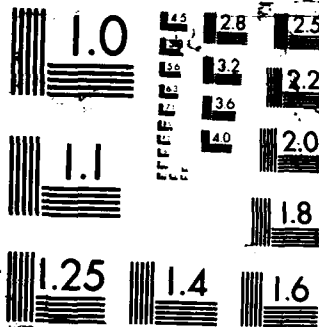
2/2

UNCLASSIFIED

F/G 7/4

NL





outgassed, annealed, activated, and operated B-cathode Mossbauer source versus a six-line standard iron foil absorber.

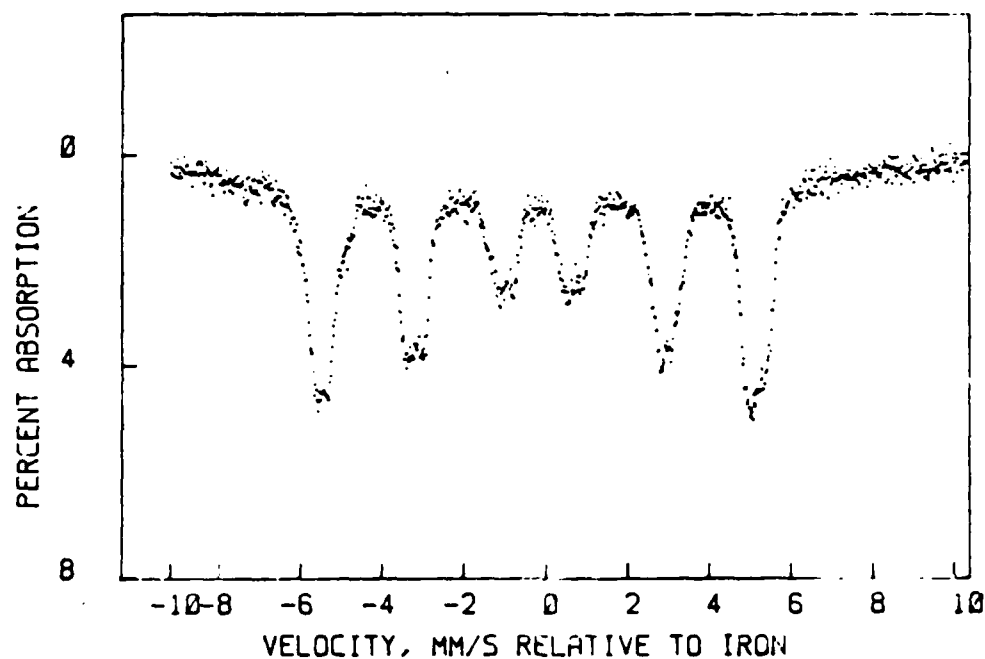


Figure 34

B-cathode source after activation and operation vs iron 57 foil absorber;
room temperature, pressure 10^{-8} Torr

III.B: DISCUSSION OF MOSSBAUER RESULTS

One of the goals of my research was to show the efficacy of employing the Mossbauer effect (ME) to investigate the electronic and steric properties of IDC's. The recorded data clearly distinguishes these characteristics, indicating the influence of crystalline electric fields on the nuclear energy levels of the Mossbauer probe isotopes. Whereas the ME is usually associated with bulk properties, the surface features can be distinguished from the bulk contributions by analyzing the respective intensities of the adsorption minima (41). For this reason, attention was paid primarily to those absorption dips accounting for more than 25% of the total intensity.

The interpretation of the temperature dependent spectra is complicated due to the sensitivity of the Mossbauer nucleus to the surrounding perturbations, especially those arising from hyperfine magnetic fields. These interactions are due to core electron polarization as well as distributions of hyperfine fields due to the presence of nonmagnetic atoms and local compositional and chemical disorder. In addition, the different contributions to the electric field gradient (EFG) and the influence of the amorphous nature of the host matrix must also be considered. However, the 3d electrons of iron serve as an excellent probe of the environment due to the 3d splitting caused by any deviation from cubic symmetry, as well as the

change in the 3d radial component due to covalency. For this reason, attention must be focused on the quadrupole-isomer shift correlation in the recorded Mossbauer Spectra. Figure 35 depicts the isomer shift-quadrupole correlation for iron compounds.

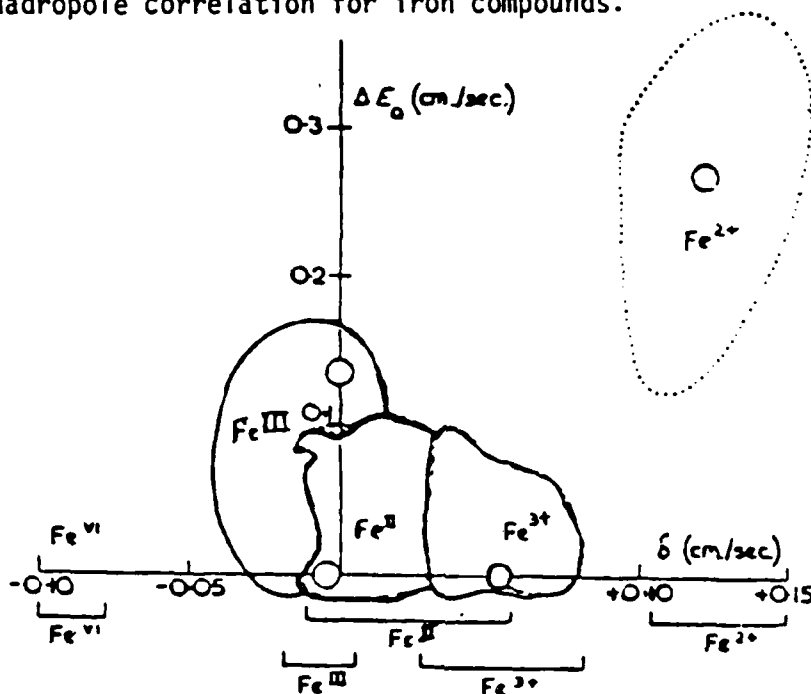


Figure 35

Isomer Shift and Quadrupole Correlation for Iron Compounds

In order to obtain the magnitude of the quadrupole splitting and the isomer shift, as well as the sign of the isomer shift, a record of the gamma ray counts as a function of velocity is needed. The computer based data acquisition system of my spectrometer then searched for the respective minima, and assigned a velocity and absorption value. Using the ASA curve-fitting routine,

these values were printed out, and employing the techniques described previously, Figures 6-6, the isomer shift and the quadrupole splitting could be numerically obtained. These values were then interpreted by reference to Figure 35 in order to identify the oxidation state and spin nature of the Mossbauer atom.

In the following discussions, Roman numerals, e.g., Fe III, refer to low spin states, whereas Arabic numerals, e.g., Fe 3+, refer to high spin states.

Upon comparison of Figures 25 and 34, an obvious distinction can be seen between the M-type IDC and the B-type IDC. Referring to these two spectra respectively, the initial complicated spectra resolve into a well defined Fe III quadrupole doublet for the M-cathode source and a singlet Fe 2+. Remember that these spectra were taken in the emission mode so that the sense of the velocity must be reversed for comparison with standard absorption spectra.

Once the oxidation state and spin nature were identified, the Mossbauer parameters for each source spectrum were cross-referenced against existing data with the constraint that the structure must belong to one of the ten surface molecule or symmetry groups. This latter condition is necessary if the surface monolayer is to have the proper dipole polarity advantageous for thermionic emission. The results revealed that the B-cathode source was indicative of Co 57 in pure tungsten (42), while the M-cathode source data coincided very favorably with previous work, e.g., barium

titanate (43). The identification of this structure would prove to be very serendipitous.

Reviewing these results of the Mossbauer experiments, specifically those on the M-cathode source, it seemed logical to investigate those compounds that duplicated the low-spin state spectra. This naturally led to the assumption that such a surface site group could possibly be optimal for thermionic emission, and, if this configuration could be identified, the next logical step would be the actual fabrication of a thermionic cathode with this preferred structure existing at the very beginning of life.

In light of these Mossbauer results, a low-spin state ion on the M-cathode surface and a high-spin state ion on the B-cathode surface, existing experimental results and theories may now be interpreted to formulate a new theory of optimum thermionic emission.

In order to establish the background necessary for the appreciation of the Mossbauer results, I must first present the existing theory of the electronic structure of the cathode emissive surface responsible for the operation of the IDC.

Figure 3b illustrates the relative dimensions that are important to the operation of the typical IDC.

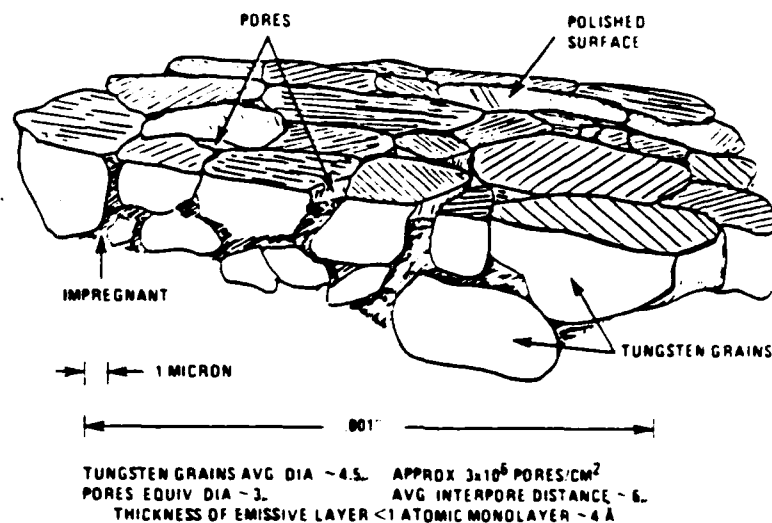


Figure 36

Scale of Cathode Features

The porous, sintered, impregnated tungsten matrix has an overall depth of .254 cm, while the emissive layer is less than one monolayer. This latter statement was once the source of much disagreement among cathode researchers. Models presented by Rittner, Rutledge and Ahlert (44) provide evidence for a barium monolayer with the presence of oxygen inferred to account for the low evaporation rate of barium (as referenced to the earlier work by Langmuir). Springer and Haas (45) and Forman (46) employed Auger spectroscopy on both model surfaces and actual cathode surfaces and their conclusions supported an emitting surface consisting of a monolayer or less of

barium over oxygen upon tungsten. Druzhinin (47) published evidence for the formation of barium oxide crystallites as the active sites, and Beck and Ahmed (48) reported evidence for the presence of thick oxide layers on cathode surfaces. Zhang (49) invalidates the classical dipole theory, stating that the high-energy electrons of the barium atoms and the low potential field exerted by the doubly charged oxygen ion are the two important factors for providing a low work function. The controversy regarding the specific nature of the emissive layer remained so until the 1980 Tri-Service Cathode Workshop. Papers presented by a majority of the cathode researchers were in support of the partial monolayer model. These particular investigations included the M-type IDC and its derivatives, but the results are easily transitioned to the B-type; in summary, the results were:

a) the emissive layer of the cathode types consist of a barium-oxygen monolayer vertically oriented with barium over oxygen

b) the barium-oxygen stoichiometry is so close to 1:1 in the stabilized cathode surface as to suggest that each barium atom is bonded with one oxygen atom

c) the oxidation state of barium is not that of the free metal, but it is intermediate between this state and that barium in the bulk BaO

d) the chemical environment of oxygen is different from that of oxygen in the bulk oxide of the impregnant

e) the substrate metal of the matrix or the sputtercoat is not oxidized. During the activation process, any oxide previously present is reduced and the activated surface is metallic. There are indications that electron density has been transferred to the metal

f) the emission enhancement exhibited by the M-type and its derivatives relative to the B-type results from increased barium-oxygen coverage arising from some difference in the bonding between the emissive layer and the 4-d or 5-d transition metal sputtercoat.

These principles are represented in Figure 37.

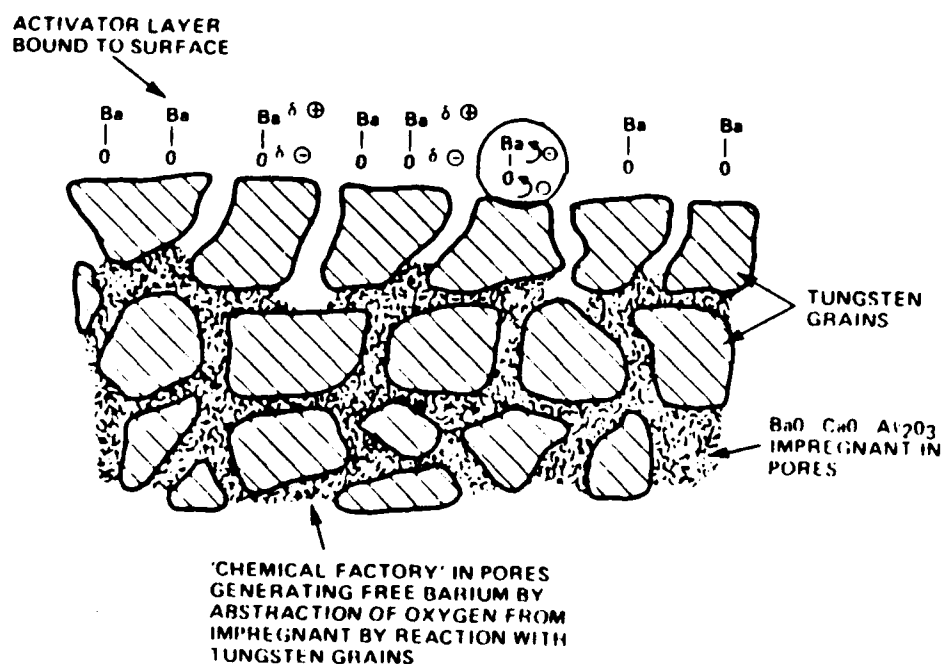


Figure 37

Schematic Representation of IDC Operating Principles

The transition to the M-type IDC can be facilitated with reference to Figure 38 which depicts the influence of select 5-d transition metal sputtercoats on the electron emission of otherwise B-type IDC's.

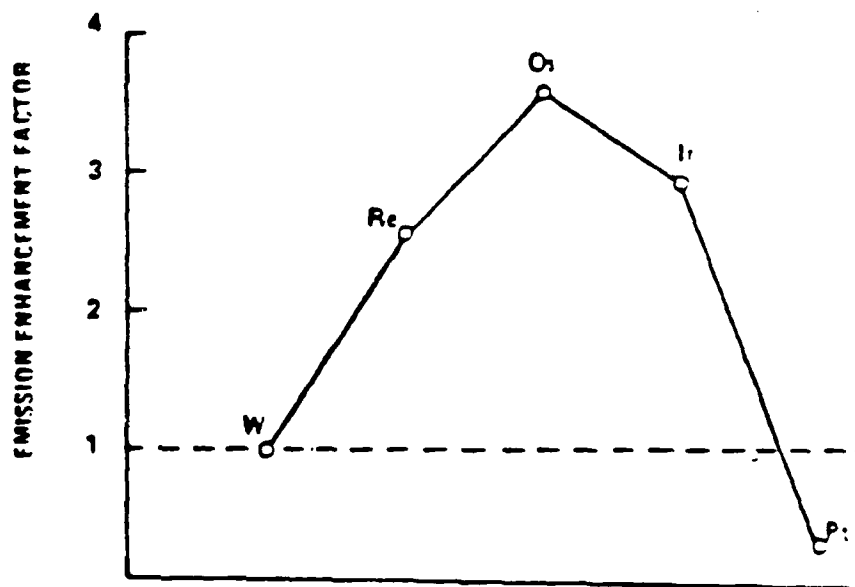


Figure 38
Transition Metal Influence on Thermionic Emission

Early efforts to explain this influence were based on the experimental fact that the larger the clean surface substrate work

function, the lower the attainable minimum work function for Group I and II adsorbates on transition metal substrates (50). This is certainly a plausible explanation for the emission enhancement of the M-type IDC, but upon inspection of Figures 38 and 39, the emission degrading behavior of platinum cannot be explained by this argument.

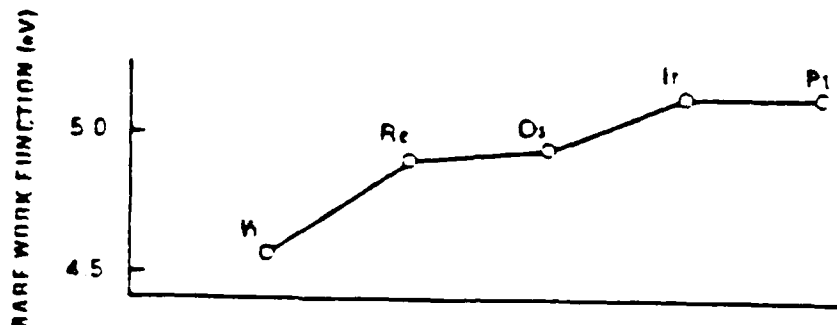


Figure 39

5-d Transition Metal Work Functions

Assuming that the Mossbauer results identify the enhanced thermionic emission surface configuration, the elements in Figure 39 can be investigated from the principles of group theory as described in section II.8.

Recalling the experimental evidence that the substrate metal of the matrix or the sputtercoat is not oxidized, it is logical to assume that the Hund's rule configurations presented in Table 1 (p.38) are valid representations of the cathode emissive surface metal atoms. However, upon inspection of these configurations it is

evident that none of the so called "enhancers" exhibit the optimal low-spin state in their free atom configurations. The obvious question now arises; what is the origin of the d-orbital low-spin state configuration?

Recalling the major points of section II.B, the d-orbitals of the transition metals are the outer-most orbitals and are thus strongly influenced by their crystalline environment. In a crystal, the effective potential at an atomic site has the symmetry of the crystal structure rather than the spherical symmetry appropriate to free atoms in space. The atomic orbital representation given by Hund's Rule may thus be violated because the eigenvalues and eigenfunctions of the electron must now belong to the irreducible representations of the symmetry group of the Hamiltonian of the system in which the electron finds itself. These configurations were presented in Figure 8.

Since the important enhancing elements used in the M-type IDC have d-4, d-5, d-6, and d-7 configurations, it seems reasonable to conclude that the emission enhancement found in these cathodes can be explained by the strong CFT hypothesis.

At this point, it is interesting to note that Green (51) has also postulated a theory to explain the emission enhancement of M-type IDC's. Arguing from advances in the field of catalysis, he divides the transition metals into three classes, as depicted in Figure 40.

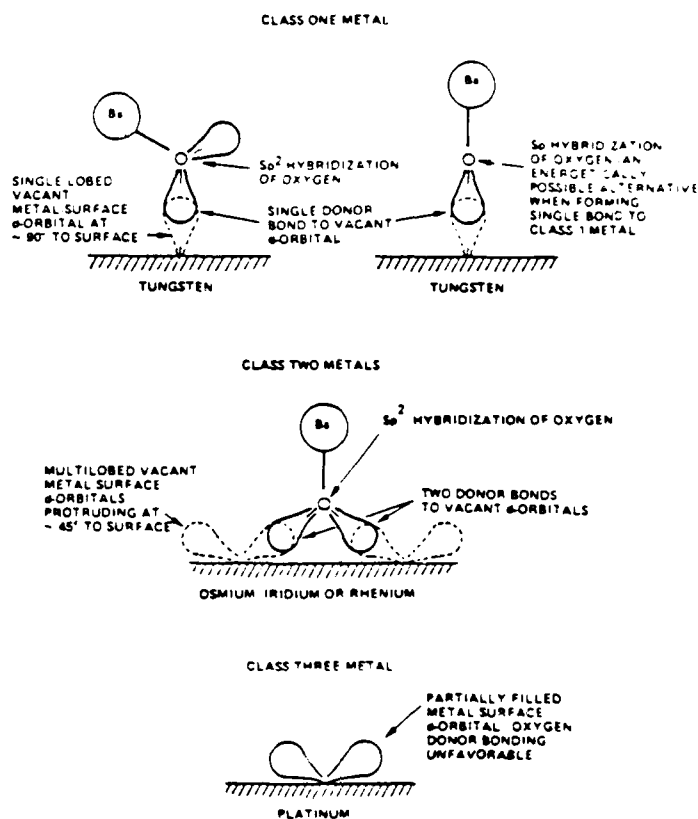


Figure 40

Surface classification of Transition Metals

As postulated by Green, the oxygen orbitals not involved in bonding to barium and available for bonding to the surface d-orbitals are the sp^2 hybrids; these orbitals are filled and thus require vacant surface orbitals into which they can donate their electron pair to form oxygen donor bonds. However, the references used by Green to formulate his theory present an extremely vague basis for the surface classification (52). Therefore I present the following theory.

Mossbauer results clearly show that the M-cathode has the empty surface orbitals necessary for stable monolayer bonding; these result from the formation of a surface site group possessing symmetry that removes the degeneracy of the transition metal d-orbitals and energetically favors a low-spin state configuration. This low-spin state means that there are empty d-orbitals available for the Ba-O ligand to bond to. The low symmetry of the alloy at the M-cathode surface provides the precursor for the optimal emissive center, as shown by the activated M-cathode spectrum, but this alloy formation on the M-type surface requires time. At the 1984 Tri-Service Cathode Workshop, Falce (53) reported on the effects of aging on the diffusion of the M cathode sputter coated with 5000 Angstroms of 80/20 Os/Ru. (The Ru is added by some manufacturers to suppress the formation of OsO_4 , as well as to make the emissive layer easier to machine.) The results of his study showed that W diffuses to the surface of M cathodes virtually from the beginning of life. Either the sintering of the cathode during fabrication or initial activation is sufficient to bring between 25% and 35% W to the surface. He also showed that an alloy forms within the region of the original coating thickness that is quite stable. The composition of the alloy changes very slowly at 1273K, having 60% W after 50,000 hours. Private discussions with Falce revealed however, that his SEM data were taken with no particular intention to reveal the alloy phase structure.

This alloying results in the creation of a sigma phase W/Os, possessing tetragonal symmetry. The Mossbauer results of the M-cathode source clearly indicate this low symmetry before the arrival of the barium, whereas the results of the B-cathode source indicate cubic symmetry, i.e., no strong crystal field to remove the degeneracy of the d-orbitals. The subsequent Ba-O monolayer on either cathode surface must result in the formation of the most stable surface configuration subject to the constraint of the cathode operating temperature. The B-cathode surface cannot offer completely empty d-orbitals for this structure, whereas the M-cathode does, due to the strong crystal field. This in turn, creates a more stable monolayer, in agreement with previous studies conducted on the M-cathode. This theory is also self-consistent in that it can explain the emission degradation of Pt; even in the strong field case, Pt must spin pair its d-orbitals to accommodate all 9 or 10 electrons (depending on which ground state electron configuration is chosen).

The CD eliminates the initial time required for the alloy formation, and suggests that precursor optimal emissive sites can be established during the fabrication sequence. Reviewing these results of the Mossbauer experiments, it seemed logical to investigate those compounds that duplicated the low-spin state spectra. This naturally led to the assumption that such a surface site group could possibly be optimal for thermionic emission, and, if this configuration could

be identified, the next logical step would be the actual fabrication of a thermionic cathode with this preferred structure at the very beginning of life.

Since the surface configuration that establishes the template for barium adsorption has been identified by Mossbauer spectroscopy, i.e. a barium titanate type structure, the next step is the investigation of the impregnant thermochemistry in order to facilitate the arrival and dispersal of this active element.

IV.A: DTA RESULTS

Figures 41-44 are the DTA traces of the starting materials for the Philip's-Emet impregnant fabrication sequence. The first trace represents a 5:3:2 molar ratio of the barium-calcium carbonates and alpha alumina. The subsequent Figures are representative of the pure starting materials subjected to the identical experimental procedures, in order to determine possible chemical reactions.

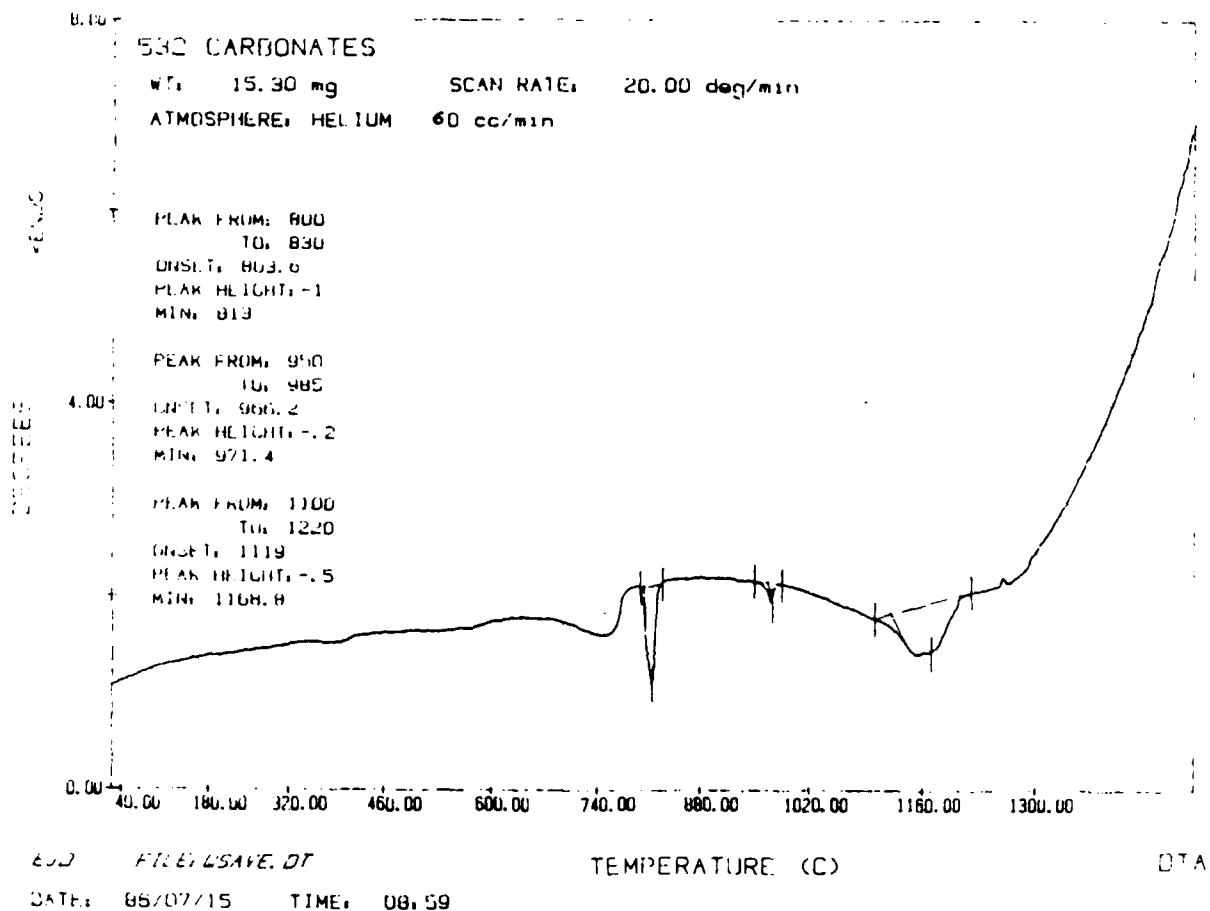


Figure 41

DTA trace of 5:3:2 carbonate mixture taken at a heating rate of 20 degC/min in a 60 cc/min helium atmosphere.

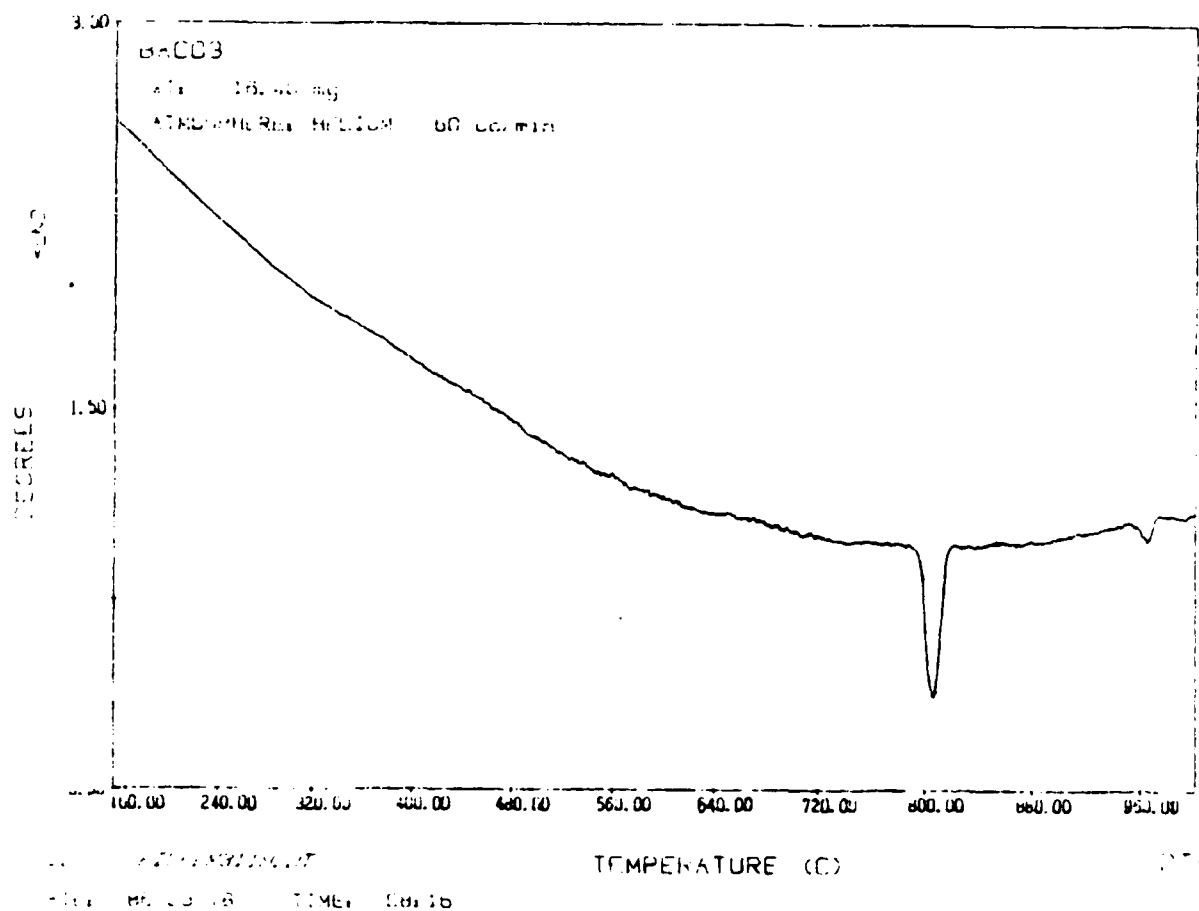


Figure 4z

DTA trace of puratronic grade barium carbonate taken at a heating rate of 20C/min in a 60 cc/min atmosphere of helium.

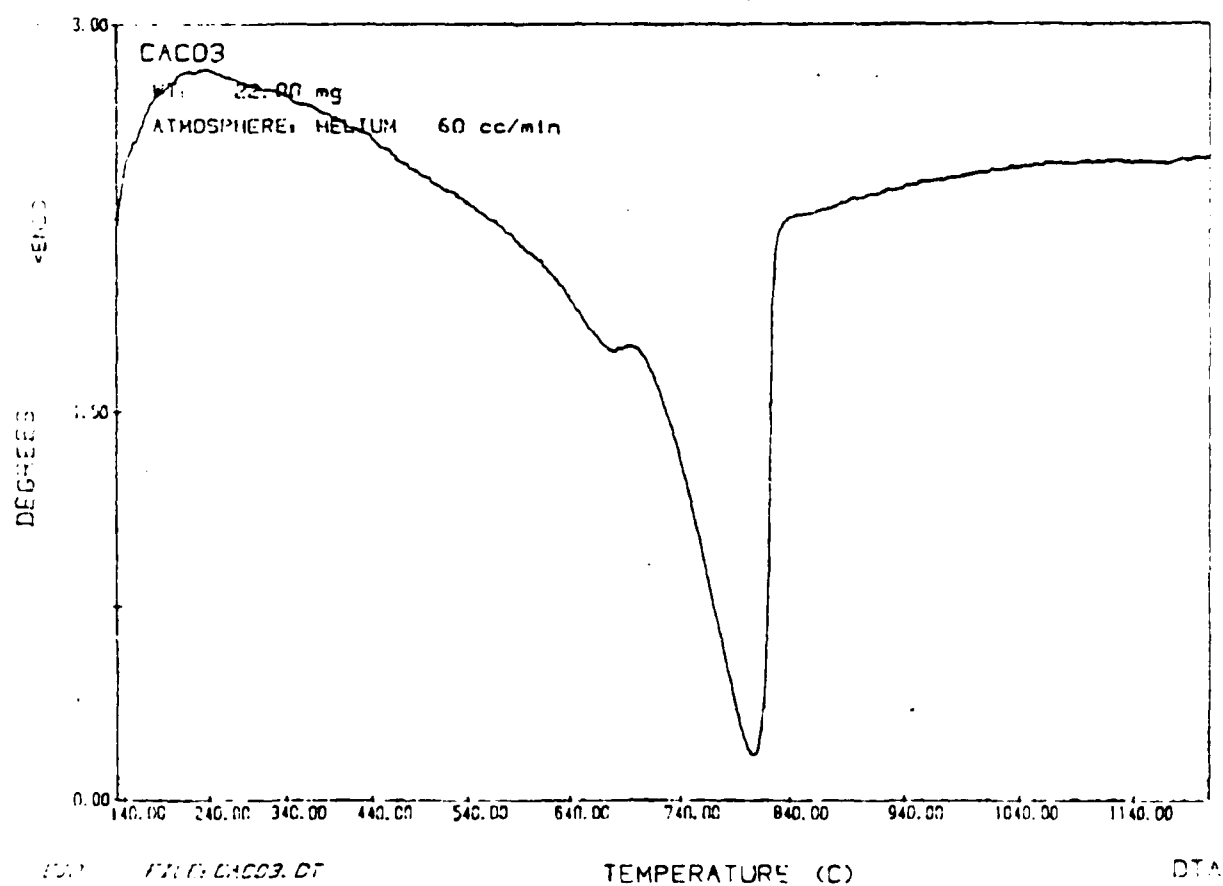


Figure 43

DTA trace of a puratronic grade calcium carbonate taken at a heating rate of 20C/min in a 60 cc/min atmosphere of helium.

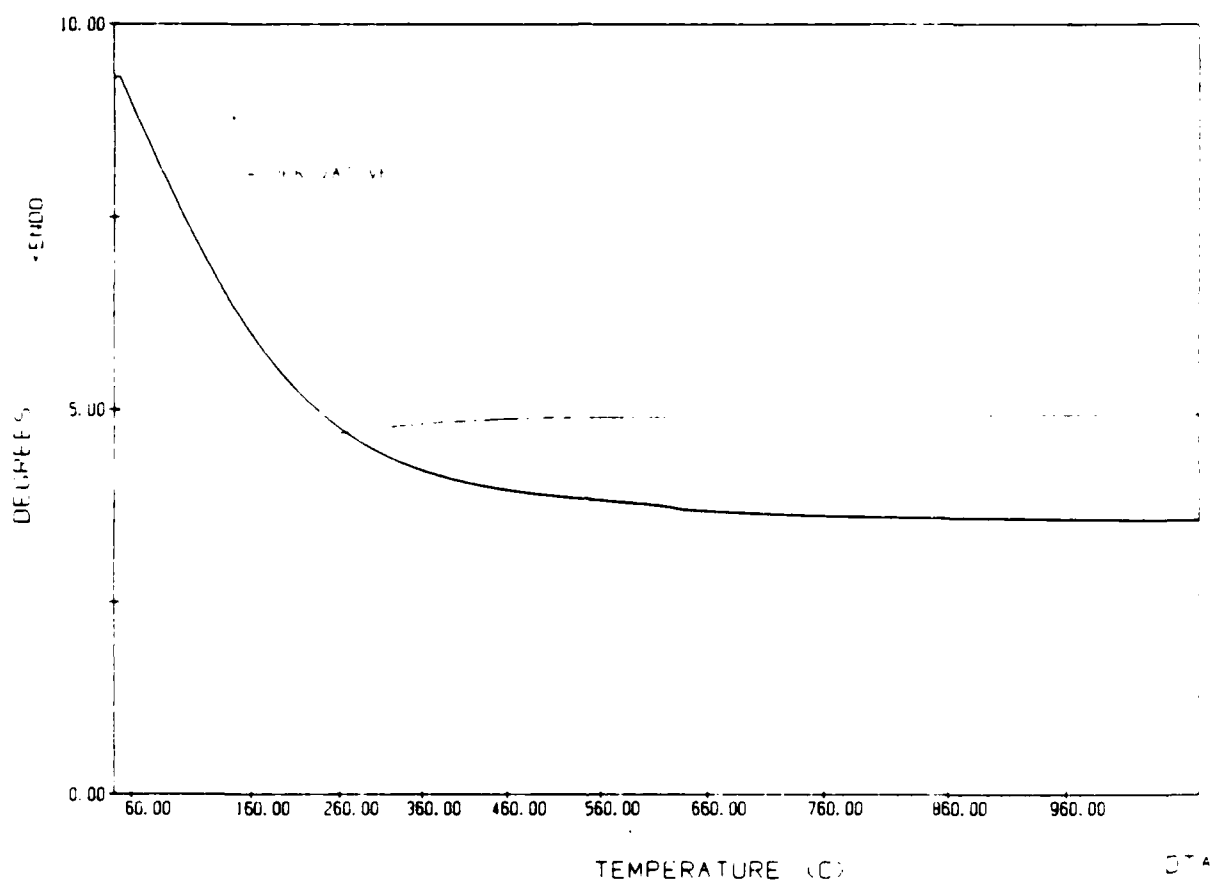


Figure 44

DTA trace of a puratronic grade alpha alumina taken at a heating rate of 20 degC/min in a 60 cc/min atmosphere of helium.

Figures 45-47 depict DTA traces of the carbonate system that were taken after the activation sequence was followed. In this case, the only variable changed was the particle size of the aluminum oxide; the traces represent, in order, aluminum oxide particle size from the three regions described in the experimental section.

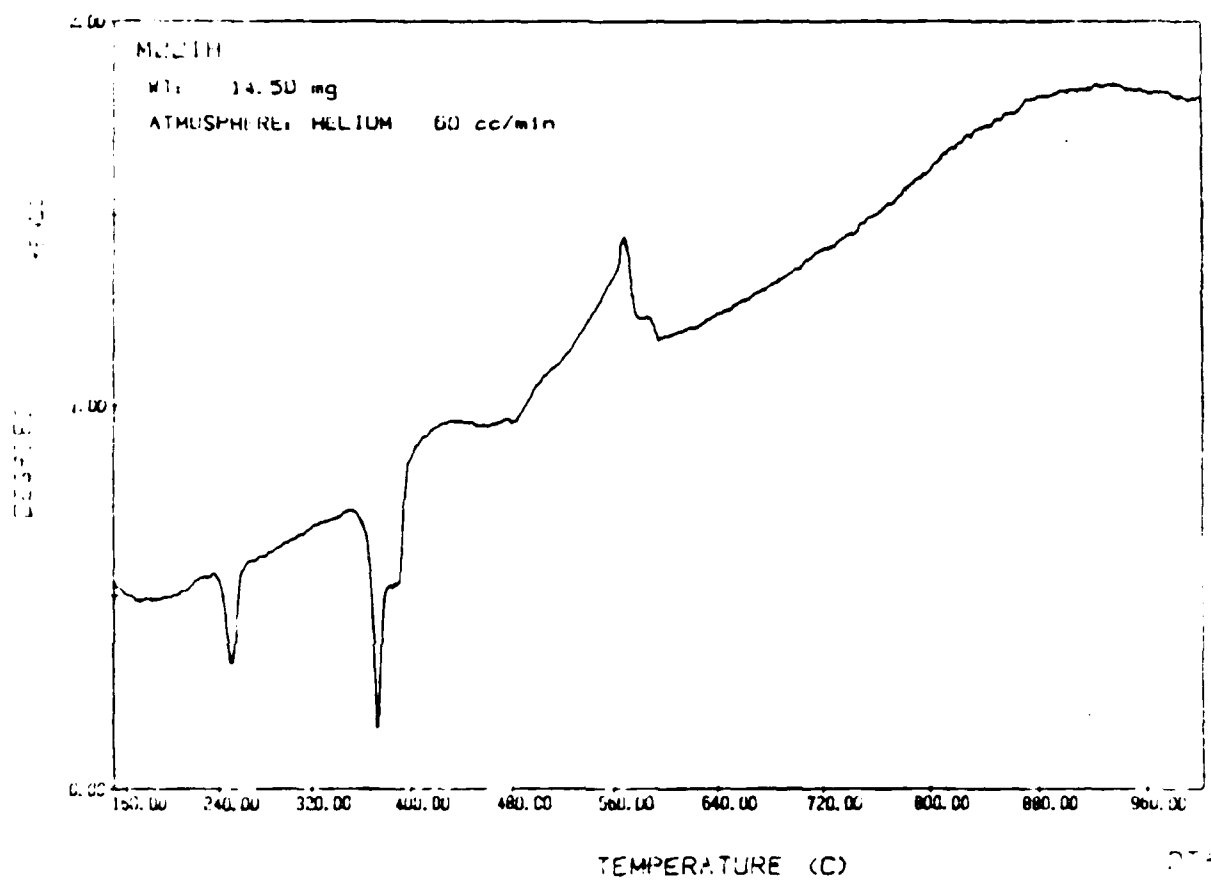


Figure 45

DTA trace of calcined 5:3:2 carbonates; aluminum oxide 40 mesh,
heating rate of 20 degC/min in 60 cc/min helium atmosphere.

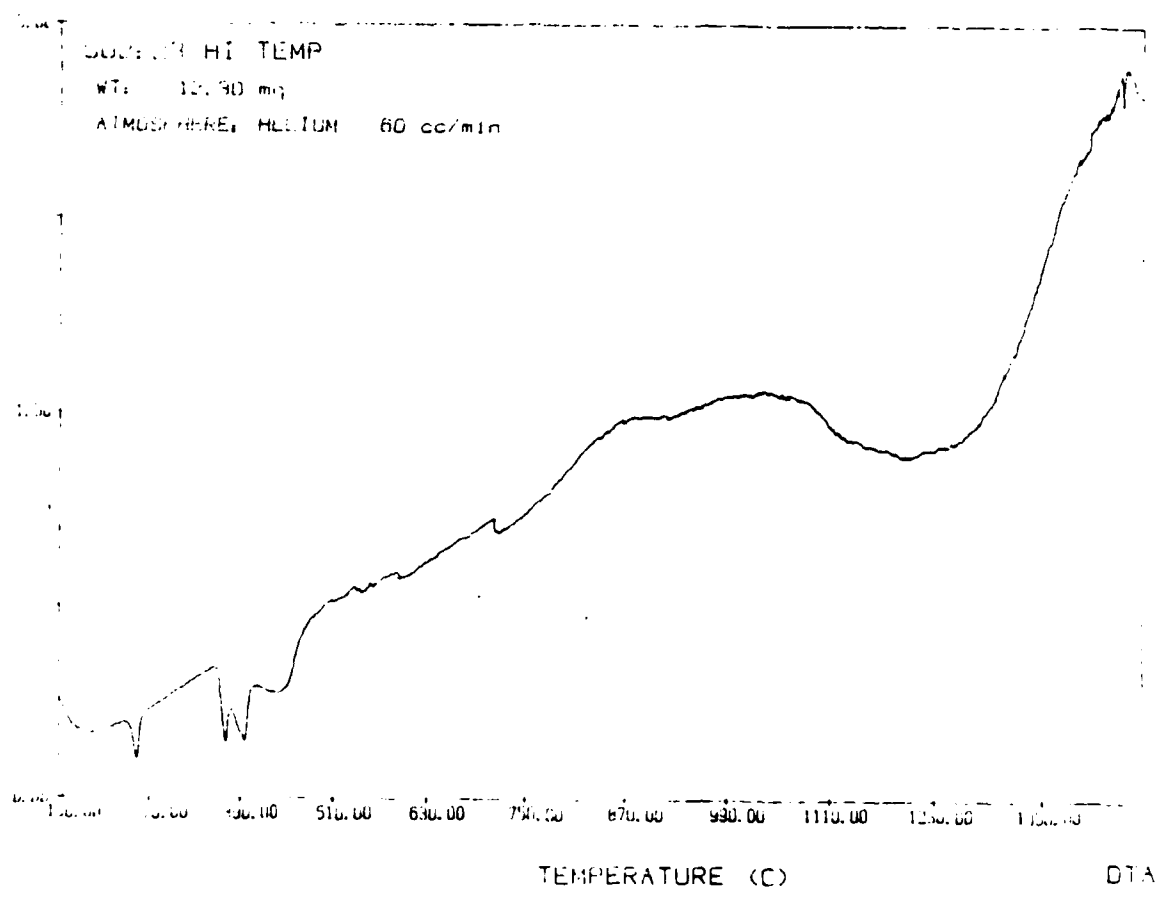


Figure 46

DTA trace of calcined 5:3:2 carbonates; aluminum oxide between 40 and 80 mesh, heating rate 20 degC/min in a 60 cc/min helium atmosphere.

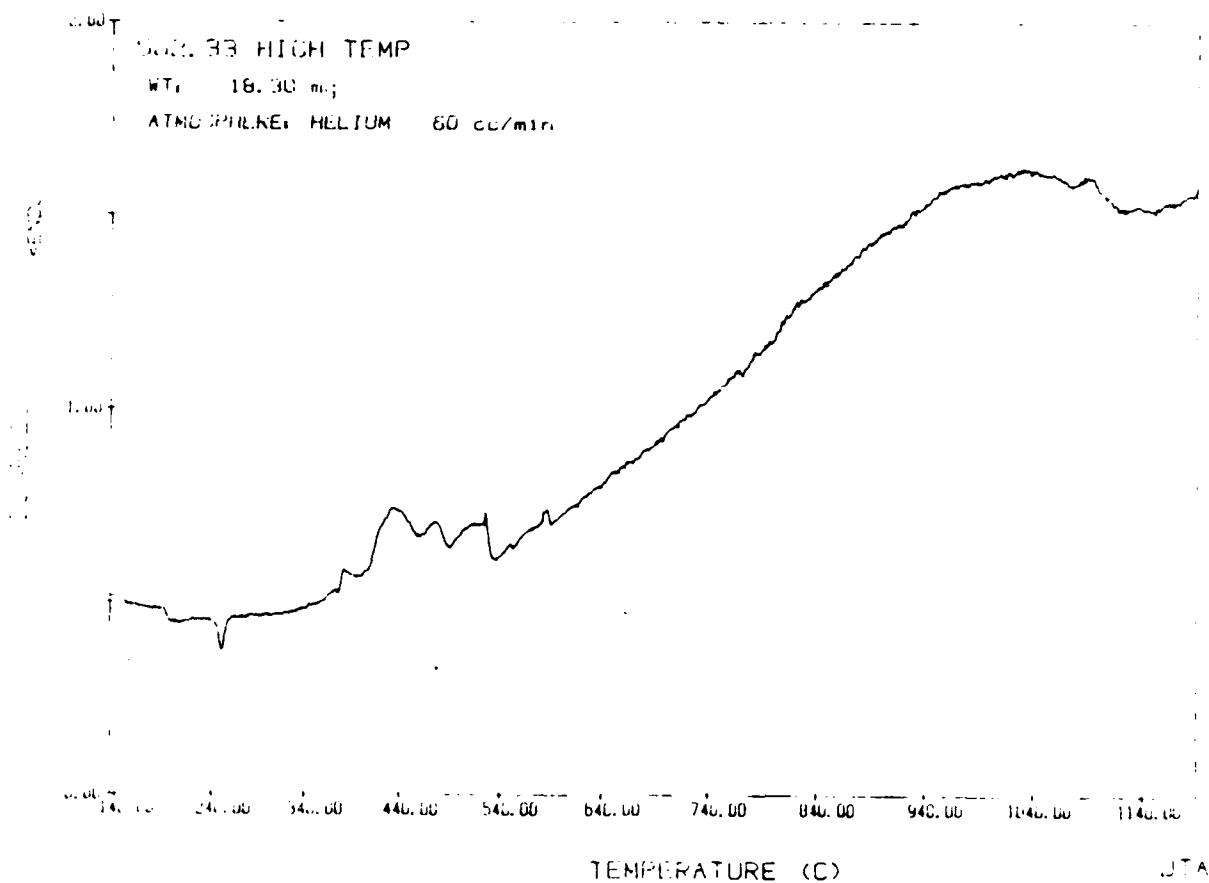


Figure 47

DTA trace of calcined 5:3:2 carbonates; aluminum oxide 80 mesh, heating rate of 20 degC/min, in a 60 cc/min helium atmosphere.

In contrast, figure 48 is the DTA trace of a 5:3:2 molar ratio of the barium-calcium-aluminum oxide system.

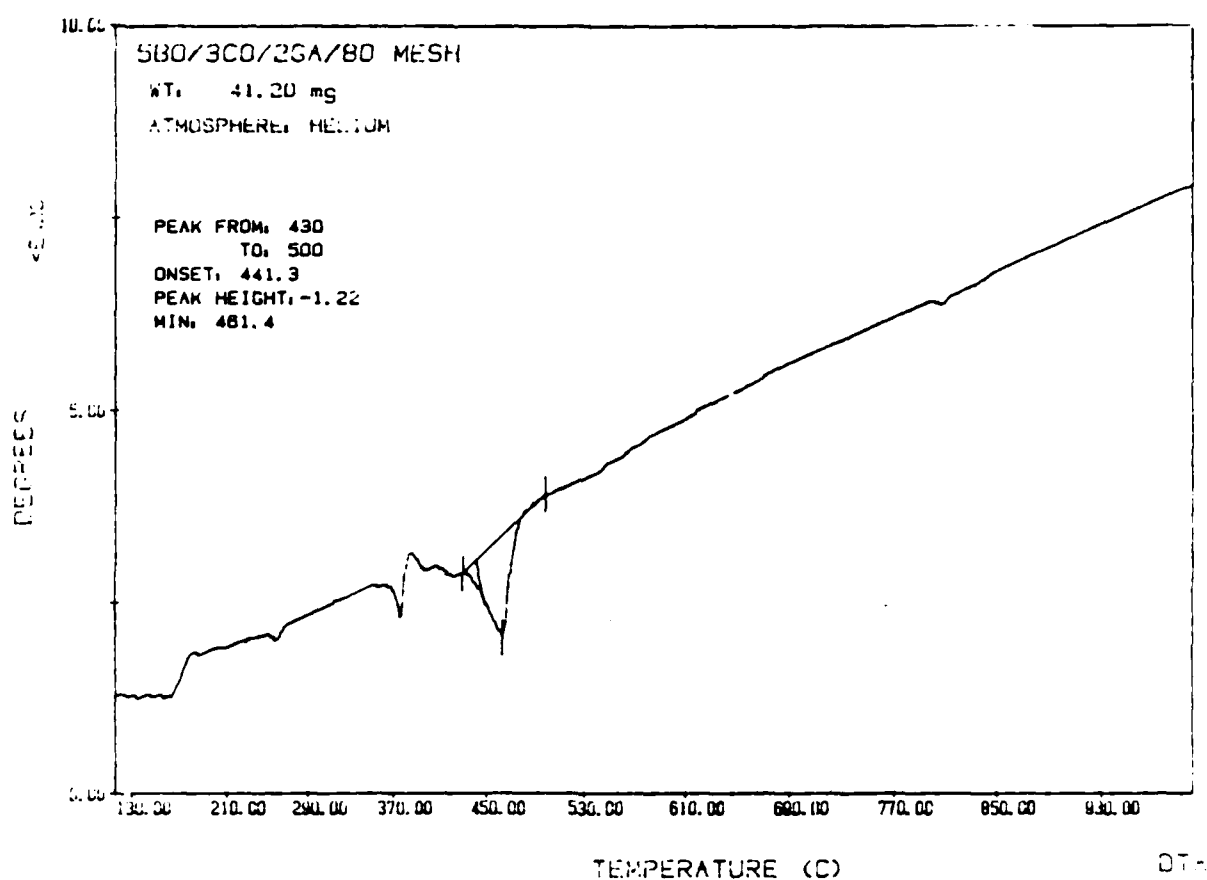


Figure 48

DTA trace of 5:3:2 oxide mixture, heating rate of 20 degC/min, in a 60 cc/min helium atmosphere.

IV.B: DTA DISCUSSION OF RESULTS

The DTA traces shown in the last section are representative of those recorded during the entire experimental procedure. Owing to the number of experimental variables and the possible combinations, it is impractical to present them all. However, one general trend is obvious; the impregnant fabrication scheme is difficult, if not impossible, to duplicate. Figures 45-48 certainly indicate this last statement. This fact has a significant bearing on cathode fabrication because this mixture must still be melted and drawn into the porous tungsten matrix. Based on the DTA traces of traditional cathode impregnant compositions and fabrication techniques, it is obvious that it is extremely difficult to prepare uniform and reproducible impregnants. In addition, from the principles of DTA theory, Figures 45-48 also indicate incomplete chemical reactions, and, in conjunction with Figures 41-44, unknown chemical reactions due to incomplete decompositions. This unwieldy number of component and preparation variables precludes any "hit or miss" procedures applied to determining the optimal cathode fabrication sequence.

In support of this research there has been complimentary work in the field of cathode preparation. Maloney and Richardson (54), in 1980, reported that unless carefully cleaned, the surface of an impregnated dispenser cathode before activation is covered with patches of impregnant material which may be many microns thick and

tens of microns across. SEM and Auger studies indicated that much of this material remains after activation and evaporates only slowly during life. This leads to emission patchiness early in life. Frederick (55) realized the need for improvements in uniformity and reproducibility of pores in porous tungsten substrates for dispenser cathodes, and conducted a study on the use of closely graded powders as starting materials, as well as the influence of powder size, source, and of pressure on the as pressed density of isostatically pressed compacts. In addition, the interrelation of sintering time, temperature and starting density on final density and on the bonding character was also studied, and the results indicated that pore structures were in fact difficult to reproduce. Lamartine, Lampert, and Haas (56), also in 1980, conducted AES and RGA investigations of various types of cathodes during activation in ultrahigh vacuum. Three stages of behavior were apparent with increasing temperature: 1) production of CO and CO₂ in nearly equal amounts, 2) electron emission with an increase in both surface and evaporated barium, and 3) appearance of BaO. In 1982, Forman et al (57) employed Auger microprobe techniques for the chemical mapping of IDC surfaces. They reported that early in life, M-type cathodes which have a high pore density also have a multi-layered Ba-O complex overlying the surface. This multi-layered complex was felt to be related to the excess impregnant in the high pore density area that decreases the area of emission of the M-cathode. Cochran, Ogden, and Ohlinger (58) studied

the high temperature physio-chemical reactions in the barium-calcium carbonate-alumina system to characterize the oxides resulting from the reaction and sintering of the carbonates and gamma-alumina. They reported CaCO_3 decomposition at 873-973K, BaCO_3 sintering at 1023-1073K, reaction of BaCO_3 and Al_2O_3 from 1073-1123K, and sintering of the three oxides from 1323-1473K. Surface area measurement for raw materials of the B composition fired for 48 hours confirmed complete reactions by 1323K. Tarter, Hill and Ohlinger (59) conducted a study of the melting behavior and characteristics of re-solidified materials in the $\text{BaO-CaO-Al}_2\text{O}_3$ system, and reported that the materials observed upon resolidification from melts produced under typical impregnation conditions did in fact differ from the relationships expected on the basis of available phase diagrams. Lipeles and Kan (60) investigated the chemistry of barium generation from barium calcium aluminate cathode impregnants and concluded that the loss rate of barium is proportional to the barium oxide vapor pressure of the impregnant, and that this vapor pressure is, in turn, related to the phase composition of the impregnant. Eng and Kan (61) presented results in which they examined processes in cathode activation utilizing a computer assisted SAM. Their results were that carbon burns off and there is an onset of barium diffusion at 1023K, the pores oxygenate and there is a shift in the oxygen lines at 1046K, a calcium window is observed from 1123-1313K, an onset of tungsten oxidation at 1263K, and a sulphur burn off from the pores at

1333-1453k. Hill and Lampert (62) conducted an investigation of the high-BaO portion of the ternary phase diagram. The motivation for their work marked the first realization that fabrication can effect performance, since there is no clear idea what phases are frozen into the porous tungsten matrix when the cathode is impregnated, nor what changes occur in the impregnant when the cathode is reheated during activation and subsequent operation. Kan and Seaver (63) analyzed impregnant compositions inside IDC's. Electron microprobe analyses were made, pore by pore, for Ba, Ca, and Al, and the compositions were inferred from the phase diagram. In B-cathodes, all three elements show a distribution in concentration rather than the single nominal value of 5:3:2, and Ca was usually found to be deficient. In aged cathodes, three distinct regions were identified: a relatively undisturbed region in the interior containing the approximate original impregnant, CaO, and 2 BaO:CaO:W₂O₃; a transition region (.01" d .041") high in CaO, BaO:Al₂O₃, and 2 BaO:CaO:Al₂O₃; and a near surface region consisting of BaO:Al₂O₃. Tarter and Ohlinger (64) evaluated impregnated samples in order to determine the composition of the material infused into the tungsten. They examined general trends in composition shift and related them to production impregnation procedures.

In light of the DTA results, coupled with the findings just discussed, it is no wonder that cathode design has remained an art

rather than a science.

The problem of not being able to reproducibly fabricate the impregnant has a tremendous influence on cathode activation and subsequent performance.

It is interesting to note and significant to point out that the problems encountered in the preparation, activation, and performance of a heterogeneous supported catalyst are very similar to those encountered in the construction of a reliable thermionic emitter. When faced with a similar situation for the design of new catalyst systems in the field of heterogeneous supported catalysis, the catalytic scientist had to rely on developing a first principles' understanding of the factors which contribute to optimum catalytic performance.

To demonstrate the one-on-one comparison between the preparation and activation procedures of cathodes and the preparation of catalysts, which consists of dispersing transition metals on high surface carriers, a brief digression is required. In the following, the reader is advised of the following two facts:

- 1) the identity of the support matrix and the adsorbate are reversed, but

- 2) the surface phenomena which lead to desired performance in both cases are controlled by the interactions that occur in the surface layer and thus this reversal of identity is on no consequence.

To proceed, the bonding of transition metal-oxides to inorganic supports can be viewed as a subclass of functional groups on solid surfaces (65). For example, three primary models of the supported phase oxide structure of these metal oxides on alumina have been proposed: a surface compound consisting of one layer on the oxide surface of isolated transition-metal oxide units, a surface compound consisting of one layer on the oxide surface of polymeric, octahedrally coordinated units, and a surface structure consisting of bi- and trilayer structures of the transition metal oxide. The structures of the supported phase are controlled by many factors, one of the factors being the relative surface coverage. This factor was clearly demonstrated in a recent study of an important cracking catalyst used to process crude petroleum on low molecular weight components, viz., tungsten oxide supported on alumina (66). Recall, the support matrix and adsorbate take on, in this case, obverse but chemically identical roles as the surface layer present in a working impregnated cathode. In the referenced work, the influence of activation temperature upon the solid state chemistry of WO_3 and Al_2O_3 was examined. The technique employed was Raman spectroscopy, a surface sensitive probe that can be employed under activation temperatures in a manner similar to DTA. The results of this study of a supported catalyst revealed that below monolayer coverage of WO_3 on Al_2O_3 , the tungsten oxide phase is present as a highly dispersed and amorphous surface complex on the support. A close packed

monolayer of the tungsten oxide surface complex on alumina is formed as the surface area of the alumina support decreases at high activation temperatures. The lower the tungsten oxide weight loading, the more severe the activation temperature must be to reach the close packed monolayer. The close packed tungsten oxide monolayer accommodates the further desurfacing at still higher temperatures by forming the bulk tungsten oxide phases, WO_3 and $Al_2(WO_4)_3$. The latter phase is formed from the reaction of WO_3 crystallites with the Al_2O_3 support. The promoter controlling the phases present in the WO_3 on Al_2O_3 system is the surface density of the tungsten oxide species on the alumina surface. In the case of cathode preparation there is a similarity of the surface structures produced when transition metal oxides and other refractory oxides are in intimate contact during thermal activation. The importance of the relative coverages of these components as well as their oxidation states are apparent when one considers both the description of IDC operation which has been described throughout this thesis, and the results of the DTA traces of this section. The surface and near surface region of the cathode critically determine the performance of the activated cathode, and clearly, the existence of strong two-dimensional surface molecules cannot be controlled by conventional preparation and activation sequences.

The surface has a distinct advantage when compared to the bulk. For example, surface phase oxide structures are indeed highly

refractory and have coordinately unsaturated sites associated with the transition-metal center (67,68). The coordinated unsaturated sites in the epi-phase of transition-metal oxides may be associated with isolated transition-metal centers, polymeric oxide phases, or even multilayer phases. Thus it seems reasonable to speculate that some strong metal-metal bonding pairs cannot be realized in an oxide lattice due to incompatibility of their respective anion polyhedra. At the surface, however, the ligand coordination of a metal in the epiphase need not complement that of an endophase metal in any way whatever. This line of demarcation is not clearly understood. It is likely to vary from compound to compound as well as within a given compound subjected to varying activation temperatures. In the discussions to follow this strong metal-metal bond terminology from synthetic inorganic chemistry will be used to describe the spatial and chemical identity of these regions. The lability of oxygen at a surface confers an advantage in terms of establishing the desired anion coordinations. Recalling the desirable features of an active thermionic cathode, they suggest that optimum performance will be achieved when there exists a surface metal-metal bond (69,70). This defines a relatively new type of solid characterized by the direct bonding of neighboring metal atoms or cations. In the 1950's and the 1960's there occurred a rapid growth in solid-state inorganic chemistry in the area of metal-cluster compounds. These comprise a large number of transition metal compounds in which direct chemical

bonding, involving d-electrons and d-orbitals, takes place between neighboring metal atoms and cations. The prime example of such compounds are the hexagonal barium titanates, the prototype structure already identified by Mossbauer spectroscopy. Therefore, it seems reasonable at this juncture to hypothesize a structure for the metal-cluster compounds that could be formed on a cathode surface. The strong metal-metal interaction would be between barium and tungsten which could be electronically and structurally stabilized by oxygen ligands. The structure of a binary oxide supported on a refractory tungsten porous plug, whose surface, itself, contains a strongly adsorbed oxide layer, appears well suited for thermionic emission.

The conclusion of this section, based on the DTA traces and other works quoted, is that an alternative impregnation sequence must be developed in order to guarantee reproducible structures. In addition, the fortuitous identification of the hexagonal barium titanate structure and the possibility of establishing the steric properties that would facilitate the strong metal-metal interaction, clearly indicate the adoption of an alternative impregnant thermochemistry system. It could be argued at this point that conventional cathode materials could also exhibit the strong metal-metal interaction. However, in light of the DTA traces which indicate both lack of reproducibility, as well as incomplete and unknown chemical reactions, the establishment of this optimal surface structure on a conventional IDC appears unlikely. If the high

activation and operation temperatures are also considered, the necessary monolayer coverage could be destroyed due to surface sintering and creation of the bulk oxide, BaAl_2O_4 .

Therefore, combining the Mossbauer and DTA results, along with the realization of the strong metal-metal interaction of the barium titanates, it was decided to investigate an alternate cathode architecture, based on the accepted practices of heterogeneous supported catalysis. Thus it was necessary to fabricate a large pore tungsten matrix, in order to use wet impregnation techniques. In addition, the surface of this matrix needed to be modified with a strongly adsorbed oxide layer which would control and stabilize the strong metal-metal interaction .

V.EMISSION RESULTS

V.A: FABRICATION AND TESTING

Four key areas were targeted during this portion of the research. They were:

- 1) high surface area modified tungsten matrix
- 2) optimized compounds for precursors of emission sites
- 3) controlled impregnation procedures
- 4) conditions for generating strong metal-metal surface

interactions

The SEM photos, Figures 48-50, illustrate the large pore size of this matrix.

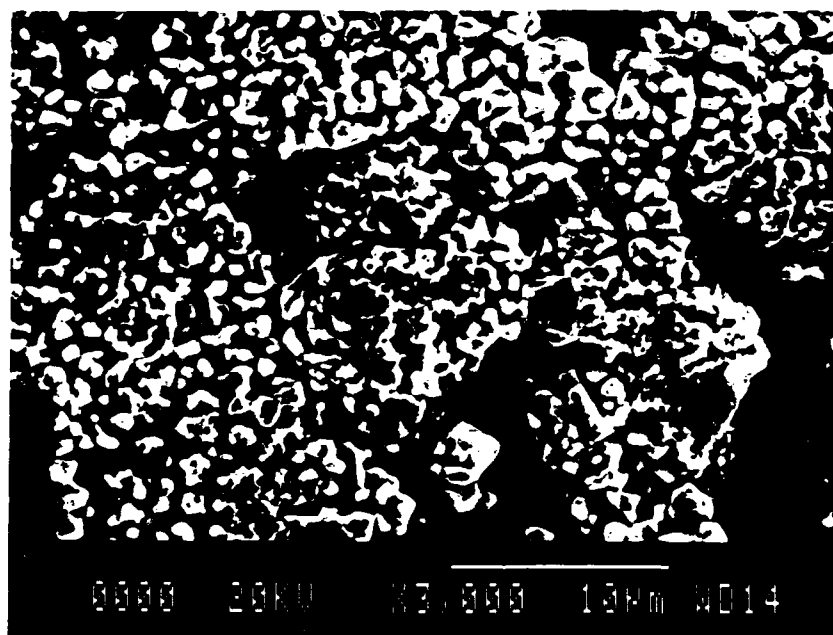


Figure 48

SEM of matrix, 3000 x magnification

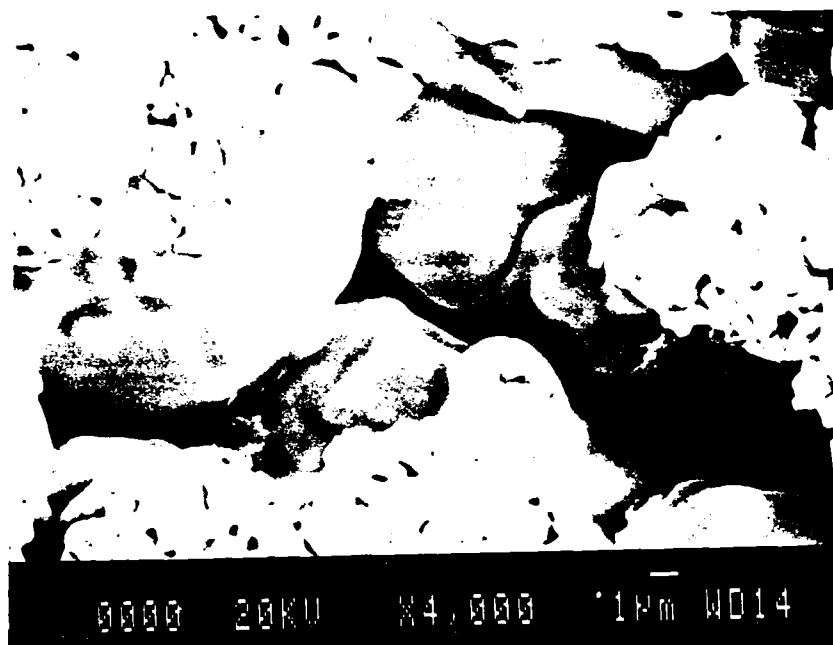


Figure 49

SEM of matrix, 4000 x magnification

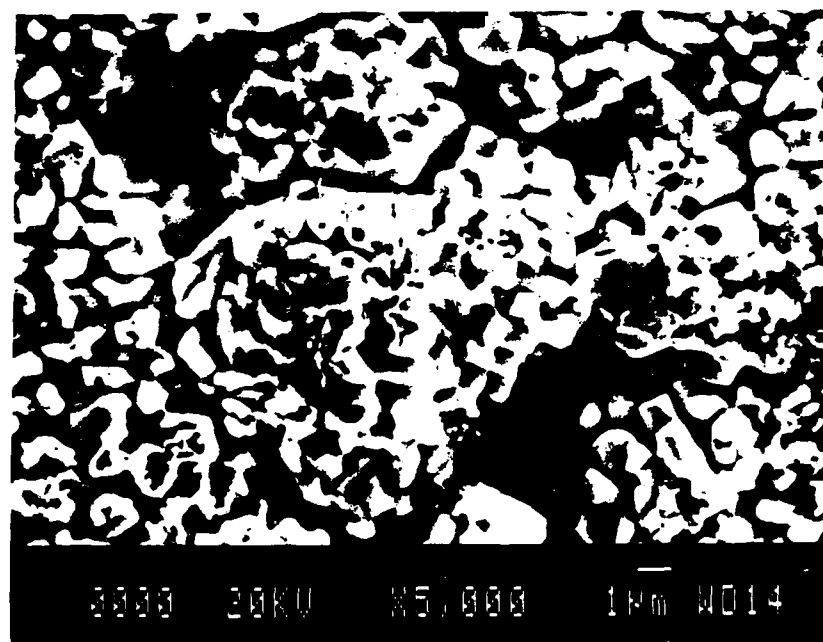


Figure 50

SEM of matrix, 5000 x magnification

Using the standard BET area measurement technique of nitrogen physisorption at liquid nitrogen temperature, the surface area of this modified bulk tungsten matrix was found to be $2.3 \text{ m}^2/\text{gm}$. In direct contrast, a tungsten matrix produced under conventional conditions did not yield any surface area.

The incipient wetness factor for this sample was determined to be $.15 \text{ cc/gm}$; however, since the solubility of barium nitrate lies between 8.7 and 34.2 gms/100 cc (depending on water temperature), it was decided to impregnate the matrix using wet impregnation techniques.

In addition to the limited incipient wetness factor, the following was also considered. Recall that barium must be present in at most a monolayer coverage in order to effectively lower the work function of the surface it is adsorbed on. If the surface area is taken as $2.3 \text{ m}^2/\text{gm}$, and assuming the diameter of the barium ion is 1.28 Angstroms, then one monolayer corresponds to roughly 76 milligrams of barium nitrate. The average matrix that was impregnated was on the order of 3 grams; thus only 45% of 3 grams of solution could be taken up into the porous matrix, and the number of barium atoms for the necessary monolayer tripled. This exceeded the solubility limit of the barium nitrate. Therefore it seemed appropriate to use wet impregnation techniques.

This prototype "cathode", cathode 1, was subjected to DTA,

shown in Figure 51. Note the low activation temperature and the simplicity of the decomposition reaction.

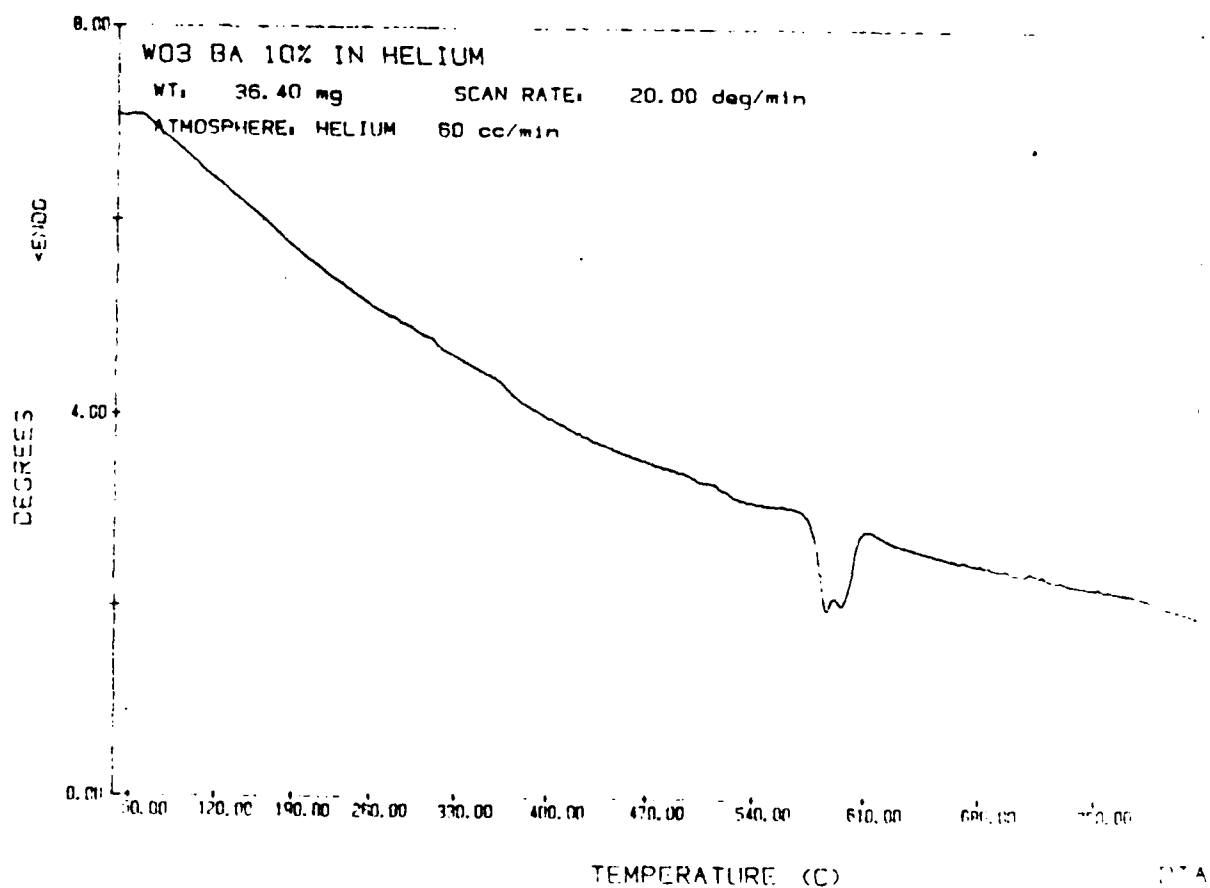


Figure 51

DTA trace of activation of cathode 1.

20 C/min heating rate in a 60 cc/min atmosphere of helium

The Raman Spectra conducted to verify the impregnation are given in Figures 52 and 53. Note the existence of the bridge bonded oxide line at 50 cm^{-1} and the oxygen metal stretch at 1050 cm^{-1} ; the matrix support did not interact significantly with the supported oxide during the impregnation and activation procedure.

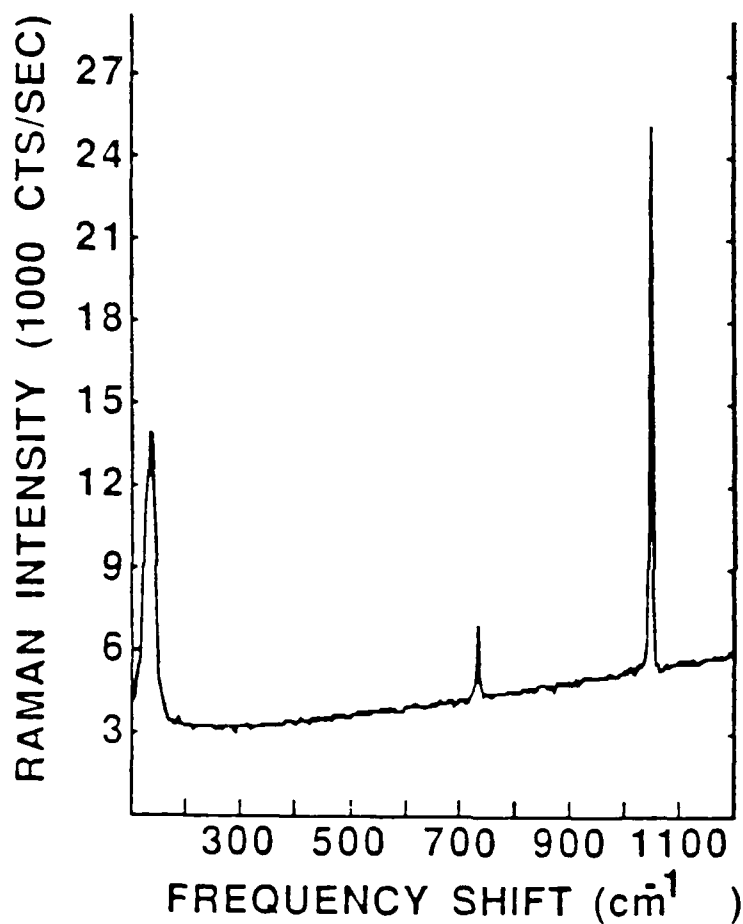


Figure 52

Raman spectra of matrix impregnated with $\text{Ba}(\text{NO}_3)_2$;
taken with the 5145 Å line of Ar^+ laser

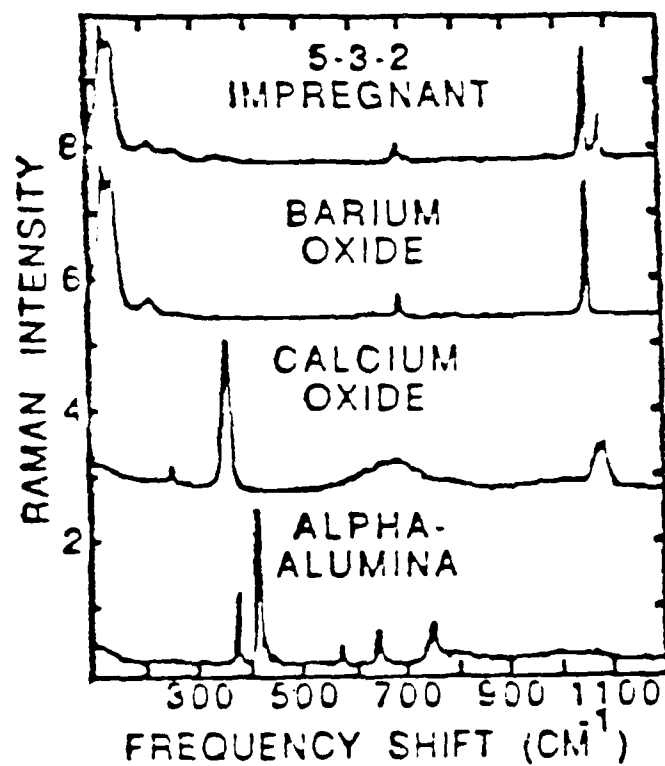


Figure 53
Raman spectra of reference materials;
taken with 5145 Å line of Ar^+ laser

From the DTA trace, the important temperatures were chosen; dehydration at 373K overnight (allowing for the increased sample size) followed by activation at 873K for 1 hour. The temperatures

were ascertained by extrapolating the heater power curve.

The preliminary emission data was very disappointing, and it was concluded that the Ba-O did not fully coat the entire available surface area. (Based on comparable physical surface area, this new device represented a 100,000 amps/gm potential.) Referring to the Mossbauer results, titanium oxide was incorporated into the fabrication sequence and cathode 2 was subjected to exactly the same conditions as the first cathode. The DTA trace detailing activation is shown in Figure 54.

In direct analogy to conventional IDC development, chloroiridic acid (.2 molar) was the next "ingredient" to be tried, in place of the titanium oxide. The fabrication was the same as the second cathode, and Figure 55 is the DTA activation "fingerprint" for this sample. Of importance is the exothermic reaction centered at 550C (823K), indicating a possible solid state reaction.

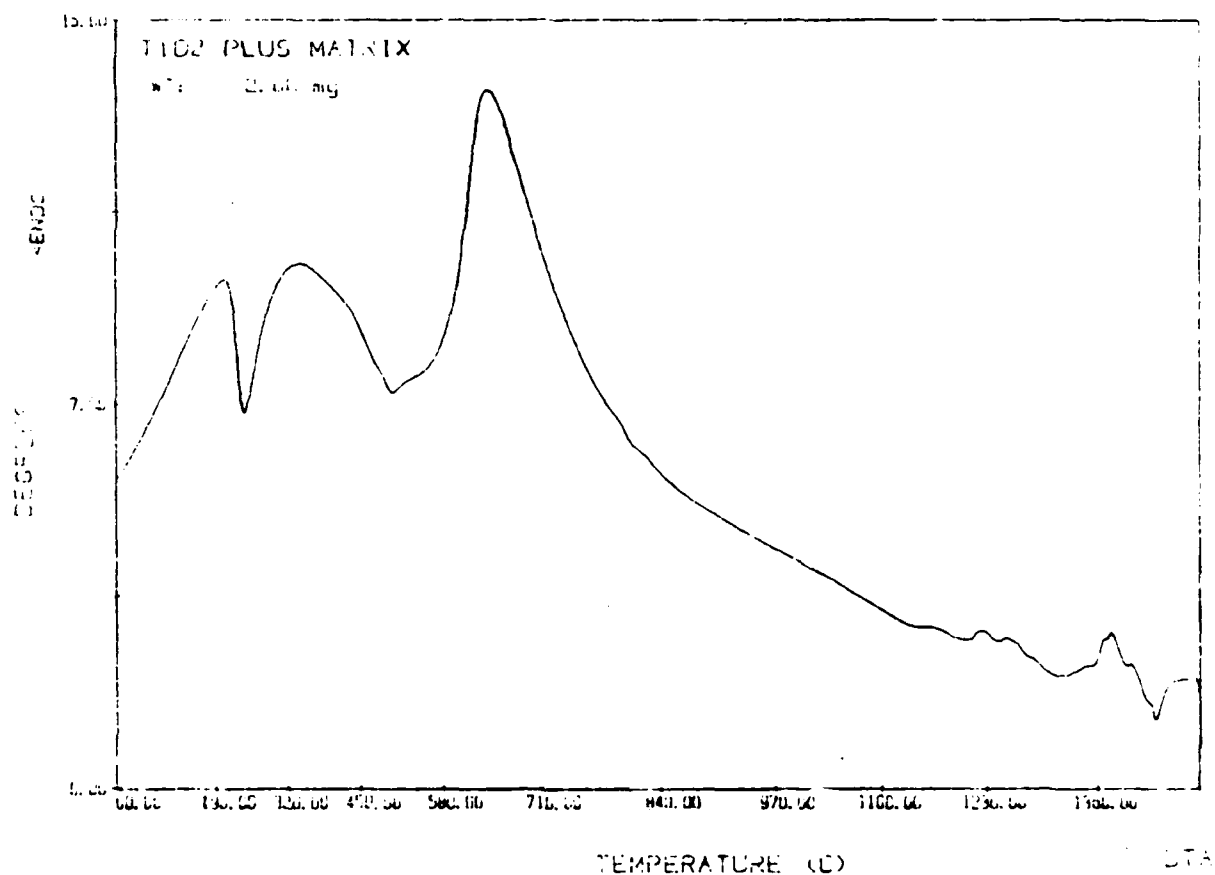


Figure 54

DTA trace cathode 2 activation;
20C/min heating rate, 60 cc/min helium atmosphere

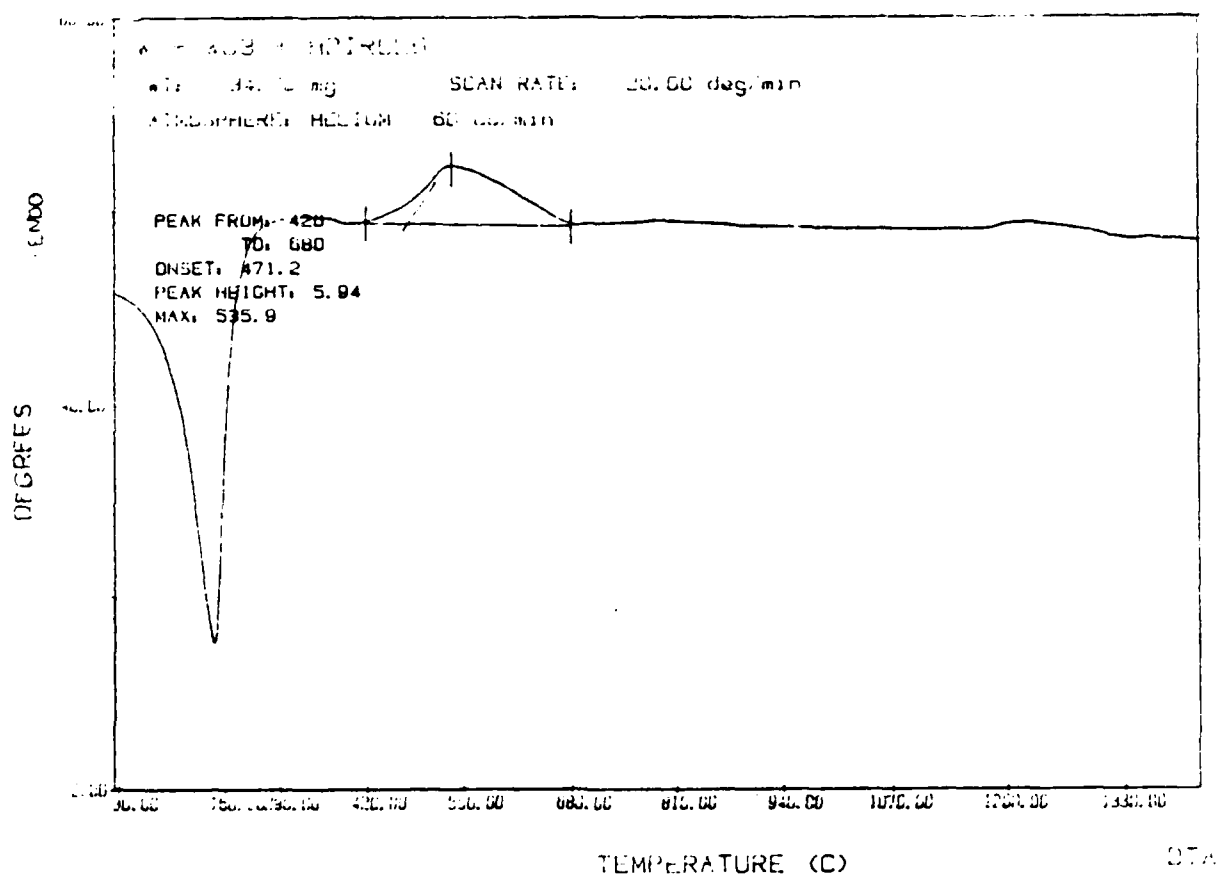


Figure 55

DTA trace of cathode 3 activation;
 20C/min heating rate, 60 cc/min helium atmosphere.

All three cathode zero field emission curves are given in
 Figure 56.

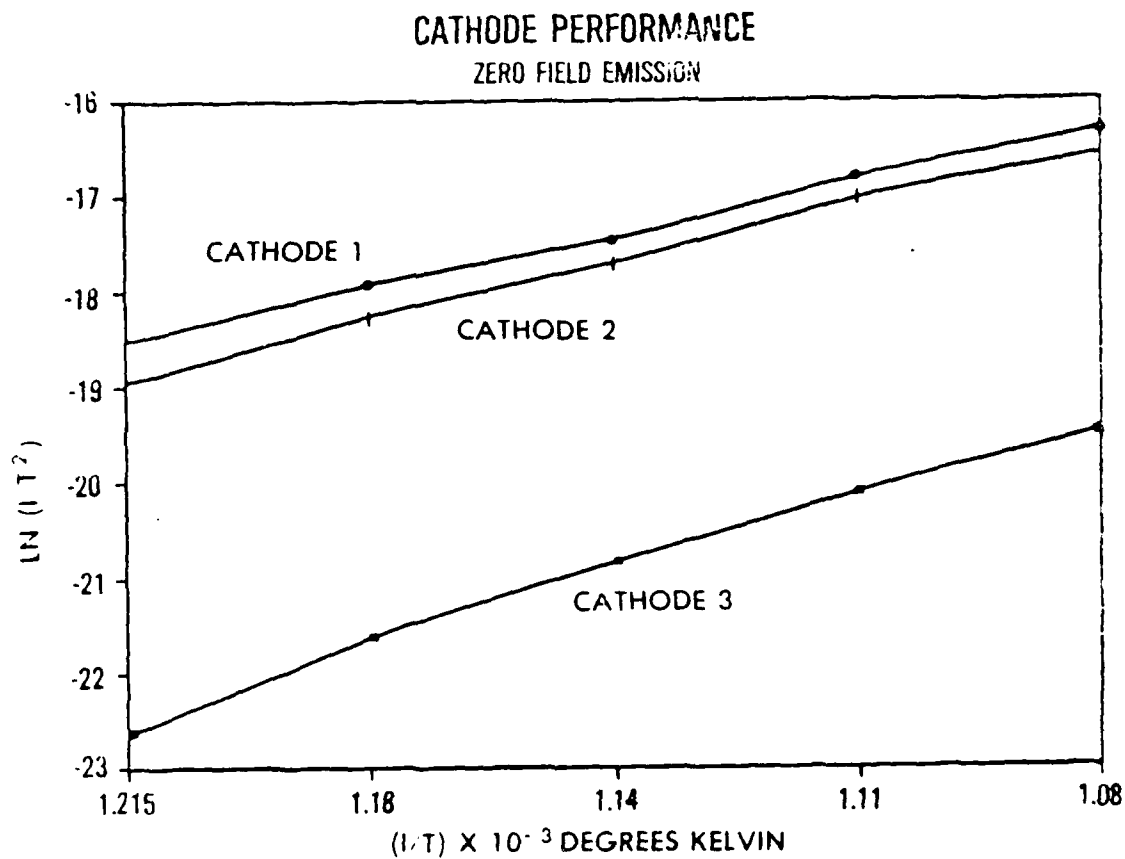


Figure 5b

Cathode Zero field emission plots

Cathode 1 is the modified matrix impregnated with $\text{Ba}(\text{NO}_3)_2$; cathode 2 is the modified matrix impregnated with TiO_2 and then $\text{Ba}(\text{NO}_3)_2$; and cathode 3 is the modified matrix impregnated with H_2IrCl_6 and then $\text{Ba}(\text{NO}_3)_2$.

V.B. DISCUSSION OF RESULTS

Figure 56 illustrates clearly the effect of preparation on performance. (The data recorded was current and the corresponding temperature.) From Richardson's Equation (2), a plot of $\ln(I/T^2)$ vs $1/T$ should be a straight line, the slope of which is related directly to the work function. This slope is then inserted back into Equation (2) in order to determine the pre-exponential value. Table 6 summarizes the results for the three prototype thermionic cathodes.

| <u>CATHODE</u> | <u>WORK FUNCTION</u> | <u>A</u> |
|----------------|----------------------|----------|
| 1 | 2.1 ev | 112 |
| 2 | 1.5 | 117 |
| 3 | 1.2 | 119 |

Table 6

Thermionic Emission Constants

(Cathode 1 is the modified tungsten matrix impregnated with barium nitrate, analogous to a B-type cathode; cathode 2 is the modified tungsten matrix impregnated with titanium oxide and then barium nitrate, which represents an incorporation of the Mossbauer results

and the strong metal-metal bond; cathode 3 is the modified tungsten matrix, impregnated with chloroiridic acid and then barium nitrate, which is analogous to the M-type cathode.)

There are two practical realizations that arise from these data. First, upon comparison of Figure 54 with Figure 2, note the temperature difference for comparable current density. Second, the emission data for the new cathodes fits the theoretical equations extremely well. I feel this latter statement proves my earlier hypothesis that cathode preparation and emission performance are intimately related. This of course depends upon the identification of the fundamental electronic and steric properties inherent to the physics of thermionic emission.

The preliminary results of this research task clearly point to systematic design procedures for future thermionic cathodes. There are a half a hundred elements that form oxides which are solid in the temperature range relevant to cathode operation, and I have investigated but a few of these. However, the number can systematically be reduced by considering the results of this particular research task in conjunction with the accepted experimental practices of heterogeneous supported catalysis.

As has been shown, the desirable features of an active cathode are the adsorption of a two-dimensional electropositive monolayer onto the surface of a conductor, and, the existence of strong chemical bonds of these adsorbates to the metal surface. The

former was determined by the Mossbauer experiments, while the latter was realized through an investigation of the barium titanates from the standpoint of catalysis. The actual fabrication sequence that will be responsible for these two factors can be divided into three main areas; 1) cathode materials, 2) impregnation procedures, and 3) activation procedures. The "proof of the pudding" has been established by actual emission testing of the cathodes.

The formation of active and stable cathode structures occurs as the result of chemical reactions during activation. This process is dynamic in which both solid-state as well as new surface compounds are formed. Previous studies have focused on interpreting the structure of the cathode subsequent to activation. This research project, built on the significant contributions of past and present cathode scientists, has elucidated those factors prior to activation that are of extreme consequence to ultimate thermionic emission. It is my hope that these results, when synergistically combined with conventional and novel design criteria, will form the scientific basis for the formation of efficient and reliable thermionic emitters.

VI. SUMMARY

The main effort has been to try to bring together in a simplified manner both experimental and theoretical studies basic to the analysis of thermionic emission from impregnated dispenser cathodes as it is understood at this time. These studies revealed two major areas of uncertainty: 1) the electronic and steric nature of the cathode emissive surface, and 2) the lack of a reproducible impregnation procedure.

Mossbauer spectroscopy, which can investigate exceedingly small perturbations in the nuclear levels caused by the solid state properties of the local environment of the Mossbauer isotope, was used to probe the cathode surface. Both a B-type and M-type IDC were impurity doped with cobalt 57 and the subsequent in situ Mossbauer emission spectra from these two cathodes illustrated the different surface crystalline electric fields of the respective cathodes. The B-type cathodes yielded a broadened single line Mossbauer spectrum, while the M-type cathodes exhibited a low-spin Fe III spectrum. The existence of the low-spin state results in a more effective bonding configuration for the adsorbed electropositive monolayer, hence emission enhancement and lower monolayer evaporation rate for the M-type IDC.

The existence of the low spin Mossbauer isotope led to a formulation of a hypothetical surface molecular configuration

consistent with the constraints imposed by surface symmetry considerations. This model had a striking parallelism with similar systems in the field of heterogeneous supported catalysis (HSC). In the latter case, the appropriate stoichiometry is a major goal of preparation, whereas in the former it is assumed "a priori". Further investigation of these analogous systems led to the realization that IDC fabrication procedures might be oblivious to the advances that have been made in the preparation and performance of supported catalysts. Whereas the utility of a catalyst and a cathode differ significantly, the similarity of the resultant "optimal" chemical configurations is identical. Hence the decision was made to establish a causal relationship between IDC preparation and performance according to the accepted practices of HSC.

Published reports on IDC thermochemistry clearly indicate the influence that this chemistry and the impregnation process has on thermionic emission. Of particular relevance, is the recently published work of Norman et. al. (71). In their work, they conducted surface extended x-ray-absorption fine structure (SEXAFS) experiments in order to determine the structure of the adsorbates on B-type and CD-type IDC's. They concluded that there is a unique, well defined surface complex, with Ba atoms coordinated directly to oxygen, and substrate atoms as next nearest neighbors, for the two types of cathodes. They postulated a surface structure for each cathode, based on a body-centered-cubic surface for the B-type and a

hexagonally closed packed surface for the CD type. The more open structure of the CD-type surface planes has a Ba atom bridging two O atoms, while the B-type structure has a Ba atom directly on top of an O atom. These two different structures are consistent with the Mossbauer data reported earlier, and certainly lend credence to the efficacious bonding structure that was postulated. However, the importance of surface modification, i.e. the removal of excess oxygen, is the key step in the fabrication sequence that results in the formation of the strong metal-metal bond. These findings were complimented by the utilization of differential thermal analysis (DTA), which revealed that if standard accepted practices of impregnant preparation were followed, the effects of particle size, mixing time and method, dehydration time and temperature, and atmospheric composition, must be considered if the optimal impregnant composition was to be achieved. Corroborating the conclusions of previous work with those of this portion of the research, it was possible to establish the causal relationship between preparation and performance, as well as account for noted emission discrepancies through DTA data interpretation.

The next step was to eliminate those factors that had been identified as having a legitimate bearing on thermionic emission. Reviewing the results of the research to this point, it was decided to attempt, in principle, the formation of a stable 2-dimensional electropositive adsorbate ligand onto the surface of a 5-d transition

metal. The Mossbauer results of the low spin complex revealed an ideal model, the hexagonal barium titanates (HBT).

The structure of the HBT appeared quite advantageous to thermionic emission, because it exhibits the strong metal-metal surface bond which culminates in a covalent bond between a d-electron dono cation, or atom, in an epiphase, and an acceptor cation at the surface of an oxide. This ultra-strong bond appears to be the optimum cathode surface configuration.

Utilizing the standard practices of HSC, and monitoring the solid state chemistry with Raman spectroscopy and DTA to insure reproducibility, three prototype cathodes were fabricated. Zero field thermionic emission from these devices were in excellent agreement with the theoretical Richardson equation, and the emission densities of two of the cathodes were comparable to state of the art IDC's, but at a much lower temperature (900K vs 1200K).

REFERENCES

1. W. B. Nottingham, "Encyclopedia of Physics", Volume 21, p. 7, Springer-Verlag, (1956).
2. W. H. Preece, Proc. Roy. Soc. Lond., 219, (1885).
3. J. J. Thomson, Phil. Mag. 48, 547 (1899).
4. O. W. Richardson, Proc. Cambridge Phil. Soc. 11, 286 (1902).
5. W. Wilson, Proc. Roy. Soc. A93, 359 (1917).
6. S. Dushman, Phys. Rev. 21, 623 (1923).
7. A. Sommerfeld, Z. Physik 47, 1 (1928).
8. L. Nordheim, Z Physik 30, 177 (1929).
9. loc. cit.
10. W. Schottky, Phys. Z. 15, 872 (1914)-Z. Physik 14, 63 (1923).
11. "Encyclopaedic Dictionary of Physics", J. Thewlis editor; Oxford-London-New York-Paris: Pergamon Press (1961).
12. ibid.
13. ibid.
14. ibid.
15. A. Wehnelt, Ann Phys. 14, 425 (1904).
16. A. Eisenstein, "Advances in Electronics", New York: Academic Press, pp. 1-62 (1948); P. Zalm, Advances in Electronics and Electron Physics", New York: Academic Press, pp. 211-271 (1968).
17. I. Langmuir and W. Rodgers, Phys. Rev. 4, 544 (1914) .
18. I. Langmuir and J. B. Taylor, Phys. Rev. 44, 423 (1933).
19. H. J. Lemmens, M. J. Jansen and R. Loosjes, Philips techn. Rev. 11, 341 (1950).
20. R. Levi, J. Appl. Phys. 24, 233 (1953).
21. P. Zalm and A. J. van Stratum, Philips techn. Rev. 27, 69 (1966).
22. L. R. Falce, U.S. Patent No. 4, 165, 473.
23. M. C. Green, H. B. Skinner, R. A. Tuck, App. of Surf. Science, 8, pp. 13-35, (1981).
24. ibid.

25. L. R. Falce, and R. E. Thomas, Proc. Int. Electron Devices Meet; Washington, pp. 156-159, (1978)
- * 26. M. C. Green, RADC Report TR-86-32, "Optimized Dispenser Cathode", (1986). Distribution limited to U. S. Government agencies and their contractors, critical technology.
27. loc. cit.
28. N. N. Greenwood and T. C. Gibb, "Mossbauer Spectroscopy", London: Chapman and Hall Ltd, pp. 330-351 (1971).
29. C. H. Herzfeld and P. H. E. Meijer, "Solid State Physics", Academic Press, vol. 12, pp. 2-87.
30. S. Sugano, Y. Tanabe, and H. Kamimura, "Multiplets of Transition Metal Ions in Crystals", Academic Press, New York and London; pp. 6-81, (1970).
31. loc. cit.
32. A. Gupta and C. O. Young, "The Manufacture of M-type Impregnated Dispenser Cathodes", NASA-Lewis Research Center (1977).
33. I. Brodie and R. O. Jenkins. Brit. Jour. Appl. Phys. 8, 27, (1957).
34. E. S. Rittner, W. C. Rutledge and R. H. Ahlert, J. Appl. Phys. 28, 1468 (1957).
35. ibid.
36. R. Levi, J. Appl. Phys., 26, 639 (1955)
37. loc. cit.
38. loc. cit.
39. R. Forman, J. Appl. Phys., 47 5272 (1976).
40. E. E. Rittner, J. Appl. Phys., 48, 4344 (1977).
41. loc. cit.
42. J. P. Schiffer, P. N. Parks, and Juergen Heberle, Phys. Rev., 133, 6A, A1553, (1964).
43. V. G. Bhide and M. S. Multani, Phys. Rev., 139, 6A, A1983, (1965).
44. E. S. Rittner, R. H. Ahlert and W.C. Rutledge, J. Appl. Phys 28, 1468, (1957).

*Although this report references a limited document, no limited information has been extracted.

45. R. W. Springer and T. W. Haas, J. Appl. Phys., 45, 5260 (1974).
46. R. Forman, J. Appl. Phys. 47, 5272 (1976).
47. A. V. Druzhinin, Radio Eng. Electron. Phys. 10, 425 (1965)
48. A. H. Beck and H. Ahmed, J. Electron. Control 14, 623 (1963)
49. E. Q. Zhang, Int. J. of Electronics 58, 141, (1985).
50. E. P. Gyftopoulos and J. D. Levine, J. Appl. Phys. 33, pp. 67-73, (1962).
51. loc. cit.
52. O. Johnson, J. Catalysis, 28, 503, (1973).
53. L. R. Falce, Hughes Corp., at the 1984 Tri-Service Cathode Workshop at Washington DC.
54. C. E. Maloney and N. Richardson, Appl. of Surf. Sci., 8, 2 (1981).
55. S. F. Frederick, Aerospace Corporation, at the 1980 Tri-Service Cathode Workshop, Rome NY.
56. B.C. Lamartine, W. V. Lampert and T. W. Haas, Appl. Surf. Sci., 8, 171 (1981).
57. R. Forman, E. G. Wintucky, G. G. Lesny and B. G. Lindow, NASA-Lewis Research Center, at the 1982 Tri-Service Cathode Workshop, Fort Monmouth, NJ.
58. J. Cochran and O. Ogden, Georgia Institute of Technology, and W. Ohlinger, Semicon Associates Inc., at the 1982 Tri-Service Cathode Workshop, Fort Monmouth, NJ.
59. J.O. Tarter and D.N. Hill, Georgia Institute of Technology and W.L. Ohlinger, Semicon Associates, Inc., at the 1982 Tri-Service Cathode Workshop, Fort Monmouth, NJ.
60. R. Lipeles and A. Kan, App. Surf. Sci., 16, 189 (1983).
61. G. Eng and A. Kan, Appl. Surf. Sci., 16, 181 (1983).
62. D. N. Hill and J. E. Lampert, Georgia Institute of Technology, at the 1984 Tri-Service Cathode Workshop, Washington, DC.
63. A. Kan and R. R. Seaver, Aerospace Corporation, at the 1984 Tri-Service Cathode Workshop, Washington, DC.

64. J. O. Tarter and W. Ohlinger, at the 1984 Tri-Service Cathode Workshop, Washington, DC.
65. H. P. Boehm and H. Knozinger, "Catalysis, Science and Technology", J.R. Anderson and M. Boudart Eds; Springer-Verlag: West Berlin, (1983).
66. S.C. Chan, I.E. Wachs, L.L. Murrel, and N.C. Dispenziere, J. Catal. 92, 1 (1985).
67. J.B. Peri, J. Phys. Chem. 86, 1615 (1982).
68. J.M. Basset and R. Ugo, in "Aspect of Homogeneous Catalysis"; R.Ugo, Reidel: Dordrecht, The Netherlands, 1976, Vol. III, p. 170.
69. S.J. Tauster, S.C Fung, and R.L. Garten, Jour. A. Che. Soc. 1004, 170 (1978).
70. S.J. Tauster, S.C. Fung, R.T.K. Baker and J.A. Horsely, Science 211, 1121 (1981).
71. D. Norman, R.A. Tuck, H. B. Skinner, P. J. Wadsworth, T. M. Gardiner, I. W. Owen, C. H. Richardson, and G. Thornton, Phys. Rev. Lett., Vol. 58, No. 5, 519 (1987).

A thick, dark, textured border runs along the outer edge of the page. Inside this, a rectangular frame with a repeating diamond-shaped decorative pattern encloses the central text.

MISSION of *Rome Air Development Center*

RADC plans and executes research, development, test and selected acquisition programs in support of Command, Control, Communications and Intelligence (C³I) activities. Technical and engineering support within areas of competence is provided to ESD Program Offices (POs) and other ESD elements to perform effective acquisition of C³I systems. The areas of technical competence include communications, command and control, battle management, information processing, surveillance sensors, intelligence data collection and handling, solid state sciences, electromagnetics, and propagation, and electronic, maintainability, and compatibility.

END

DATE

FILMED

5-88

DTIC